Stochastic Models of Drug Resistance Development

Inaugural dissertation
of the Faculty of Science,
University of Bern

presented by

Juan Antonio Magalang

from the Philippines

Supervisor of the doctoral thesis:
Prof. Dr. Riccardo Gatto
Institute of Mathematical Statistics and Actuarial Sciences
University of Bern

PD Dr. Daniel Sanchez-Taltavull
Department of Visceral Surgery and Medicine
Inselspital, Bern University Hospital

Stochastic Models of Drug Resistance Development

Inaugural dissertation
of the Faculty of Science,
University of Bern

presented by

Juan Antonio Magalang

from the Philippines

Supervisor of the doctoral thesis:
Prof. Dr. Riccardo Gatto
Institute of Mathematical Statistics and Actuarial Sciences
University of Bern

PD Dr. Daniel Sanchez-Taltavull
Department of Visceral Surgery and Medicine
Inselspital, Bern University Hospital

Accepted by the Faculty of Science

Bern, December 13, 2024

The Dean
Prof. Dr. Jean-Louis Reymond

Contents

Acknowledgements

Padayon!

I would like to first express my heartfelt appreciation to my supervisors, Prof. Dr. Riccardo Gatto and PD Dr. Daniel Sanchez-Taltavull for their unwavering support and patience with me throughout the entirety of my PhD journey. I am immensely grateful for their mentorship for the past years which has helped me grow more as a researcher in this field. Coming from a physics background, navigating through both biology and mathematics was not an easy task for me, but their guidance has helped me through it.

I would also like to express my appreciation to our collaborators who have helped me build this project and this thesis since the beginning. I would like to thank Prof. Dr. Édgar Roldán and Prof. Dr. Jose Perico Esguerra both of whom, along with Daniel, have introduced me to the field of modelling biological phenomena with stochastic processes and continued to guide me through it. I would also like to thank Prof. Dr. Tyll Krüger for allowing me to visit and work with him in Wroclaw, for introducing me to the larger community of academics in infectious disease dynamics, and for agreeing to be an external referee of this thesis. I would also like to thank Dr. Riccardo Turin and Dr. Laetitia Colombani for their contributions especially in the earlier years of the PhD project. Finally, I would like to thank Dr. Javier Aguilar for his enormous contributions to this work; this thesis would have taken much longer to finish without his input.

I would like to thank my colleagues at the Visceral Surgery Research Lab, especially to Prof. Dr. Deborah Stroka and Prof. Dr. Guido Beldi for allowing me to join and participate in the lab. I would also like to thank my colleagues at the Institute of Mathematical Statistics and Actuarial Sciences, especially to Prof. Dr. David Ginsbourger for his guidance in the earlier years of the PhD and for allowing me to work on this project with everyone. I know that I have not had the opportunity to work with everyone in either DBMR or IMSV directly, but all of the events, lunches, apéros, or just the random chats in the office or coffee room have made this work a lot easier.

Lastly, I would also like to thank my family and friends. To my parents and my brothers for supporting me throughout all of my endeavors, even if it means that we are all physically apart. *Mahal na mahal ko kayo.* To my friends, both old and new, both near and far, thank you for always being there for me throughout this journey.

Maraming salamat po sa inyong lahat!

Abstract

Antimicrobial resistance is a growing threat to public health as therapies designed to treat pathogenic infections lose their efficacy over time. This loss in the efficacy is due to pathogenic evolution which is inherently stochastic. Hence, estimating the times at which pathogens will develop drug resistances is an important quantity to study since it is equivalent to the time that a therapy will fail. Common strategies to mitigate drug resistance development are combination therapies, where two or more therapies are administered simultaneously, and therapy switching, where therapies are replaced or cycled out. This thesis aims to develop a model of drug resistance development within a patient infected with a chronic infection by modelling the within-host infection rate as a bounded and multidimensional Brownian motion with stochastic resetting. Features of this stochastic process reflect therapy administration strategies: multidimensionality represents combination therapies, while stochastic resetting, where a stochastic process returns to its initial position at random times, represents therapy switching. The boundaries of the model are either reflecting or absorbing. Reflecting boundaries prohibit the full recovery of the host as it is under chronic infection, while absorbing boundaries signify the failure of the therapy. The times at which the stochastic process reaches the absorbing boundary is of interest as this also symbolizes the time that drug resistance has emerged. Two scenarios will also be studied in detail: single therapy and multiple therapy protocols. In single therapy protocols, the analytical probability distribution of the resistance development time will be derived in Laplace space, and novel methods in approximating its inversion and in obtaining simulated values with a controllable error. In multiple therapy protocols, analogous stochastic processes will be proposed that are optimized for either combination therapy or therapy switching. This will allow for a thorough investigation of optimal choices of the number of therapies and switching rates, and also the imposition of constraints in terms of the maximum allowed switching rate, total number of therapies available, and costed therapy switching.

Chapter 1

Introduction

Pathogens such as viruses or bacteria cause infections by rapidly multiplying within a host. This rapid multiplication often leads to genetic errors, or mutations, that change certain traits of the offspring of the pathogen [1–3]. While specialized therapies are designed to eliminate these pathogens, mutations can sometimes result in offspring with a natural resistance to the therapies, thereby reducing their efficacy. This phenomenon, known as drug resistance, poses a global threat to modern medicine and public health.

This thesis aims to mathematically model the fluctuations in the level of drug resistance caused by the mutation of an infecting pathogen and how different strategies of administering antimicrobial therapies impact drug resistance development.

1.1 Mutation and evolution

The evolution of any organism, including pathogens, requires diversity in terms of genetic traits within its population [1]. This diversity is crucial since it provides a range of genetic traits that may be advantageous when exposed to changing environments. This evolutionary pressure may be due to the presence of natural predators or diminishing sources of food and nutrients.

Genetic diversity is typically generated through mutations that occur when organisms replicate theor genetic material to produce their offspring. The process of transferring or copying the genetic material is not always perfect and at times, errors known as mutations occur. Mutations have the potential to change certain traits of the offspring. Mutations are typically either neutral having no effect, or deleterious which hinder the chances of survival of an organism [1, 4]. Advantageous or adaptive mutations, though rare, increase the chances of survival of a organism. These mutations are often preserved and propagated through the population through mechanisms like natural selection and genetic drift [5].

Organisms with advantageous mutations are selected since they have the potential to reproduce or replicate further, while organisms with neutral and deleterious mutations are removed as the threat from external factors continue to grow. Over time, the mutations compound and the organism deviates from its ancestors, successfully evolving.

1.2 Drug resistance development

Pathogens must replicate quickly since they are vulnerable to the immune system of a host and external pressure such as antimicrobial treatments accelerate this further. Because of this rapid replication, errors in the genetic material vary by orders of magnitude [4] and different pathogen strains emerge. The increase of pathogen strains with advantageous mutations lead to drug resistance development, a phenomenon that causes an antimicrobial therapy to lose efficacy over time. The presence of resistant strains make treating infections significantly more difficult as conventional treatments gradually become ineffective.

The growing burden of drug resistant pathogens is increasingly becoming a public health crisis, especially in the global south. In 2019, of the 1.27 million deaths directly attributable to drug-resistant infections, the majority come from sub-Saharan Africa and South Asia [6]. In the worst case scenario, forecasts of up to 8.22 million deaths associated to antimicrobial resistant infections have been predicted in the year 2050 [7]. These deaths were primarily due to resistant strains of widespread infections such as HIV, malaria, and tuberculosis, which are especially prevalent in these regions [8].

Since mutations occur during treatment, it can be argued that antimicrobial therapies themselves contribute to the emergence of drug resistance. Hence, it has been suggested that the complete eradication of drug resistance is unrealistic as modern medicine continues to rely on antimicrobial therapy [9]. Antimicrobial stewardship is the most practical way to mitigate the development of drug resistance. This entails the improvement of surveillance of the prevalence of drug resistance, alternative therapies such as vaccines, and the proper and strategic administration of antimicrobial drugs of which will be studied in detail [8, 10].

1.3 Mechanisms of drug resistance

The emergence of drug resistance is accelerated by misuse and mismanagement of antimicrobial drugs in agricultural, environmental, and medical use [11, 12]. Resistant pathogens that have developed within a single host may also have the potential to spread to other hosts, thereby increasing its risk to public health [13, 14]. Drug-resistant pathogens are known to spread through water and airborne transmission, and vectors such as insects potentially transmit pathogens across vast areas [14, 15].

At a cellular level, pathogens evolve different mechanisms to escape treatment and develop drug resistance. However, these mutations commonly have evolutionary trade-offs that reduce other traits in order to increase resistance, this is also called *collateral sensitivity* [16–18]. Examples of mechanistic trade-offs are with bacteria such as *E. coli*. These mutate to survive while taking in less extracellular material including nutrients since it consequently takes in less of the drug [19]. Similarly, viruses such as HIV-1 can increase their latency period within their hosts cells to avoid being affected by treatment but results in a slower reproduction rate [20].

Trade-offs also occur in terms of the therapies being administered. These are due

to mutations changing the susceptibility of the pathogen to certain drugs. It has been found that when *Pseudomonas* develops a resistance to the antibiotic ciprofloxacin, it develops a sensitivity to another antibiotic tobramycin [21]. Likewise, *Klebsiella* that is found to be resistant to either colistin or fosfomycin individually, are found to be sensitive to combinations of these two drugs [22].

1.4 Therapy administration strategies

To manage and reduce the emergence of drug resistance, physicians use different strategies when administering antimicrobial drugs. These strategies exploit therapeutic trade-offs that pathogens undergo after mutation. Common methods that are used are combination therapy [22–24] or through therapy switching [16, 25]. Combination therapy is the use of two or more drugs at the same time, while therapy switching replaces a drug being used with a different one but with the same class.

These strategies come with risks as therapies may interact for both combination therapy and therapy switching. These interactions may be classified as synergistic, suppressive, or additive [26] and are dependent on the cellular targets of the drugs within a host during treatment. Synergistic interactions are beneficial to the host as it improves the antimicrobial efficacy non-linearly. On the other hand, suppressive interactions worsen the situation for the host as the therapies counteract each other, resulting to an ineffective therapy. Finally, additive therapies are null models of drug interaction, where therapies are assumed to not interact with each other [27, 28].

There are also various physiological and economical limitations to switching or adding a therapy [29–31]. Changing treatments for resistant infections may also lead to increases in complications, as there have been cases where switching drugs would lead to adverse outcomes for patients with certain comorbidities [32]. These constraints highlight the complexity of managing drug resistance development and the importance of modelling optimal strategies that mitigate the impact of drug resistance given the potential limitations is a critical area of research in the field.

1.5 Mathematical modelling of drug resistance

Analytical approaches such as mathematical models are valuable tools in studying drug resistance development since they can simulate epidemiological and physiological events such as transmission dynamics of resistant strains, co-infection of different strains, and introduction of alternative pharmaceutical interventions, without the need of experimental procedures [13].

Mathematical models have been used to study drug resistance development in a variety of diseases with pathogenic origins such as AIDS [33–38], tuberculosis [39], pneumonia [40], and malaria [41]. These models have been used to study mechanisms of evolutionary trade-offs to develop drug resistance [19, 20, 36, 37], stochastic viral evolution [38, 42] and competition between resistant strains [43, 44]. In larger scales, the epidemiological impact of drug resistant infections have been modelled [11, 13], along

with estimates to the economic burden due to hospitalizations and costs of treatment [45]. Furthermore, these models have shown to have significant applications to public health, as mathematical models have been used to study the effectiveness of non-pharmaceutical public health interventions such as hygiene and surveillance [11].

1.6 Goals and overview of the thesis

The combination of mechanisms of mutation, collateral sensitivity, and therapy administration strategies shows the complex interactions that comprise drug resistance development. Given the dynamic nature of these interactions, stochastic processes provide an ideal modelling framework as they capture the inherently noisy pathogenic mutations that occur while undergoing treatment. This thesis will feature reports of models of the level drug resistance, and consequently, the efficacy of therapy as a multidimensional and bounded Brownian motion. This aims to quantify the distributions of the resistance development time (RDT), which is important in characterizing the amount of time needed for a therapy to fail. This will be done in two scenarios: single therapies and multiple therapies.

1.6.1 Single therapies

The mean RDT for a single therapy model had been analytically defined previously [42]. However, the mean does not represent the entire distribution since features such as uncertainty, median, and quantiles are unavailable. Indeed, having knowledge of the full distribution provides a robust description of the model which has potential applications to biology and medicine. However, only the Laplace transform of the full RDT distribution is known in literature [42] and straightforward methods to invert this expression are currently not known [46, 47].

The inversion of the distribution is instead approximated using the proposed Padé-partial fraction (PPF) method, which approximates the RDT distribution as ratio of polynomials that can then be decomposed and inverted. Furthermore, a novel simulation method called the multiresolution algorithm (MRA) is also proposed, that generates finer values of a given process up to an arbitrary error.

The goal of the PPF method is to obtain an approximant with a Laplace inversion that can be solved using standard methods. As mentioned previously, the Padé approximation is used to obtain a fraction of polynomials with degrees equal to the order of the approximation. This method is known to be more robust than the typical Taylor series approximation and can converge even when the Taylor series does not [48]. Furthermore, the rational expression obtained from Padé is ideal since it can be decomposed into a sum of fractions with binomial denominators through partial fraction decomposition. Fractions with binomial denominators have a known inverse Laplace transform.

On the other hand, the MRA is an algorithm that yields a sample RDT by simulating a stochastic trajectory that passes through the absorbing boundary. The MRA exploits the property of Wiener processes that the intermediate point among three consecutive

points is normally-distributed with a mean given by the average of the two other points [49]. Points of the trajectory that pass through the absorbing boundary can be made finer through the MRA, yielding sample RDTs that are closer to the actual RDT. The MRA can also be combined with the standard Euler-Maruyama algorithm [50], which increases the computational efficiency of the algorithm while keeping the accuracy.

1.6.2 Multiple therapies

The Laplace transform of the RDT distribution found in [42] is limited only to a stochastic process in one dimension, i.e. only one therapy. However, combination therapy has been proven to mitigate drug resistance development which can be modeled as stochastic processes in higher dimensions. Straightforward methods to derive the RDT distribution for a higher dimension model do not work due to the unique boundary conditions of this model [51–53].

We instead introduce two phenomenological models that pattern the fluctuations of the therapy efficacy given two or more therapies with switching. The first model, called the coupled continuous model, is a rotationally-invariant stochastic process with dimensions that can be increased freely. The second model, called uncoupled discrete model, is a discrete-space stochastic process comprised of a lattice of states that explicitly accounts for the efficacy of each therapy individually.

The coupled model is a continuous-space stochastic process in polar coordinates that is rotationally-invariant. As a phenomenological model, a continuous-space scheme is considered since it models the small, incremental mutations of the infecting pathogen over short time scales [54]. The coupled model allows for the investigation of the behavior of the RDT at higher dimensions since it reduces the efficacies of all therapies being simultaneously administered to a single value, as a consequence, stochastic resetting occurs simultaneously for all dimensions.

On the other hand, the uncoupled model allows for independent resetting for all dimensions. The uncoupled model is a Markov chain of states arranged as a lattice and is controlled by a master equation. The discrete-space scheme models significant changes of the therapy efficacy over longer periods of time [3]. The statistics of the RDT for this model can be obtained by manipulating the transition matrix of the Markov chain [55], however it is computationally expensive.

1.6.3 Overview of the thesis

This thesis is organized as follows: A discussion on the different mathematical techniques that have been used to approximate the RDT from both reports, along with the full description of the drug resistance model is first presented in Chapter 2. This is followed by the two reports that discuss the single and multiple therapy scenarios in Chapters 3 and 4, respectively. Finally, a discussion of possible extensions to the work are presented in Chapter 5.

Chapter 2

Mathematical framework

The previous chapter has discussed how mutations that lead to drug resistance are random and unpredictable [1, 5]. To account for the complexity of this process, stochastic processes may be used as models for the fluctuations of the level of drug resistance [38, 42]. These processes can also be extended to model therapy administration strategies such as combination therapy and therapy switching. This chapter will discuss the mathematical background of the different elements that will be used to build the final model for drug resistance development with therapy administration strategies.

2.1 Stochastic processes

For a probability space $(\Omega, \mathcal{F}, \mathbb{P})$, a measurable state space S, and a set T called an *index set*, a collection of random variables $\{X_t\}_{t\in T}$ defined on the probability space that maps onto the state space is called a *stochastic process* [56, 57],

$$\begin{aligned} X : T \times \Omega &\to S \\ (t, \omega) &\mapsto X_t(\omega). \end{aligned} \tag{2.1}$$

Common choices for the state space is over the real numbers $S = \mathbb{R}$ or a multivariate case $S = \mathbb{R}^N$. The index set is typically interpreted as time and the choice of the index set further classifies stochastic processes into two common types: The first is for a choice $T = \mathbb{N}$ and are called *discrete-time* stochastic processes. The second is for $T = \mathbb{R}$, called *continuous-time* stochastic processes.

An important property that certain stochastic processes possess is called the *Markov property*, where for a state of a stochastic process $X_{t_{n+1}}$ at time t_{n+1}, a stochastic process has the Markov property if it satisfies the conditional probability

$$\mathbb{P}(X_{t_{n+1}} | X_{t_n}, X_{t_{n-1}}, \ldots, X_{t_1}) = \mathbb{P}(X_{t_{n+1}} | X_{t_n}), \tag{2.2}$$

for $t_{n+1} > t_n > \ldots > t_1$. The Markov property implies that the future states of the stochastic process only depends on the present state, and disregards the past states

hence, Markov processes are also called *memoryless* processes. All of the stochastic processes considered in this thesis follow the Markov property.

An example of a stochastic process is a *random walk* on a discretized state space. Consider a real-valued state space partitioned into equally-spaced sub-intervals with length $1/M$, thus $S = \{i/M \,|\, i \in \mathbb{Z}\}$. The stochastic process $\{X_t\}$ now evolves within this space that may be visualized as a discrete chain of states. The process only transitions from a state $x_i = i/M$ to its adjacent states $x_{i\pm1} = (i \pm 1)/M$. A differential equation that describes the time evolution of the random walk is called the *master equation*.

Proposition 2.1.1 (Master equation)**.** *Let x_0 be the initial state of the random walk on a chain of states. The probability that gives the position x of a random walk at any time t conditioned to the initial state is given by the master equation*

$$\frac{\mathrm{d}}{\mathrm{d}t}P(x,t|x_0) = p\,P\left(x - \frac{1}{M}, t\middle|x_0\right) + q\,P\left(x + \frac{1}{M}, t\middle|x_0\right) - (p+q)\,P(x,t|x_0), \tag{2.3}$$

for $x \in \{i/M \,|\, i \in \mathbb{Z}\}$. The rates p and q are called transition rates, and rate $-(p+q)$ is also called the escape rate from state x. The probability distribution $P(x,t|x_0)$ is also called the propagator.

The proof is outlined in Appendix A.1. Consider a finite and bounded state space partitioned into M equally-spaced states, e.g. $S = \{a + (b-a)(i/M) \,|\, i = 1, \ldots, M\}$ for $a < b$ and $a, b \in \mathbb{R}$ bounding the state space in an arbitrary interval $[a, b]$. The transition rates and dynamics of the random walk still follow eq. (2.3) away from the boundaries, but the transition rates may now be written as an $M \times M$ *transition matrix* $\mathbf{W}$, with elements W_{ij} denoting transitions from state x_j to x_i. The corresponding representation of the master equation will be

$$\frac{\mathrm{d}}{\mathrm{d}t}P(x,t|x_0) = \mathbf{W}P(x,t|x_0), \tag{2.4}$$

The propagator is now a column vector of probabilities for all M states. Solving for the propagator in Equation (2.4) is possible, however it will almost always be in terms of matrix operations [55, 58, 59]. Obtaining an analytic form of the propagator without matrix operators is challenging, but the system may be approximated to have a form that results to a propagator that is easier to solve.

The Kramers-Moyal expansion is a second-order Taylor expansion of the master equation [60, 61] that results into a partial differential equation. This expansion also transforms the state space from sub-intervals of $\mathbb{R}$ to the entire set $S = \mathbb{R}$. The resulting partial differential equation is called the *Fokker-Planck* or the *forward Kolmogorov* equation.

Proposition 2.1.2 (The Fokker-Planck equation)**.** *Let $x \in \mathbb{R}$ be a position in the continuous space approximated from the Kramers-Moyal expansion. The Fokker-Planck equation reads*

$$\frac{\partial}{\partial t}P(x,t|x_0) = -v\frac{\partial}{\partial x}P(x,t|x_0) + D\frac{\partial^2}{\partial x^2}P(x,t|x_0), \tag{2.5}$$

where v is called the drift parameter and D is called the diffusion parameter, dependent on the transition rates p and q taken from the master equation,

$$v = \frac{p-q}{M}, \quad D = \frac{p+q}{2M^2}. \tag{2.6}$$

The proof is outlined in Appendix A.2. The Fokker-Planck equation has a propagator that may be solved given appropriate boundary conditions [51, 62]. These conditions define the limits at which the stochastic process is allowed to evolve. Some common boundary conditions that have been considered are absorbing and reflecting boundaries and the theory of stochastic processes with these boundaries is a classical topic in probability theory [62]. Reflecting boundaries are regions where diffusing particles cannot permeate [63]. On the other hand, absorbing boundaries are regions where diffusing particles can enter but cannot leave.

The Fokker-Planck equation describes the probability distribution of the process at a certain position, however it neglects the dynamics of the stochastic trajectory itself [64]. The equation that captures the dynamics of the trajectory as it fluctuates through a continuous space is controlled by the stochastic differential equation (SDE). Let $\{X_t\}_{t\geq 0}$ be a stochastic process, the SDE of this process described in eq. (2.5) is given by

$$\mathrm{d}X_t = -v\,\mathrm{d}t + \sqrt{2D}\,\mathrm{d}W_t, \quad \forall t \geq 0, \tag{2.7}$$

where v is the drift constant, and D is the diffusion constant, and W_t is called the *Wiener process* or the *standard Brownian motion* [53, 56, 57].

Definition 2.1.3 (Wiener process)**.** The Wiener process $\{W_t\}_{t\geq 0}$ is a stochastic process that has the following properties,

1. At $t = 0$, $W_0 = 0$.
2. Independent increments: Let $t_i, t_j, t_k \in T$ with $t_i > t_j > t_k$. The increments of the Wiener process follows
$$\mathbb{P}((W_{t_i} - W_{t_j}) \cap (W_{t_j} - W_{t_k})) = \mathbb{P}(W_{t_i} - W_{t_j})\mathbb{P}(W_{t_j} - W_{t_k}), \quad \forall t_i, t_j, t_k \in T. \tag{2.8}$$
3. Stationary Gaussian increments: Let $t_i, t_j \in T$. The increments of the Wiener process follows
$$W_{t_i} - W_{t_j} \sim \mathcal{N}(0, t_i - t_j), \quad \forall t_i, t_j \in T \tag{2.9}$$
where $\sim$ denotes that the increment is normally distributed with mean 0 and variance $t_i - t_j$. It is emphasized that any increment of the Wiener process is identically distributed or is distributed in the same manner.

The Fokker-Planck equation (2.5) may be obtained from the SDE (2.7) using Itô's formula. The derivation is outlined in Appendix A.3. Itô's formula states that for a twice differentiable test function $g(x,t)$,

$$\mathrm{d}g(x,t) = \frac{\partial}{\partial t}g(x,t)\mathrm{d}t + \frac{\partial}{\partial x}g(x,t)\mathrm{d}x + \frac{1}{2}\frac{\partial^2}{\partial x^2}g(x,t)\,(\mathrm{d}x)^2 \tag{2.10}$$

This formula is obtained from the second-order Taylor expansion of a general function, and then setting $\mathrm{d}t^2 = 0$ since this term is now negligibly small.

2.2 Generalizations

Stochastic processes may be generalized to consider *stochastic resetting* [65, 66] which allows the process to return to its initial position at random times and intrinsically exhibit non-equilibrium stationary distributions [65, 67, 68]. This introduces an auxiliary process χ, which is the set of *arrival times of a homogeneous Poisson process.*

Definition 2.2.1 (Arrival times of a homogeneous Poisson process)**.** A homogeneous Poisson process $\{N_t\}_{t\geq 0}$ is a counting process that counts the number at which a random event occurs up to time t. The set of arrival times $\chi = \{t^* | t^* \geq 0\}$ is the set of all times at which the Poisson process increases.

1. Independent increments: Let $t_i^*, t_j^*, t_k^* \in \chi$ with $t_i^* > t_j^* > t_k^*$. The increments $t_i^* - t_j^*$ and $t_j^* - t_k^*$ are independent as defined in eq. (2.8).
2. Exponentially-distributed increments: Let $t_i^*, t_{i+1}^* \in \chi$ for $i \geq 1$ be consecutive arrival times. The time in between two arrival times, also known as the *waiting time*, is distributed as a random variable

$$t_{i+1}^* - t_i^* \sim \text{Exp}\,(r) \tag{2.11}$$

where $\text{Exp}(r)$ denotes an exponential distribution with rate r and mean $1/r$.

The set of arrival times is used to write an appropriate SDE for the process with stochastic resetting,

$$\mathrm{d}X_t = (1 - \mathbf{1}_\chi(t)) \left(v\,\mathrm{d}t + \sqrt{2D}\,\mathrm{d}W_t \right) + \mathbf{1}_\chi(t)(x_0 - X_t)\,\mathrm{d}t, \quad \forall t \geq 0. \tag{2.12}$$

The function $\mathbf{1}_\chi(t)$ is an indicator function dependent on the set of arrival times,

$$\mathbf{1}_{\chi(t)} = \begin{cases} 1, & t \in \chi \\ 0, & t \notin \chi \end{cases} \quad \text{where } \chi = \{0, t_1^*, t_2^*, \ldots\}, \tag{2.13}$$

where the increments of the arrival times $t_{i+1}^* - t_i^*, i \geq 1$, or the waiting times, are characterized by a rate r, called the *resetting rate*, as introduced in eq. (2.11).

Note that in [65, 66], an SDE-type equation was written in terms of the position of the stochastic process at the next infinitesimal time step,

$$X_{t+\mathrm{d}t} = \begin{cases} x_0, & \text{with probability } r\,\mathrm{d}t \\ X_t + (v\,\mathrm{d}t + \sqrt{2D}\,\mathrm{d}W_t), & \text{with probability } (1 - r\,\mathrm{d}t). \end{cases} \tag{2.14}$$

This is equivalent to the SDE in eq. (2.12) since the set of arrival times χ has an underlying Poisson counting process $\{N_t\}$ and has a known mean of events within an interval of time $\mathrm{d}t$ equal to $\mathbb{E}\{N_t\} = r\,\mathrm{d}t$.

With the formulation of the process in eq. (2.14), it has been shown in [66] that it is possible to write the equivalent Fokker-Planck equation with resetting by averaging over events in the interval $t + \mathrm{d}t$.

Proposition 2.2.2 (The Fokker-Planck equation with resetting)**.** *The appropriate Fokker-Planck equation with stochastic resetting reads*

$$\frac{\partial}{\partial t}P(x,t|x_0) = -v\frac{\partial}{\partial x}P(x,t|x_0) + D\frac{\partial^2}{\partial x^2}P(x,t|x_0) - r\,P(x,t|x_0) + r\delta(x-x_0), \quad (2.15)$$

where $\delta(x-x_0)$ is a Dirac delta function centered at the displacement from the initial position x_0, and r is the resetting rate.

One other generalization of the stochastic process is higher dimensions and with time and position-dependent drift and diffusion parameters [69]. An N-dimensional stochastic process is denoted as a vector by $\boldsymbol{X}_t = \{X_t^{(1)}, X_t^{(2)}, \ldots, X_t^{(N)}\}_{t\geq 0}$. Without stochastic resetting, the Itô SDE for this process is

$$\mathrm{d}\boldsymbol{X}_t = \boldsymbol{\mu}\left(\boldsymbol{X}_t, t\right)\,\mathrm{d}t + \boldsymbol{\sigma}\left(\boldsymbol{X}_t, t\right)\,\mathrm{d}\boldsymbol{W}_t, \quad (2.16)$$

where $\boldsymbol{\mu}$ is a drift vector that affects all components of $\boldsymbol{X}_t$ individually, and $\boldsymbol{\sigma}$ is a diffusion matrix which accounts for the interactions of each component of $\boldsymbol{X}_t$. A diffusion matrix with zero nondiagonal elements is called *isotropic* diffusion and assumes that the components of the stochastic process are independent of each other. From this SDE, an appropriate Fokker-Planck equation in higher dimensions may also be derived using the known multivariate version of Itô's formula for the SDE in eq. (2.16) [53]

Proposition 2.2.3. *For a multivariate SDE, Itô's formula gives the following for a test function $g(\boldsymbol{x}, t)$*

$$\begin{aligned}\mathrm{d}g(\boldsymbol{x},t) = &\left[\frac{\partial}{\partial t}g(\boldsymbol{x},t) + \sum_{i=1}^{N}\boldsymbol{\mu}(\boldsymbol{x},t)\frac{\partial}{\partial x_i}g(\boldsymbol{x},t) + \sum_{i=1}^{N}\sum_{j=1}^{N}D_{ij}\frac{\partial}{\partial x_i}\frac{\partial}{\partial x_j}g(\boldsymbol{x},t)\right]\mathrm{d}t \\ &+ \sum_{i=1}^{N}\sum_{j=1}^{N}\sigma_{ij}(\boldsymbol{x},t)\frac{\partial}{\partial x_i}g(\boldsymbol{x},t)\,\mathrm{d}W_t^{(j)},\end{aligned} \quad (2.17)$$

where $W_t^{(j)}$ is the j^{th} component of the multivariate Wiener process $\boldsymbol{W}_t$ and D_{ij} refers to the elements of the tensor $\boldsymbol{D} = \boldsymbol{\sigma}\boldsymbol{\sigma}^\top$, and is given by

$$D_{ij} = \frac{1}{2}\sum_{k=1}^{N}\sigma_{ik}(\boldsymbol{x},t)\sigma_{jk}(\boldsymbol{x},t). \quad (2.18)$$

The proof is outlined in Appendix A.4. Hence, the multivariate Fokker-Planck equation is given by the following.

Proposition 2.2.4 (The N-dimensional Fokker-Planck equation)**.** *The appropriate Fokker-Planck equation in N dimensions reads*

$$\frac{\partial}{\partial t}P(x,t|x_0) = -\sum_{i=1}^{N}\frac{\partial}{\partial x_i}\boldsymbol{\mu}(\boldsymbol{x},t)P(\boldsymbol{x},t|\boldsymbol{x}_0) + \sum_{i=1}^{N}\sum_{j=1}^{N}\frac{\partial}{\partial x_i}\frac{\partial}{\partial x_j}D_{ij}P(\boldsymbol{x},t|\boldsymbol{x}_0), \quad (2.19)$$

where D_{ij} refers to elements of the diffusion tensor defined in eq. (2.18).

This equation is obtained using the procedure shown in Proof A.2 for the 1-dimensional case where the expectation of both sides of Itô's formula is taken.

Boundary conditions in higher dimensions are no longer points or levels, but now span curves and surfaces. This makes solving for the propagator a challenge since conventional methods such as Laplace transforms, solving the Greens function, method of images, and the like [42, 51–53, 70] are no longer straightforward to perform. As an alternative, phenomenological models that patterns the fluctuations of the stochastic process in Equation (2.16) in higher dimensions may be used which are reducible and exploit certain symmetries of the boundary conditions. Symmetries are easier to exploit when the process is transformed, for example, into polar coordinates using Itô's rule [53] and then considering SDEs such as Rayleigh and Ornstein-Uhlenbeck processes [71, 72].

2.3 First passage times and distributions

Absorbing boundaries can be used as a stopping condition, and the time at which the process has reached the stopping condition is called the *first passage time* (FPT) [51].

Definition 2.3.1 (First passage time)**.** Suppose that the absorbing boundary is at $X(t) = a$, then formally, the FPT is written as a stopping time

$$T = \inf\{t \geq 0 \,|\, X(t) \leq a\}. \tag{2.20}$$

Since the first passage time is dependent on a stochastic process, it is also a random variable with a probability distribution $f(t)$. To obtain the FPT distribution, the propagator of the Fokker-Planck equation must be solved first. An important quantity from the Fokker-Planck equation is the *probability flux* or *probability current*. For the 1-dimensional Fokker-Planck equation (2.5), the probability flux is defined as follows.

Definition 2.3.2 (Probability flux)**.** The probability current $J(x,t)$ is the rate of influx of trajectories of the stochastic process at the position x given by

$$J(x,t) = v\,P(x,t|x_0) - D\frac{\partial}{\partial x}P(x,t|x_0)\,. \tag{2.21}$$

For an absorbing boundary at $x = a$, it is known that [51, 73]

$$f(t) = J(a,t) = v\,P(a,t|x_0) - D\frac{\partial}{\partial x}P(a,t|x_0). \tag{2.22}$$

Hence, the FPT distribution may be obtained provided that the propagator is solved. This is related to the derivation of the inverse Gaussian distribution using the method of images [74, 75]. The propagator also allows for the computation of another important quantity called the *survival probability* [51].

Definition 2.3.3 (Survival probability)**.** The survival probability is the probability that the process does not reach the absorbing boundary, given by

$$S(t) = \int_a^b P(x,t|x_0)\,\mathrm{d}x, \tag{2.23}$$

for a process bounded, for example in $[a, b]$ with a as the absorbing boundary.

This quantity is important for extending the process to stochastic resetting as renewal equation methods that computing for the FPT distributions with resetting may be obtained [66].

In general, solving for the propagator may be a challenging process, however methods such as solving for the Greens function and method of images [51–53] have been used successfully for certain configurations of the boundary conditions. One more standard method of solving for the propagator involves taking the Laplace transform.

Definition 2.3.4 (Laplace transform of $f(x,t)$)**.** The Laplace transform with respect to t is given by

$$\tilde{f}(x,s) = \mathcal{L}\{f(x,t)\}(x,s) = \int_0^\infty f(x,t)\exp(-st)\,\mathrm{d}t, \tag{2.24}$$

where $\tilde{f}(s)$ is the Laplace transform of $f(t)$.

Given the appropriate boundary conditions, e.g. reflecting and absorbing boundary conditions at certain positions in space, the Laplace transform of the propagator may be solved using standard techniques such as the separation of variables and undetermined coefficients [42, 51]. With this, the FPT distribution in Laplace space may be obtained.

However, inverting this Laplace transform back to the time domain is difficult and is not always possible to obtain analytically. There are numerical methods that are available for inversion [76, 77], such as the Gaver-Stehfest algorithm [78, 79] and the Talbot method [80]. However, since these are numerical algorithms, analytical quantities such as derivatives will be not as straightforward to obtain.

The straightforward inversion of the Laplace transform necessitates that $\tilde{f}(x,s)$ be in a form that can be found in standard tables of conversion for the Laplace transform, see e.g. [81]. This form may be obtained by either algebraic manipulation or approximation. The Padé approximation is a method used to obtain a fraction of polynomials with degrees equal to the order of the approximation.

Definition 2.3.5 (Padé approximation)**.** Let m, n be nonnegative integers and let $g(s)$ be a real-valued, $n+m$ times differentiable function. The Padé approximation of orders m and n to g is the rational function

$$g_{m,n}(s) = \frac{p_m(s)}{q_n(s)} = \frac{a_0 + a_1 s \ldots a_m s^m}{b_0 + b_1 s \ldots b_n s^n} \tag{2.25}$$

where the coefficients $a_0, \ldots, a_m$ and $b_0, \ldots, b_{n-1}$ are obtained by solving the $m+n+1$ linear equations

$$\begin{cases} \displaystyle\sum_{j=0\vee(i-n)}^{i} \frac{g^{(j)}(0)}{j!} b_{i-j} = a_i, \text{ for } i = 0, \ldots, m, \\ \displaystyle\sum_{j=0\vee(i-n)}^{i} \frac{g^{(j)}(0)}{j!} b_{i-j} = 0, \text{ for } i = m+1, \ldots, m+n. \end{cases} \tag{2.26}$$

The notation $g^{(j)}(0)$ denotes the j^{th} derivative of the function $g(s)$ evaluated at $s = 0$.

This method is known to be more robust than the typical Taylor series approximation and can converge even when the Taylor series does not [48]. Furthermore, the rational expression obtained from Padé is ideal since it can be decomposed into a sum of fractions with binomial denominators through partial fraction decomposition or the residue method. Fractions with binomial denominators have a known inverse Laplace transform, hence providing an analytical approximation to the FPT distribution that can be inverted.

2.4 Numerical simulations

Simulation methods provide numerical results of the FPT distribution without the need of approximations and alternative formulations. These methods are also versatile, allowing for different simulation conditions such as stochastic resetting and non-trivial boundary conditions for higher dimensions.

A widely used simulation algorithm for generating stochastic processes is the Euler-Maruyama algorithm [82]. This algorithm is extended to consider stochastic resetting as well.

Definition 2.4.1 (Euler-Maruyama algorithm with resetting)**.** A stochastic process generated by the Euler-Maruyama algorithm has values of time given by $t = \{n\Delta t | n \geq 0\}$, where $\Delta t > 0$ is a fixed time increment. The stochastic process is generated recursively for $n \geq 0$

$$X_{(n+1)\Delta t} = \begin{cases} x_0, & \text{with probability } r\,\Delta t \\ X_{n\Delta t} + v\Delta t + \sqrt{2D}\,\Delta W, & \text{with probability } 1 - r\,\Delta t \end{cases} \tag{2.27}$$

where x_0 is the initial position of the stochastic process and $\Delta W \sim \mathcal{N}(0, \Delta t)$ is a finite Wiener increment.

While the Euler-Maruyama is simple to implement, it has several limitations, especially when it comes to computing for the FPT.

Proposition 2.4.2. *Let T be the FPT generated by a Brownian SDE (2.12) and T_{EM} be the FPT generated by the Euler-Maruyama algorithm, hence $T_{EM} \geq T$.*

Proof. At an absorbing boundary at a, the stopping condition of the Euler-Maruyama algorithm is defined as

$$T_{EM} = \Delta t \cdot \inf\{n \geq 0 | X_{n\Delta t} \leq a\}. \tag{2.28}$$

It can also be written that $T_{EM} = n'\Delta t$ for an n' that satisfies the condition above. By Definition 2.3.1 for the true FPT, it is implied that $T \in [(n'-1)\Delta t, n'\Delta t]$ but the Euler-Maruyama algorithm is defined to take the FPT at $n'\Delta t$. Thus, $T_{EM} \geq T$, almost surely.

□

This shows that the Euler-Maruyama algorithm will overestimate the true FPT due to the finite time increment Δt. It is possible to still numerically simulate an FPT with a variable error. Wiener processes have a property following from the formula for conditioning the multivariate normal distribution [50],

$$W_{t+h} \mid [W_t = a, W_{t+2h} = b] \sim \mathcal{N}\left(\frac{a+b}{2}, \frac{h}{2}\right), \quad h > 0, \tag{2.29}$$

where $\mathcal{N}(\mu, \sigma^2)$ denotes a normally-distributed random variable with expectation μ and variance σ^2. Following this property recursively, one may obtain a new points on the stochastic process in between $t \in (t, t+h)$ and $t \in (t+h, t+2h)$. This creates finer points while still keeping the same stochastic trajectory. Hence, using this to compute for the FPT allows for arbitrary accuracy as long as new intermediate points are being generated.

For simulating the master equation formulation of the stochastic process in Equation (2.4), the Gillespie algorithm or the stochastic simulation algorithm [83] is a classic approach. This algorithm returns a possible stochastic solution of the master equation and gives an exact stochastic trajectory. However, the computational cost increases significantly the more connected each state is to one another on the graph.

2.5 Stochastic models of physical phenomena

Stochastic processes are widely used as scale-free models that describe a wide range of physical phenomena. The mathematical framework of stochastic processes allows one to obtain insights from systems despite undergoing fluctuations over time. By analyzing these processes, one may measure behavior such as phase transitions and rare events. Stochastic processes in both discrete and continuous state spaces have been widely used as models of search strategies [84], synchronization of complex phenomena [85], predator-prey behavior [86] and epidemiology [87, 88].

First passage times have also been used as models in various fields such as solid state physics [89], cosmology [90], economics [91] and finance [92–94]. Specifically in biology, FPTs have been used to study how fast two DNA segments in the genome have physical contact [95], coordinated cell migration [96], and in cellular channel transport and receptor binding [97].

As an extension to FPT problems, stochastic resetting problems have also been used as models for biological systems. It has been used to model hunting behavior in animals, where animals return to specific sites to look for food [98], cellular focal adhesions [99], and backtrack recovery in RNA polymerization [100]. Stochastic resetting has also developed new experimental models, where in a colloidal diffusion, particles are reset [101, 102].

However, analytical solutions to these models have been challenging due to the reasons presented in the previous sections. Solutions to the Fokker-Planck equation with resetting have been previously investigated for systems with a specific configurations of absorbing boundaries [66, 103–105]. Analytical properties of random walks on discrete

state spaces have also been widely studied [58, 106, 107]. Finally, stochastic resetting has been generalized further to power-law distributed resetting [108], time-dependent resetting [109], resetting with costs [110, 111], as well as with Lévy flights [112] and Ornstein-Uhlenbeck processes [113].

2.6 Stochastic model of drug resistance

This thesis aims to model drug resistance development with therapy switching using a bounded and biased diffusion process with stochastic resetting [42]. The process aims to quantify the change in therapy efficacy of a drug given to a host over time as it treats an infection. The efficacy of the therapy being administered to a host is inversely proportional to drug resistance development of the infecting pathogen.

This parameter of therapy efficacy η is coupled to the infection rate of a host-pathogen model for chronic infection, such as HIV-1 [36, 37]. The host-pathogen model tracks three cell populations: healthy cells H, latently-infecting cells L, and actively-infecting cells I:

$$\frac{\mathrm{d}H}{\mathrm{d}t} = \alpha - \lambda_H H - \beta H I \prod_{i=1}^{N_T}(1-\eta_i), \tag{2.30a}$$

$$\frac{\mathrm{d}L}{\mathrm{d}t} = \epsilon\beta H I \prod_{i=1}^{N_T}(1-\eta_i) + pL\left(1-\frac{L}{K}\right) - a_L L - \lambda_L L, \tag{2.30b}$$

$$\frac{\mathrm{d}I}{\mathrm{d}t} = (1-\epsilon)\beta H I \prod_{i=1}^{N_T}(1-\eta_i) + a_L L - \lambda_I I. \tag{2.30c}$$

Healthy cells are generated with a constant rate of α and die at a rate of $\lambda_H H$, where λ_H is a death constant for healthy cells. Furthermore, these healthy cells are turned into either latently-infecting or actively infecting cells with a rate $\beta H I \prod_{i=1}^{N_T}(1-\eta_i)$, with β as a constant of infection and η as the therapy efficacy. Constant ϵ is a probability that infection will yield a latently-infected cell, which means $1-\epsilon$ will give the probability that the infection will yield and actively-infecting cell. Latently-infecting cells proliferate with a rate pL, with p as a constant of proliferation, limited by a carrying capacity K with a rate $(pL^2)/K$, and die off with a rate $\lambda_L L$. Finally, latently-infecting cells can transform to actively-infecting cells with a rate aL, with a as a constant of activation. Actively-infecting cells die off with a rate of $\lambda_I I$.

The therapy efficacy is used to scale the base rate of infection in the model βHI. Based on how Equations (2.30) are written, therapy efficacy is bounded: $\eta_i \in [0, 1)$. A therapy efficacy of $\eta_i = 1$ signifies a perfect therapy, as it removes the term for the infection rate. On the other hand, $\eta_i = 0$ signifies a failure of the therapy, which maximizes the infection rate.

Let $\boldsymbol{\eta}$ be a vectorial representation of N_T dimensions of a stochastic process, i.e. $\boldsymbol{\eta}(t) = \{\eta_1(t), \ldots, \eta_{N_T}(t)\}$. This vector represents all N_T simultaneous therapy effica-

cies that are being administered. The stochastic differential equation that controls this process is written as

$$\begin{aligned} \mathrm{d}\boldsymbol{\eta} = &\operatorname{diag}\left(\boldsymbol{I} - \boldsymbol{\mathcal{I}}_{\boldsymbol{\chi}}(t)\right)\left[\boldsymbol{\mu}(\boldsymbol{\eta}, t)\mathrm{d}t + \sqrt{2D}\,\mathrm{d}\boldsymbol{W}(t)\right] \\ &+ \operatorname{diag}\left(\boldsymbol{\mathcal{I}}_{\boldsymbol{\chi}}(t)\right)(\boldsymbol{\eta}_0 - \boldsymbol{\eta}), \end{aligned} \tag{2.31}$$

where $\boldsymbol{v}$ is a drift vector and $\boldsymbol{\eta}_0$ is a vector of initial positions of the N_T therapies. The operator $\operatorname{diag}(\cdot)$ refers to transforming the vector argument into a square diagonal matrix and the vector $\boldsymbol{I}$ refers to a vector of ones with length N_T. Function $\boldsymbol{\mathcal{I}}_{\boldsymbol{\chi}}(t)$ is a vector of indicator functions dependent on N_T independent Poisson processes, i.e. $\boldsymbol{\chi}(t) = \{\chi_1(t), \ldots, \chi_{N_T}(t)\}$. As such, $\boldsymbol{\mathcal{I}}_{\boldsymbol{\chi}}$ has elements $\mathbf{1}_i(\chi_i(t))$

$$\mathbf{1}_i(\chi_i) = \begin{cases} 1, & t \in \chi_i \\ 0, & t \notin \chi_i \end{cases} \quad \text{where } \chi_i(t) = \{0, t_1^*, \ldots\}_i, \text{ for } i = 1, \ldots, N_T. \tag{2.32}$$

These elements represent stochastic resetting, reminiscent of the SDE in Equation (2.12). Stochastic resetting represents switching the therapies that are being administered to a patient, which is a common strategy used by physicians to avoid the development of drug resistance [16, 25, 114]. Changing the therapy exposes the pathogen to a new stimulus, which resets the resistance back to its initial value and in terms of the corresponding stochastic process, the process resets to its initial position.

The model includes N_T simultaneous therapies being administered to the patient, each having a therapy efficacy $\eta_i, i = 1 \ldots N_T$. This models combination therapies which is one of the therapy strategies that will be studied. Note the form of the infection rate $\prod_i (1-\eta_i)$ changes non-linearly as each of the η_i changes over time. The effective therapy efficacy of all N_T simultaneous therapies is considered to be multiplicative of each other, assuming an additive model of drug interaction, as discussed in Section 1.4.

It has been observed that solving for the equilibrium points of eq. (2.30) in terms of the therapy efficacies η_i reveal regions greater than $\eta_i > 0, \forall i$ where the population of healthy cells are below a critical threshold, signifying that the host has reached a critical status due to the low therapy efficacy without reaching complete therapy failure at $\eta_i = 0$. Let $\boldsymbol{\eta}^*$ be the set of therapy efficacies that make the population of healthy cells go below the aforementioned threshold. Since $\boldsymbol{\eta}$ is a stochastic process that fluctuates over time, this set may now be used as a new absorbing boundary, with the FPT

$$T = \inf\{t \geq 0 \,|\, \boldsymbol{\eta} \in \boldsymbol{\eta}^*\}. \tag{2.33}$$

Therefore, the final model of drug resistance development within a host experiencing a chronic infection is given by eq. (2.30) with an infection rate that is coupled to a stochastic process, following the SDE (2.31). The model then follows two time scales: the first is the slower scale of host-pathogen dynamics assumed to be at equilibrium, and the second is the faster scale of fluctuating pathogenic evolution. As such, the SDE then drives the dynamics of the host-pathogen model.

Chapter 3

Analytic and Monte Carlo Approximations to the Distribution of the First Passage Time of the Drifted Diffusion with Stochastic Resetting and Mixed Boundary Conditions

The contents of this chapter are available on arXiv as:
Magalang, J., Turin, R., Aguilar, J., Colombani, L., Sanchez-Taltavull, D., & Gatto, R. (2024). *Analytic and Monte Carlo Approximations to the Distribution of the First Passage Time of the Drifted Diffusion with Stochastic Resetting and Mixed Boundary Conditions*. arXiv. https://doi.org/10.48550/ARXIV.2311.03939

Analytic and Monte Carlo Approximations to the Distribution of the First Passage Time of the Drifted Diffusion with Stochastic Resetting and Mixed Boundary Conditions

Juan Magalang[a,b,*], Riccardo Turin[a,c,*], Javier Aguilar[d,**], Laetitia Colombani[a], Daniel Sanchez-Taltavull[b,***], Riccardo Gatto[a,***]

[a] *Institute of Mathematical Statistics and Actuarial Science, University of Bern, Alpeneggstrasse 22, Bern, 3012, Switzerland*
[b] *Department of Visceral Surgery and Medicine, Inselspital, Bern University Hospital, University of Bern, Murtenstrasse 35, Bern, 3008, Switzerland*
[c] *Group Risk Management, Swiss Re Management Ltd, Mythenquai 50/60, Zurich, 8022, Switzerland*
[d] *Laboratory of Interdisciplinary Physics, Department of Physics and Astronomy "G. Galilei", University of Padova, Padova, Italy*

Abstract

This article introduces two techniques for computing the distribution of the absorption or first passage time of the drifted Wiener diffusion subject to Poisson resetting times, to an upper hard wall barrier and to a lower absorbing barrier. The first method, which we call "Padé-partial fraction" approximation, starts with the Padé approximation to the Laplace transform of the first passage time, which is then exactly inverted by means of the partial fraction decomposition. The second method, which we call "multiresolution algorithm", is a Monte Carlo technique that exploits the properties of the Wiener process in order to generate Brownian bridges at increasing levels of resolution. Our numerical study reveals that the multiresolution algorithm has higher efficiency than standard Monte Carlo, whereas the faster Padé-partial fraction method is accurate in various circumstances and provides an analytical formula. Also, a closed-form exact expression for the expected first passage time is derived.

Keywords: absorbing barrier, Brownian bridge, Euler-Maruyama scheme, Fokker-Planck equation, hard wall reflection, Laplace transform, Padé approximation, partial fractions decomposition, Poisson resetting times, Wiener process.
PACS: 02.50.-r, 05.10.Gg, 05.10.Ln, 05.40.-a, 02.30.Mv, 02.60.-x, 02.50.Ng
2000 MSC: 41A58, 60G18, 60G40, 60J65, 65C05, 35G15

*Equal contribution
**Corresponding author: javier.aguilarsanchez@unipd.it
***Scientific group leaders

Contents

1. Introduction

Drift-diffusion processes represent a cornerstone in the mathematical modeling of systems whose evolution includes stochastic components. The central one is Brownian motion and it finds frequent applications in most scientific fields, such as physics [1, 2, 3, 4], biology [5, 6, 7, 8], insurance mathematics [9, 10, 11] and it builds the basis of mathematical finance. Through this work, we will focus on a drifted and bounded Brownian motion for which the particle returns to its original position at random times following the Poisson process. Such stochastic resetting has gained importance in the past decade [12, 13, 14, 15, 16, 17, 18, 19, 20, 21]. Particularly, in the context of biology, stochastic resetting has been used to model hunting behavior in animals, where animals return to specific sites to look for food [22]. At the cellular level, this scheme can model cellular focal adhesions [23]. At the biomolecular level, it has been applied to model backtrack recovery in RNA polymerization [24]. In our previous work, we have shown that stochastic resetting can be used to model the role of changes in therapies to palliate drug resistance development [25]. As new models and experimental realizations of processes with stochastic resetting continue to emerge [26, 27], there is a growing need for more refined approximation and simulations techniques to comprehensively characterize real-world resetting protocols [15], which we tackle to some extent in this study.

By means of the Laplace transform and of the underlying stochastic differential equation (SDE) [28, 29], we are able to derive an analytic and a Monte Carlo technique for computing the distribution of the first passage time (FPT) to the null level of the process [30, 31, 32, 33, 34, 35, 36, 37]. With other methods existing in the literature the mean FPT can be obtained analytically. However, this first moment does not provide sufficient information the entire FPT distribution: quantities such as standard deviation, median, and upper quantiles are often relevant in applications to biology and medicine, for example.

In this context, this article introduces two computational methods for obtaining the probability distribution of the FPT of the drifted Brownian motion subject to Poisson resetting times and to upper hard wall barrier. The first of these two techniques makes use of the Laplace transform of the FPT [25]. It is difficult to find a general and accurate method for inverting Laplace transforms. Moreover, most methods are purely numerical. Accurate analytical approximation formulae are however useful in various situations, for example for computing sensitivities of the approximated probabilities. Our method uses the Padé approximation and partial fractions decomposition to approximate the Laplace transform inversion. We call it Padé-partial fraction (PPF) approximation. Besides high computational speed, it provides a simple closed-form expression for the distribution of the FPT. The second method is a Monte Carlo algorithm that exploits a bridge property of the Wiener process, which allows to obtain trajectories at increasing level of detail [38, 39]. We call it multiresolution algorithm (MRA), following the terminology of wavelet analysis. The MRA allows for very high accuracy. We introduce two versions of the MRA: the standard MRA (SMRA), which directly exploits the bridge property of the Wiener process to our model, and the hybrid MRA (HMRA), which starts with the classical Euler-Maruyama algorithm to generate the initial approximation of the FPT and which improve it further by using the MRA.

This article has the following structure. We first derive the Laplace transform of the FPT

(Section 2). Then we introduce the PPF approximation (Section 3). This section presents also a simple expression of the mean FPT. Next, we present the SMRA and HMRA (Section 4). These methodological sections are followed by an intensive numerical study, aiming to show the accuracy of our techniques (Section 5). A short summary of the methodological and numerical results followed by a discussion on future research concludes the article (Section 6).

Notation

- $f^{(k)}(x) = (d/dx)^k f(x)$, for $k = 0, 1, \ldots$, where $f : \mathbb{R} \to \mathbb{R}$.
- $\partial_t f(t,x) = (\partial/\partial t) f(t,x)$, $f'(t,x) = (\partial/\partial x) f(t,x)$ and $f''(t,x) = (\partial/\partial x)^2 f(t,x)$, where $f : [0,\infty) \times \mathbb{R} \to \mathbb{R}$.
- $\tilde{f}(s) = \int_0^\infty e^{-st} f(t)\, dt$ is the Laplace transform of $f : [0,\infty) \to \mathbb{R}$.
- $\delta(x)$ is the Dirac delta function, which assigns mass 1 at $x = 0$ and is null $\forall x \neq 0$.
- $X \sim Y$ means that the random variables X and Y have same distribution.
- $f(x) = o\,(g(x))$, as $x \to a$, means that $\lim_{x\to a} \frac{f(x)}{g(x)} = 0$, where $f, g : \mathbb{R} \to \mathbb{R}$.[2]

2. Laplace transform of propagator and mean FPT

The distribution of FPTs is often the essential element in the study of absorption phenomena. This distribution crucially depends on the drift-diffusion processes, the number of dimensions of the diffusion space, and the boundary conditions [30, 40, 41, 42]. Of particular interest are problems with absorbing or reflecting boundaries. Absorbing boundaries are regions in the diffusion space where diffusing particles can enter but cannot leave [43]. Reflecting boundaries are regions in which diffusing particles cannot permeate [44]. In the following, we will focus on problems with mixed boundary conditions, meaning that the process is bounded between one absorbing and one reflecting boundary.

Obtaining the closed-form expression for the distribution of the FPT is in general difficult, because it involves solving a Fokker-Planck equation with absorbing boundaries [30, 41, 42]. Nonetheless, we are still able to characterize the FPT through the Laplace transform. In this section, we derive the Laplace transform of the FPT distribution and obtain a novel formula for its expectation. Starting with the process without resetting, we obtain the Laplace transform of the propagator by solving the Laplace transform of the Fokker-Planck equation with boundary conditions [43] (Section 2.1). From the propagator, we obtain the Laplace transform of the FPT distribution [30, 25] that will relate to the process with resetting through the survival function [16, 17] (Section 2.2). Finally, by using the aforementioned expressions, we show that the expected FPT with resetting can be expressed in terms of the Laplace transform of the FPT distribution without resetting.

[2] It is mplicitely assumed that g is nonnull over some neighborhood of a, if $|a| < \infty$, or for all extreme large (small) values, if $a = \infty$ $(-\infty)$.

2.1. Laplace transform of the propagator

The underlying stochastic process is the basic Brownian motion or Wiener process with drift, here denoted $Y = \{Y_t\}_{t\geq 0}$, which solves the SDE

$$dY_t = v\,dt + \sqrt{2D}\,dW_t,\ \forall t \geq 0\,, \tag{2.1}$$

with fixed initial condition $Y_0 = x_0 \in (0, 1]$, where the drift v and the volatility D are respectively real and nonnegative real constants. We then impose that the paths of this process are bounded between 0 and 1 and use the same name Y for the bounded process. The level 1 is a *reflecting boundary of type hard wall* [30]. On the one hand, the definition of this reflecting boundary at the level of the Fokker-Planck equation requires the concept of probability current and will be given in Eq. (2.4). On the other, the action of the reflecting boundary at the level of sample path will be provided along with its discretization scheme in Section 4.3. We refer to [45] for a detailed discussion of SDEs with reflecting boundaries.

We note that this process is neither the formal reflection of a trajectory, as would be the absolute value of a diffusion, nor the regulated Brownian motion. These two cases are described in the introduction of [46]. Regarding the null level, it is an *absorbing state* and our goal is precisely to evaluate the probability of reaching this state.

Our prior work [25] showcases the practical relevance of the model in describing biological phenomena. Specifically, we utilized a drift-diffusion process with mixed boundary conditions in order to model drug resistance development resulting from mutation – a stochastic process biased towards the survival of the infecting pathogen [47, 48]. Our approach employed a bounded drift-diffusion process to quantify changes in therapy efficacy against the mutating infecting pathogen. The reflecting boundary represented perfect therapy, while the absorbing boundary denoted drug failure, since infecting pathogens develop complete resistance to therapies due to mutation [49].

Denote by $p(\cdot, t)$ the probability density of Y_t, $\forall t > 0$, and $p(\cdot, 0) = \delta(\cdot - x_0)$, called *propagator*. Let $x \in \mathbb{R}$ and $t \geq 0$. The *forward Kolmogorov* or *Fokker-Planck equation* determines the probability distribution of the process Y and it is given by the PDE

$$\partial_t p(x, t) + vp'(x, t) - Dp''(x, t) = 0. \tag{2.2}$$

We refer e.g. to [43] for the construction of Eq. (2.2).

The propagator is indeed a defective probability density, viz. with total mass below 1, because it does not account for the probability mass at the absorption state. This reflects the physical interpretation of Y as the location of a particle moving between two boundaries that as soon as touches the absorbing boundary gets immediately removed from the system.

Let us further introduce the *probability current*

$$J(x, t) = vp(x, t) - Dp'(x, t)\,. \tag{2.3}$$

The two boundary conditions that are absorption at 0 hard wall at 1 can be weakly defined in terms of the propagator and the probability current in the following way,

$$p(0, t) = 0 \quad \text{and} \quad J(1, t) = 0, \tag{2.4}$$

respectively; see e.g. Chapter 4 of [28] or [30].

Thus we study the solution of the following system of equations,

$$\begin{cases} \partial_t p(x,t) + v p'(x,t) - D p''(x,t) = 0, \\ p(0,t) = 0, \\ J(1,t) = 0, \\ p(x,0) = \delta(x - x_0), \end{cases} \tag{2.5}$$

in which the last equation provides the initial condition. No closed-form solution to Eqs. (2.5) is available. Lemma 2.1 provides a closed-form expression for the Laplace transform of the propagator, viz. for $\tilde{p}(x,s) = \int_0^\infty e^{-st} p(x,t)\, dt$, $\forall s \geq 0$.

Lemma 2.1 (Laplace transform of propagator)**.** *Let $x_0 \in (0,1]$, $v \in \mathbb{R}$, $D > 0$ and consider p solution to Eqs. (2.5). Let $s > -v^2/(4D)$ and define*

$$\rho = \frac{v}{2D}, \quad \omega(s) = \sqrt{v^2 + 4Ds}, \quad \theta(s) = \frac{\omega(s)}{2D} = \frac{\sqrt{v^2 + 4Ds}}{2D} \tag{2.6}$$

and

$$\alpha_\pm(s) = \frac{v \pm \sqrt{v^2 + 4Ds}}{2D} = \frac{v \pm \omega(s)}{2D} = \rho \pm \theta(s). \tag{2.7}$$

Then the Laplace transform of the propagator is given by

$$\tilde{p}(x,s) = \tilde{p}(x_0,s) \times \begin{cases} \frac{e^{\alpha_+(s)x} - e^{\alpha_-(s)x}}{e^{\alpha_+(s)x_0} - e^{\alpha_-(s)x_0}}, & \forall x \in [0, x_0), \\ \frac{\alpha_+(s)\, e^{\alpha_+(s)(x-1)} - \alpha_-(s)\, e^{\alpha_-(s)(x-1)}}{\alpha_+(s)\, e^{\alpha_+(s)(x_0-1)} - \alpha_-(s)\, e^{\alpha_-(s)(x_0-1)}}, & \forall x \in (x_0, 1], \end{cases} \tag{2.8}$$

with $\tilde{p}(x_0,s)$ given by

$$\tilde{p}(x_0,s) = \frac{2\sinh(\theta x_0)\left\{\omega \cosh[\theta(x_0-1)] + v \sinh[\theta(x_0-1)]\right\}}{\omega^2 \cosh(\theta) - v\,\omega \sinh(\theta)}. \tag{2.9}$$

The ratio ρ is currently called *Péclet number*.

2.2. Stochastic resetting and stopping condition

We now modify the dynamics of the stochastic process Y by putting stochastic resetting. More explicitly, we assume that at random times $T_0 = 0 < T_1 < T_2 < \ldots$, a.s., the value of the process Y is reset to its initial value x_0. Following [15], this is expressed through the addition of a new term to the SDE, giving

$$dX_t = (1 - \chi_t) \cdot (v\, dt + \sqrt{2D}\, dW_t) + \chi_t \cdot (x_0 - X_t), \quad \forall t \geq 0, \tag{2.10}$$

where

$$\chi_t = \sum_{n=1}^{\infty} \mathbf{1}\{T_n = t\}, \quad \forall t \geq 0,$$

where **1** denotes the indicator. We assume that the stochastic process $\chi = \{\chi_t\}_{t\geq 0}$ is an independent homogeneous Poisson process with rate or intensity $r > 0$. Thus T_n the sum of n independent exponential random variables with expectation r^{-1}, for $n = 1, 2 \ldots$.

We can now define the FPT (also called absorption time) by

$$\tau_r = \inf\{t \geq 0 \,|\, X_t \leq 0\}. \tag{2.11}$$

It admits a proper probability density function denoted f_r, where the subscript $r \geq 0$ highlights the dependence on the Poisson rate r. When $r = 0$, we retrieve the dynamic without resetting.

3. Laplace transform of FPT distribution and PPF

Although the mean FPT $\mathbb{E}[\tau_r]$ properly characterizes typical absorption times, this quantity alone does not quantify the uncertainty inherent to the first passage phenomenon. Often, high-order quantiles are more relevant. Thus, besides the expectation we want to obtain the entire probability distribution of τ_r. Its Laplace transform is available, but there is no obvious and general way of inverting it. The well-known fast Fourier transform (FFT) is a purely numerical method and it does not necessarily provide accurate results, in particular for approximating upper tail quantiles, that are useful in many applications. We refer for example to [11] for a numerical comparison of methods for computing a FPT probability for the compound Poisson process perturbed by diffusion.

In this section, we propose and implement a particular method for our FPT problem. We obtain the Laplace transform of the FPT (Section 3.1), PPF approximation whose inversion will be approximated numerically. The approximated inversion begins with the Padé approximation of the Laplace transform, followed by a partial fraction decomposition of the Padé approximation and then by the simple inversion of the sum of partial fractions (Section 3.2). This is the PPF approximation. One can find some references, in particular in the engineering literature, on the problem of obtaining approximate Laplace inversions by rational approximations: some early references are [38], [50], [51], [52] and [53].

3.1. Laplace transform of FPT distribution with resetting

In this section we first provide the Laplace transform of the FPT distribution, τ_r, and then we give a simplified formula for its expectation.

Proposition 3.1 (Laplace transform of FPT distribution with resetting)**.** *Assume that X solves the SDE with resetting of Eq. (2.10), with $X_0 = x_0 \in (0, 1]$, $v \in \mathbb{R}$, $D > 0$ and $r > 0$. Denote by f_r the probability density of the absorption time τ_r, defined in Eq. (2.11). Then its Laplace transform is given by, $\forall s > -r$,*

$$\begin{aligned}\tilde{f}_r(s) &= \frac{(s+r)\tilde{f}_0(s+r)}{s + r\tilde{f}_0(s+r)} \\ &= \frac{(s+r)\{\omega(s+r)\cosh[\theta(s+r)(x_0-1)]+v\sinh[\theta(s+r)(x_0-1)]\}}{se^{\rho x_0}\{\omega(s+r)\cosh[\theta(s+r)]-v\sinh[\theta(s+r)]\}+r\{\omega(s+r)\cosh[\theta(s+r)(x_0-1)]+v\sinh[\theta(s+r)(x_0-1)]\}},\end{aligned} \tag{3.1}$$

where $\tilde{f}_0$ *is given by,* $\forall s > -v^2/(4D)$,

$$\tilde{f}_0(s) = e^{-\rho x_0} \frac{\omega(s)\cosh\{\theta(s)(x_0-1)\} + v\sinh\{\theta(s)(x_0-1)\}}{\omega(s)\cosh\{\theta(s)\} - v\sinh\{\theta(s)\}} \,. \tag{3.2}$$

Proof. We obtain from Eq. (A.4) the Laplace transform of f_r as $\tilde{f}_r(s) = 1 - s\tilde{S}_r(s)$, for all $s \in \mathbb{R}$. We combine it with Eq. (A.7) and it yields the first expression,

$$\forall s > -r,\ \tilde{f}_r(s) = \frac{(s+r)\tilde{f}_0(s+r)}{s + r\tilde{f}_0(s+r)} \,.$$

This last expression holds $\forall s < -r$ under the assumption $\tilde{f}_0(s+r) \neq -s/r$.

We deduce the closed-form expression in Eq. (3.1) by combining the first expression with $\tilde{f}_0$ in Eq. (3.2). Note that, for the function ω to be defined, we need $s + r \in (-v^2/(4D), \infty)$, viz. $s \in (-r - v^2/(4D), -r)$. □

We can make two short remarks on Proposition 3.1. First, because the Laplace transform exists over a neighborhood of the origin, all moments of τ_r exist and determine its distribution unambiguously. In contrast with this, the FPT of the driving drifted Brownian motion without hard wall reflecting boundary and resetting has infinite moments: it is known that although the FPT of the Brownian motion is finite with probability one, its expectation is infinite [30].

We also note the distribution of the model without resetting is obtained continuously, because $\lim_{r\to 0} \tilde{f}_r(s) = \tilde{f}_0(s)$, $\forall s > 0$.

We end this section with the following novel closed-form expression for the *mean absorption time* with resetting.

Proposition 3.2 (Mean FPT)**.** *Assume that the process* X *solves the SDE with resetting of Eq.* (2.10)*, with* $X_0 = x_0 \in (0, 1]$*,* $v \in \mathbb{R}$*,* $D > 0$ *and* $r > 0$*. The expectation of* τ_r *in Eq.* (2.11) *is given by*

$$\mathbb{E}[\tau_r] = \frac{1}{r}\left(\frac{e^{\rho x_0}\left(\omega(r)\cosh\{\theta(r)\} - v\sinh\{\theta(r)\}\right)}{\omega(r)\cosh\{\theta(r)(x_0-1)\} + v\sinh\{\theta(r)(x_0-1)\}} - 1\right), \tag{3.3}$$

where ρ*,* ω *and* θ *are given in Eq.* (2.6)*.*

The proof of Proposition 3.2 is in Appendix A.

3.2. PPF approximation to FPT distribution with resetting

Because we cannot invert the Laplace transform $\tilde{f}_r$ in Eq. (3.1) analytically, we now propose to approximate $\tilde{f}_r$ by a specific rational function, which is the ratio of two polynomials with degree in denominator higher than in numerator. The type of rational approximation considered here is the one suggested by Henri Padé thesis in 1892 and called Padé approximation. It has shown practical relevance in many problems of theoretical physics where power series expansions occur, as already stressed by [54]. Introductions can be found in various

books, such as in Section 4.6 of [55], in which it is mentioned that for given computational time, the Padé approximation is typically more accurate than the Taylor approximation. It has a local error of order smaller than the sum of the two degrees of the two polynomials of the ratio. We note that available tables do not provide the analytical form of the Laplace inverse of a Taylor approximation and, under some assumptions, they provide the Laplace inverse of many rational functions.

Let m, n be nonnegative integers, let I be an interval of $\mathbb{R}$ with $0 \in I$ and let $g : I \to \mathbb{R}$ be a $n + m$ times differentiable function. Then the Padé approximation of orders m and n to g is the rational function

$$g_{m,n}(s) = \frac{p_m(s)}{q_n(s)}, \tag{3.4}$$

where

$$p_m(s) = \sum_{j=0}^{m} a_j s^j \text{ ,and } q_n(s) = \sum_{j=0}^{n} b_j s^j, \quad \forall s \in I,$$

and which satisfies $g^{(k)}(0) = g^{(k)}_{m,n}(0)$, for $k = 0, \ldots, n + m$.[3] It can be shown that these conditions imply that the coefficients $a_0, \ldots, a_m$ and $b_0, \ldots, b_{n-1}$ are obtained by solving the $m + n + 1$ linear equations

$$\begin{cases} \displaystyle\sum_{j=0\vee(i-n)}^{i} \frac{g^{(j)}(0)}{j!} b_{i-j} = a_i, \text{ for } i = 0, \ldots, m, \\ \displaystyle\sum_{j=0\vee(i-n)}^{i} \frac{g^{(j)}(0)}{j!} b_{i-j} = 0, \text{ for } i = m+1, \ldots, m+n. \end{cases} \tag{3.5}$$

It can also be shown that

$$g(s) - g_{m,n}(s) = o(s^{m+n}), \quad \text{as} \quad s \to 0\,.$$

The PPF considers the restriction $m < n$. It allows for exact inversion of the Laplace transform in Eq. (3.1) approximated by Padé and re-expressed in terms of partial fractions. This leads to a simple and practical approximate closed-form expression for the density of the FPT τ_r. Precisely, let $g_{m,n}(s) = p_m(s)/q_n(s)$ be the Padé approximation of orders $m < n$ to the Laplace transform $\tilde{f}_r$. If *all roots of* q_n *are real and negative*, then there exists a Laplace inversion of $g_{m,n}$, which we denote $f_{m,n}$. Thus, $f_{m,n}$ provides an approximation to the density of τ_r, namely to f_r on $[0, \infty)$. Thus the density $f_{m,n}$ can be obtained by the following steps, under the above condition on roots of q_n.

Algorithm 3.3 (PPF approximation to FPT density).
Step 1. Padé approximation

- Select the orders $m < n$ of the Padé approximation to $\tilde{f}_r$, which we denote $g_{m,n}$.

[3] Note that these same equations hold for the Taylor approximation of order $m + n$.

- Compute $\tilde{f}_r^{(k)}(0)$, for $k = 0, \ldots, n+m$.
- Find the coefficients $a_0, \ldots, a_m$ and $b_0, \ldots, b_{n-1}$ by solving the $m+n+1$ linear equations in Eqs. (3.5).

Step 2. Partial fraction decomposition

- Decompose the Padé approximation in the partial fractions as follows,

$$g_{m,n}(u) = \frac{p_m(u)}{q_n(u)} = \sum_{j=1}^{k} \sum_{i=1}^{l_j} \frac{\gamma_{j,i}}{(u-\alpha_j)^i}, \tag{3.6}$$

  where $\alpha_1, \ldots, \alpha_k$ are the distinct roots of the denominator q_n, whose multiplicities respectively are $l_1, \ldots, l_k$ (with $l_1 + \ldots + l_k = n$).

- Compute the real coefficients $\gamma_{j,i}$, for $j = 1, \ldots, k$ and $i = 1, \ldots, l_j$. Typically, q_n has n distinct roots $\alpha_1, \ldots, \alpha_n$. In this case,

$$\frac{p_m(u)}{q_n(u)} = \sum_{j=1}^{n} \frac{\gamma_j}{u-\alpha_j},$$

  gives us

$$\gamma_j = \frac{p_m(\alpha_j)}{\prod_{k=1,k\neq j}^{n}(\alpha_j - \alpha_k)}, \qquad \text{for } j = 1, \ldots, n\,.$$

  Should not all roots of q_n be distinct, the coefficients $\gamma_{j,i}$, for $j = 1, \ldots, k$ and $i = 1, \ldots, l_j$, could be obtained by the residue method.

Step 3. Inversion
This step is possible only under the restriction $\alpha_1, \ldots, \alpha_k < 0$.

- Invert the Padé approximation $g_{m,n}$ to $\tilde{f}_r$ by exploiting its re-expression in Eq. (3.6) so to obtain the linear combination of gamma or exponential densities

$$f_{m,n}(t) = \sum_{j=1}^{k} \sum_{i=1}^{l_j} \frac{\gamma_{j,i}}{i!} t^{i-1} e^{\alpha_j t}, \quad \forall t > 0. \tag{3.7}$$

Step 4. Corrections
The following corrections to Eq. (3.7) generally improve its accuracy. In order to keep notation simple, the same name $f_{m,n}$ is used for the original approximation of Eq. (3.7) and for the corrected version.

- *Truncation of negative parts*
  Negative values are equated to null, viz.

$$f_{m,n}(t) = \max\{f_{m,n}(t), 0\}, \ \forall t > 0.$$

- *Smoothing near to origin*
  Oscillations near to the origin are removed. Find $s > 0$ the abscissa point of the last local minimum of $f_{m,n}$. If it does not exist, then no correction is required. Consider

$$f_{m,n}(t) = \begin{cases} 0, & \text{if } t \leq s, \\ f_{m,n}(t), & \text{if } t > s. \end{cases} \tag{3.8}$$

- *Normalization*
  Give integral value one, viz. consider

$$f_{m,n}(t) = \left(\int_0^\infty f_{m,n}(s) ds \right)^{-1} f_{m,n}(t), \ \forall t > 0.$$

- *Recentering to expectation*
  Give expected value $\mu = \mathbb{E}[\tau_r]$. Compute μ, through its closed-form expression in Eq. (3.2), and compute $\mu_{m,n}$, the mean of the approximate density $f_{m,n}$. Obtain the recentered approximated FPT density by

$$f_{m,n}(t) = f_{m,n}(t + \mu_{m,n} - \mu), \ \forall t > \max\{0, \mu - \mu_{m,n}\}.$$

Let us now provide some further and more precise justifications to the PPF Algorithm 3.3. The PPF approximation $f_{m,n}$ to the FPT density f_r is implicitly defined through its Laplace inversion formula $g_{m,n}(u) = \int_0^\infty e^{-ut} f_{m,n}(t) \, dt$, $\forall u \geq 0$. If $\alpha_1, \ldots, \alpha_k < 0$, we have

$$\int_0^\infty \frac{t^{i-1}}{i!} e^{(\alpha_j - u)t} \, dt = \frac{1}{(u - \alpha_j)^i}, \ \forall u > \max\{\alpha_1, \ldots, \alpha_k\},$$

for $i = 1, \ldots, l_j$ and $j = 1, \ldots, k$, This and the partial fractions decomposition of $g_{m,n}$ in Eq. (3.6) give Eq. (3.7), in Step 3.

Next, the two corrections regarding truncation to nonnegative values and smoothing near the origin concern only small neighborhoods of the origin. The corrections are due to the fact that the PPF approximation can display undesirable oscillations over these neighborhoods. However, we know that the true FPT density must vanish at the origin. Indeed, the process starts above zero. In addition to this, repeated Monte Carlo experiments have confirmed that the FPT density is smooth close to the origin and overall unimodal. Based on this theoretical or empirical evidence, the above smoothing correction assumes that the domain of the density is cut in two parts: the region where it increases from null to the maximum of the density, followed by the region where it decreases to null. Accordingly, we correct near to the origin by finding the set of points $t > 0$ such that $f'_{m,n}(t) = 0$. We assume that the largest value in this set is mode of the approximate density and so all other values of the set must be local extrema. If this set has one element only, then no correction is needed. Otherwise, we denote $t^\ddagger$ to be the second largest value in this set (which is either the last local minimum before the mode of or the last point of inflection): we remove the non-monotonic part around the origin through Eq. (3.8).

We conclude with the next remarks.

Remarks 3.4. 1. As mentioned, $f_{m,n}$ is not necessarily a probability density: as $\gamma_1, \ldots, \gamma_n$ can be negative, $f_{m,n}$ can be negative over some regions. However,

$$\int_0^\infty f_{m,n}(t)dt = \sum_{j=1}^{k} \sum_{i=1}^{l_j} \frac{\gamma_{j,i}}{(-\alpha_j)^i} = g_{m,n}(0) \longrightarrow \tilde{f}_r(0) = 1, \text{ as } m, n \to \infty,$$

so the sequence of PPF approximations has the correct normalization in the limit of large m, n.

2. If the PPF approximation $f_{m,n}$ is a proper probability density, then its expectation is given by

$$\mu_{r,m,n} = \sum_{j=1}^{k} \sum_{i=1}^{l_j} \frac{(i+1)\gamma_{j,i}}{(-\alpha_j)^{i+1}}.$$

3. If the function $f_{m,n}$ has a Laplace transform of the form of the Padé approximation Eq. (3.4), i.e. if $f_{m,n} = p_m/q_n$ for some polynomials p_m and q_n, then $f_{m,n}$ is characterized as the solution of the homogeneous linear ordinary differential equation (ODE)

$$f_{m,n}^{(k)}(t) + c_{k-1} f_{m,n}^{(k-1)}(t) + \ldots + c_1 f'_{m,n}(t) + c_0 = 0,$$

for some coefficients $c_0, \ldots, c_{k-1} \in \mathbb{R}$ with $c_0 \neq 0$ and for some positive integer k. Thus, the closeness of $g_{m,n}$, obtained in Step 3, to f_r, the true density, can be re-expressed in terms of closeness of the solution of the above ODE to the true density. This may give another way for analyzing the error of the PPF approximation.

- If we consider the process without hard wall and without resetting (Y), then the FPT follows a simple distribution, which is the inverse Gaussian. In this case, the PPF becomes meaningless. If we consider the process without either hard wall or resetting (Y), but not without the two together, then it remains interesting to compute the FPT distribution and the PPF can be adapted accordingly. This remarks extends to the Monte Carlo MRA of Section 4.

4. MRAs

We will see that, although the PPF approximation is efficient and provides analytical formulas, it is only valid for specific combinations of the models parameters. Monte Carlo methods are in general a good alternative to compute the distribution of any FPT, however, they are computationally intensive. In this section we propose a Monte Carlo method that we call the multiresolution algorithm (MRA), which leads to arbitrary accuracy and a combination of the MRA and the Euler-Maruyama algorithm, which reduces its computational time while keeping the accuracy.

4.1. MRA for the Wiener process

We describe a particular strategy for generating trajectories of Wiener processes, yielding the SMRA. We provide an algorithm that allows the generation of a single sample path of the Wiener process with arbitrary resolution. The algorithm is directly obtained from the following well-known property of the Wiener process,

$$\mathrm{P}\Big[W_{t+h} \in (x, x+dx)\Big| W_t = a, W_{t+2h} = b\Big] = \frac{1}{\sqrt{\pi h}} \exp\left\{-\frac{\left(x - \frac{a+b}{2}\right)^2}{h}\right\} dx, \ \forall t, h > 0, a, b \in \mathbb{R}. \tag{4.1}$$

Therefore, given the knowledge of the state of the process at two times ($W_t = a$ and $W_{t+2h} = b$), Eq. (4.1) allows to sample the process at intermediate time (W_{t+h}). This property can be iterated to access arbitrary small temporal scales, as sketched in Figure 1, and we will use it to obtain estimations of FPTs at arbitrary accuracy. Indeed, consider the stopping time equivalent to Eq. (2.11) but for this simpler diffusion,

$$T = \inf\{t \leq 0 \mid W_t \leq 0\},$$

where we slightly alter the standard definition of the Wiener process to have some initial condition $X_0 > 0$ that makes T non-trivial. Let us assume that a discretization $\{W_{nh}\}_{n=1,2,\ldots}$ of $\{W_t\}_{t\geq 0}$ is available, for some $h > 0$ small. Then,

$$T_h = \inf\{t \geq 0 \mid W_{nh} \leq 0\}$$

is an overestimation of T (i.e. $T_h \geq T$) that converges to T, as $h \to 0$. This tells us that applying the MRA at increasing resolutions allows us to approximate the stopping time at any desired precision.

Given a certain time-interval, for example $t \in [0, 1]$, we will note the k-th resolution level of the sample path in that interval as $\mathbf{W}_k = \{W_{k,j}\}$, for $k = 0, 1, \ldots$, and $j = 0, 1, \ldots, 2^k$. Both indices allows to evaluate the process at a particular time in $[0, 1]$, $W_{k,j} = W_{t=2^{-k}j}$. While the first index informs about the level of refinement of the path, the secondary index, j, refers to the ordinal of each element given a certain k. Therefore, at initial level $k = 0$, we have

$$\mathbf{W}_0 = \{W_{0,0}, W_{0,1}\}, \quad \text{where } W_{0,0} = 0 \text{ and } W_{0,1} \sim \mathcal{N}(0, 1). \tag{4.2}$$

Here $\mathcal{N}(\mu, \sigma^2)$ stands for a Gaussian random variable with mean μ and variance σ^2. Then, consecutive levels of refinement, $k \geq 1$, are obtained by

$$W_{k,2j} = W_{k-1,j}, \quad \text{for } j = 0, 1, \ldots, 2^{k-1} \tag{4.3a}$$

$$W_{k,2j+1} \sim \mathcal{N}\left(\frac{W_{k-1,j} + W_{k-1,j+1}}{2}, \frac{1}{2^k}\right), \quad \text{for } j = 0, 1, \ldots, 2^{k-1} - 1. \tag{4.3b}$$

For $k > 0$, the even indices of j are copied over as the resolution increases as in Eq. (4.3a). The odd indices of j are generated randomly using two consecutive variables from the previous resolution, as in Eq. (4.3b). Proceeding in this way, the overestimation of the FPT of $\mathbf{W}_k$ decreases as k increases.

Further details about the MRA can be found at p. 277-279 of [39]. In the Appendix B.1 we show a pseudocode with the implementation of the MRA for the process $\{W_t\}_{t\geq 0}$.

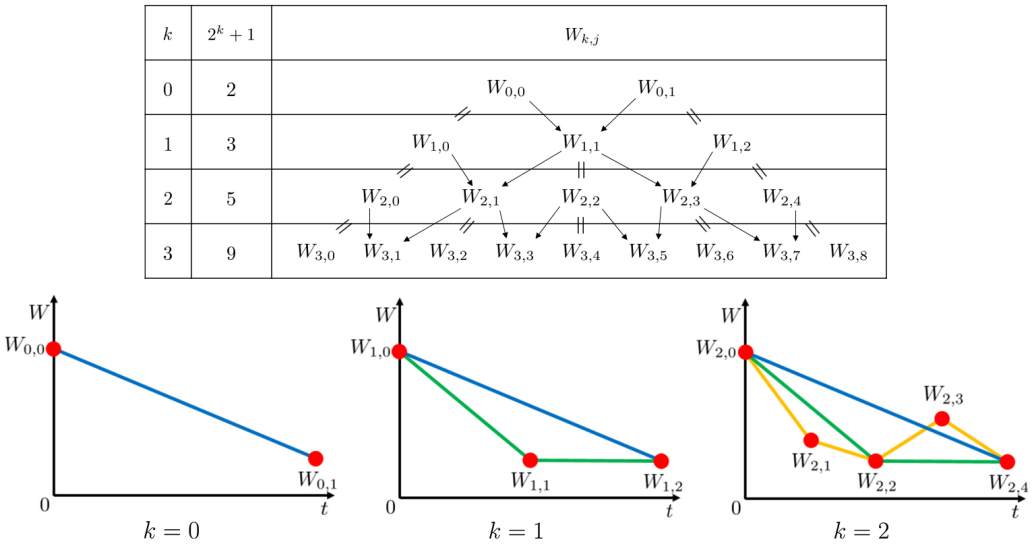

Figure 1: *Upper table: Resolution level k and corresponding number of generated variables 2^k+1 (first two columns); generated variables $W_{k,j}$ (last column). Equal signs indicate copying a variable from a previous resolution; see Eq. (4.3a). Arrows indicate generating of a new variable from a previous resolution; see Eq. (4.3b). Lower graphs: Illustrations of the trajectory generated subsequently by the MRA.*

4.2. MRA with resetting

This section describes the application of the MRA to a process with resetting, similar to the one of Section 2.1, but without considering the reflecting boundary for now. Let us call $\{B_t\}_{t\geq 0}$ the drifted Brownian motion without hard wall and without resetting,

$$dB_t = v\,dt + \sqrt{2D}\,dW_t,\ \forall t \geq 0, \tag{4.4}$$

where $B_0 = x_0 > 0$. Let us call $\mathbf{t}^\dagger$ the sequence of times at which the process experiences a reset

$$\mathbf{t}^\dagger = \{t_0^\dagger, t_1^\dagger, t_2^\dagger, \ldots\}, \quad \text{where } t_0^\dagger = 0,\ (t_{i+1}^\dagger - t_i^\dagger) \sim \text{Exponential}(1/r).$$

Let us define reset intervals from pairs of consecutive reset times: $\{(0, t_1^\dagger), (t_1^\dagger, t_2^\dagger),\ \ldots\}$. The main idea to exploit is that B_t is a normally distributed random variable with mean $\mu = x_0 + vt$ and variance $\sigma^2 = 2Dt$ within any reset interval. Therefore, we can build Brownian bridges connecting the extremes of reset intervals with arbitrary precision. We first consider the process in the first reset interval, $t \in [0, t_1^\dagger]$, and, similar to what we did with the Wiener process in Section 4.1, we define the k-th resolution level of the sample path in that interval as $\mathbf{B}_k^{(1)}$. In the first resolution level, the process starts at the initial position, $B_{0,0} = x_0$, with initial time 0, and ends at the final position, $B_{0,1}$, with final time $t_1^\dagger$. Therefore,

$$\mathbf{B}_0^{(1)} = \{B_{0,0}^{(1)}, B_{0,1}^{(1)}\}, \quad \text{where } B_{0,1}^{(1)} \sim \mathcal{N}(x_0 + vt_1^\dagger, 2Dt_1^\dagger). \tag{4.5}$$

Then, similar to Eq. (4.3), the generation of the process at the next resolution k is obtained by

$$B^{(1)}_{k,2j} = B^{(1)}_{k-1,j}, \quad \text{for } j = 0, 1, \ldots, 2^{k-1}, \quad \text{and} \tag{4.6a}$$

$$B^{(1)}_{k,2j+1} \sim \mathcal{N}\left(\frac{B^{(1)}_{k-1,j} + B^{(1)}_{k-1,j+1}}{2}, \frac{2Dt^\dagger_1}{2^k}\right), \quad \text{for } j = 0, 1, \ldots, 2^{k-1} - 1. \tag{4.6b}$$

The precise meaning of Eq. (4.6b) is that the *conditional* distribution of $B^{(1)}_{k,2j+1}$ *given* $B^{(1)}_{k-1,j}$ and $B^{(1)}_{k-1,j+1}$ is Gaussian. The same steps can be used to generate the Brownian trajectory in the second reset interval, $\mathbf{B}^{(2)}_k$, simply replacing $t^\dagger_1$ by $t^\dagger_2 - t^\dagger_1$ in Eqs. (4.5) and (4.6b). In general, the Brownian trajectory in the i^{th} reset interval, i.e. $(t^\dagger_i, t^\dagger_{i-1})$, and at refinement level k is obtained through

$$\mathbf{B}^{(i)}_0 = \{B^{(i)}_{0,0}, B^{(i)}_{0,1}\}, \quad \text{where } B^{(i)}_{0,1} \sim \mathcal{N}(x_0 + v(t^\dagger_i - t^\dagger_{i-1}), 2D(t^\dagger_i - t^\dagger_{i-1})), \tag{4.7}$$

and

$$B^{(i)}_{k,2j} = B^{(i)}_{k-1,j}, \quad \text{for } j = 0, 1, \ldots, 2^{k-1}, \quad \text{and} \tag{4.8a}$$

$$B^{(i)}_{k,2j+1} \sim \mathcal{N}\left(\frac{B^{(i)}_{k-1,j} + B^{(i)}_{k-1,j+1}}{2}, \frac{2D(t^\dagger_i - t^\dagger_{i-1})}{2^k}\right), \quad \text{for } j = 0, 1, \ldots, 2^{k-1} - 1. \tag{4.8b}$$

Since $B^{(i-1)}_{k,2^k} \neq B^{(i)}_{k,0} = x_0$, the procedure described so far generates a multivalued process when consecutive reset intervals are concatenated. Therefore, once the multiresolution algorithm has been applied until the desired level of resolution, we obtain the proper discretization of the process setting $B^{(i)}_{k,2^k} = x_0$, for $i = 0, 1, \ldots$.

4.3. Reflecting boundary

We now add the hard wall reflecting boundary [30] to the previous developments. The hard wall reflections that bound the process below level 1 annihilate the Gaussian nature of the process, which is essential to the multiresolution method. To solve this issue, we first generate an unbounded trajectory with the multiresolution method $\mathbf{B}^{(i)}_k$, at some resolution level $k \geq 1$. Then, by using the increments of $\mathbf{B}^{(i)}_k$, we define the reflected process $\mathbf{R}^{(i)}_k$ starting as follows:

$$\begin{aligned} R^{(i)}_{k,j+1} &= \begin{cases} R^{(i)}_{k,j} + \Delta B^{(i)}_{k,j}, & \text{if } R^{(i)}_{k,j} + \Delta B^{(i)}_{k,j} \leq 1, \\ 2 - (R^{(i)}_{k,j} + \Delta B^{(i)}_{k,j}), & \text{if } R^{(i)}_{k,j} + \Delta B^{(i)}_{k,j} > 1 \end{cases} \\ &= \min\left\{R^{(i)}_{k,j} + \Delta B^{(i)}_{k,j}, 2 - (R^{(i)}_{k,j} + \Delta B^{(i)}_{k,j})\right\}, \end{aligned} \tag{4.9}$$

where $\Delta B^{(i)}_{k,j} = B^{(i)}_{k,j+1} - B^{(i)}_{k,j}$, for $j = 0, \ldots, 2^{k+1}$, and $R^{(i)}_{k,0} = x_0$.

4.4. Stopping condition

Every resolution k will provide a value for the first time at which the trajectory $\mathbf{R}_k$ is observed to go below the absorbing boundary, which is the null line,

$$\tau_{r,k} = \inf\{t_{k,j}^{(i)} \in (t_{i-1}^{\dagger}, t_i^{\dagger}) \,|\, R_{k,j}^{(i)} \leq 0,\, i = 1, 2, \dots\}. \tag{4.10}$$

This time provides an approximation to the target FPT at resolution k. Increasing the resolution yields finer sample paths and therefore finer estimations according to Eq. (4.10). However, we note that estimations using Eq. (4.10) are always upper bounds to the real FPT. Furthermore, if $k > k'$, then

$$\tau_r \leq \tau_{r,k} \leq \tau_{r,k'}.$$

This inequality has important consequences for our simulation schemes. Basically, every estimation induces an effective time horizon for our Monte Carlo method. Given the estimation at some resolution k, $\tau_{r,k}$, it makes no sense to simulate the process on times $t > \tau_{r,k}$ since $\tau_r \leq \tau_{r,k}$.

An explicit condition at which we may stop the simulation can be defined by using an error threshold $\epsilon > 0$. We define the maximum resolution level $k^{\dagger}$ such that the time increment is below ϵ,

$$k^{\dagger} = -\left\lceil \frac{\log(\epsilon)}{\log(2)} \right\rceil,$$

where $\lceil x \rceil$ denotes the smallest integer $\geq x$.

We finally defined all elements required to use the MRA to sample the FPT, we denote this version of the algorithm as the *standard* MRA (SMRA). We start generating the unbounded motion from Eq. (4.4) in the first reset interval ($i = 1$) for a target resolution $k^{\dagger}$ using Eq. (4.8). Once the Brownian trajectory has been generated in the first reset interval, we compute the reflected process in this interval [through Eq. (4.9)]. If the stopping condition in the first interval is reached [Eq. (4.10)], then the simulation stops and we can sample an estimation for the FPT at resolution $k^{\dagger}$. Otherwise, we will draw the next reset time, $t_2^{\dagger}$, and proceed similarly in the second reset interval (i.e. generating the Brownian trajectory using the multiresolution scheme, then reflecting the trajectory and lastly checking if the reflecting trajectory reach the stopping criteria). This procedure is iterated until the stopping condition is reached.

Once the above process has been used to get an estimation of the FPT with resolution $k^{\dagger}$, $\tau_{r,k^{\dagger}}$, it can be further refined to reach a new resolution level $k > k^{\dagger}$. In this second phase, there are no further sampling of reset times, and the multiresolution scheme is iterated on a fixed interval $[0, \tau_{r,k^{\dagger}}]$. This is because $\tau_{r,k^{\dagger}}$ is an upper bound for the true FPT.

4.5. HMRA

Stochastic resetting can strongly increase the computational requirements of the SMRA. This is because it requires applying the multiresolution method in multiple reset intervals with a high resolution $k^{\dagger}$, which is especially costly when $1/r \ll \tau_r$ because it results in a large number of resets.

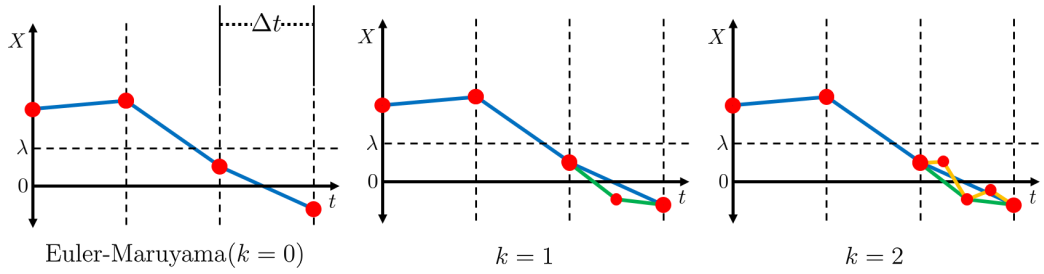

Figure 2: *Illustrations of trajectories generated from HMRA. Time increments of the Euler-Maruyama algorithm (Δt) are sketched as the separation of vertical dashed lines.*

The Euler-Maruyama algorithm partially overcomes these limitations, however it tends to overestimate the FPT and it does not have an arbitrary accuracy. We propose the *hybrid* MRA (HMRA) that refines the Euler-Maruyama trajectories with the MRA (Figure 2). In doing so, first we produce a trajectory of the Euler-Maruyama (Algorithm B.3), with a time step Δt. Close to the absorbing boundary, i.e. $X < \lambda$, for some small $\lambda > 0$, we use the MRA to refine the approximation. The details are included in Appendix B.5. Note finally that with our process the higher order Milstein scheme reduces to the Euler-Maruyama, because the coefficient of dW_t in Eq. (2.1), $\sqrt{2D}$, does not depend on X_t.

5. Numerical results

In order to illustrate the effectiveness of the PPF and the SMRA and HMRA, we analyse their performance in terms of accuracy, memory requirements, and speed. Source codes and Python packages of the PPF and MRA are available on the links provided in Appendices A and B.

5.1. PPF

The results of the approximation at order $m = 2$ and $n = 3$ are shown in Figures 3a and 3b which are compared with simulated results of the HMRA. In Figure 3 and Table 1 we observe that the PPF method is a good approximation of the entire distribution obtained by Monte Carlo, for multiple values of v, except for the percentile $p = 0.1$, for negative values of v.

For a valid result from the PPF method, we need to identify all the roots of the denominator of the Padé approximation, and ensure that they are real and negative, cf. Step 3 of Algorithm 3.3. Having at least one positive root, implies that no Laplace inverse of $f_{m,n}$ exists. On the other hand, if there is at least one non-real root, the result yields a damped sinusoidal, i.e. a signed function. Varying the parameters for drift and diffusion reveals regions at which the PPF method will not work based on these criteria, as shown in Figure 4.

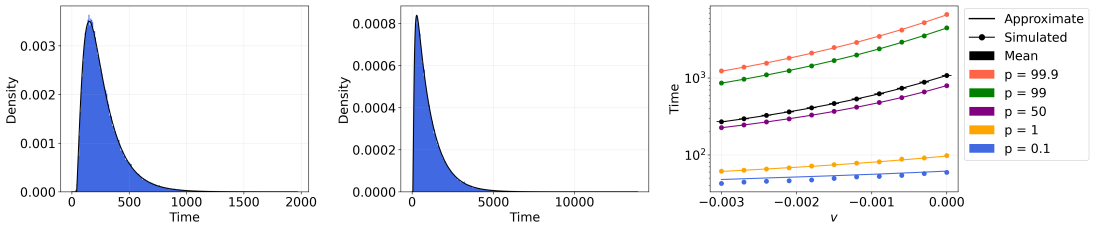

(a) $v = -3 \times 10^{-3}$ (b) $v = 0$ (c)

Figure 3: *Results of PPF approximation, parameters are* $D = 5 \times 10^{-4}$, $r = (3 \times 365)^{-1}$ *and approximation orders* $m = 2$, $n = 3$. *(a)-(b) Histograms obtained from* 10^6 *generated values and continuous curves obtained from PPF with varying drift* $v = -3 \times 10^{-3}$ *and* $v = 0$. *(c) Comparing quantiles close to the tails, medians, and means generated from PPF and* 10^6 *simulations for a varying drift.*

t	$\mathrm{P}_{HMRA}[\tau_r > t]$	$\mathrm{P}_{PPF}[\tau_r > t]$
342.140	0.25000	0.24918
379.322	0.19937	0.19800
416.503	0.15806	0.15718
453.685	0.12593	0.12470
490.866	0.10099	0.09891
528.047	0.07981	0.07843
565.229	0.06382	0.06219
602.410	0.05082	0.04931
639.592	0.04064	0.03910
676.773	0.03234	0.03100
713.955	0.02555	0.02458
751.136	0.02020	0.01949
788.317	0.01591	0.01545
825.499	0.01253	0.01225
862.680	0.01000	0.00971

t	$\mathrm{P}_{HMRA}[\tau_r > t]$	$\mathrm{P}_{PPF}[\tau_r > t]$
1445.966	0.25000	0.25089
1664.281	0.19842	0.19894
1882.596	0.15738	0.15775
2100.911	0.12428	0.12508
2319.225	0.09894	0.09919
2537.540	0.07823	0.07865
2755.855	0.06189	0.06236
2974.170	0.04967	0.04945
3192.485	0.03972	0.03921
3410.800	0.03117	0.03109
3629.115	0.02444	0.02465
3847.430	0.01964	0.01955
4065.745	0.01589	0.01550
4284.060	0.01255	0.01229
4502.375	0.01000	0.00975

Table 1: *Upper tail probabilities of HMRA and PPF in Figures 3a (left table) and 3b (right table).*

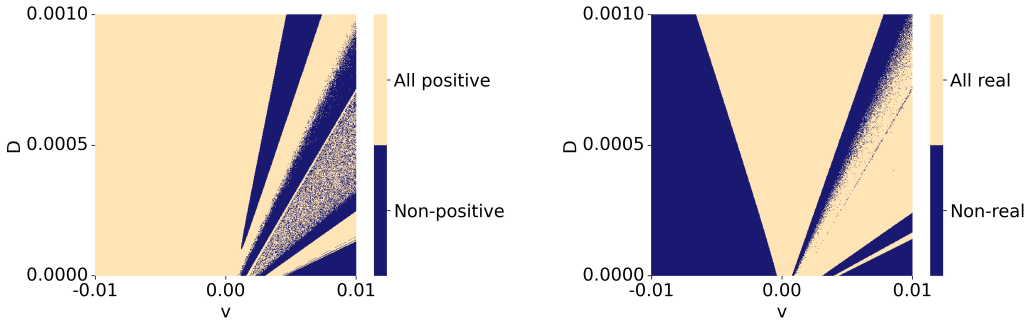

Sign of the root Presence of imaginary part of the root

Figure 4: *Regions of the parametric space* (v, D) *of validity of the PPF with orders* $m = 2$, $n = 3$, $r = (1/3) \times (1/365)$.

5.2. SMRA and HMRA

When comparing the accuracy of SMRA and HMRA by comparing their simulated mean FPT with the analytical mean FPT, we observe that as error threshold ϵ decreases, both algorithms converge to the analytical solution, whilst very small step sizes are necessary for Euler Maruyama to reach the same level of accurarcy (Figure 5). In terms of computational requirements, when we decrease ϵ, we observe a linear increase in $\langle k \rangle$, that would lead to an exponential increase in memory requirements as it is proportional to the number of points generated for each trajectory. Therefore, HMRA outperforms SMRA since it needs lesser points to reach the same accuracy (Figure 6a). Finally, in terms of speed, the HMRA outperforms the MRA by 2 to 4 orders of magnitude (Figure 6b).

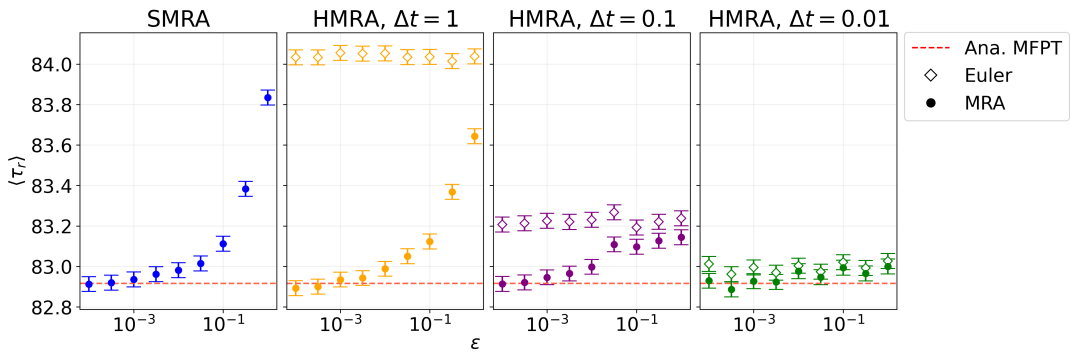

Figure 5: *SMRA and HMRA results with different Euler-Maruyama time steps* Δt*, with changing threshold* ϵ*.* $v = -10^{-2}$*,* $D = 10^{-4}$*,* $r = (3 \cdot 365)^{-1}$*,* $x_0 = 0.8$*,* 10^6 *simulations.*

Although HMRA outperforms the SMRA, HMRA requires two parameters to be set, ϵ and Δt. For this reason, we study the impact of either parameters in terms of computational time. For all the values of Δt, we identify where reducing ϵ does not correspond to a significant increase in computational time. However, as ϵ is further decreased, the computational time rapidly increases by orders of magnitude. This behavior describes a Pareto front, suggesting the existence of a critical value of ϵ which yields the best trade-off between accuracy and speed (Figure 6c).

6. Discussion

We have addressed the problem of computing the FPT distribution to the null level of the drifted Brownian motion with upper hard wall barrier and Poisson resetting times. In doing so, we have first introduced the PPF approximation, which is an analytical formula that can be immediately evaluated. We have then introduced the SMRA and HMRA, that are purely numerical but give arbitrary accuracy, and we have shown how they overcome the limitations of some other available methods in terms of accuracy and speed. Moreover, by using the survival function of the FPT, we have found a more compact expression of the mean FPT with resetting, which only uses the Laplace transform of the FPT without resetting [15, 16]. We have provided an easier derivation than one in [25].

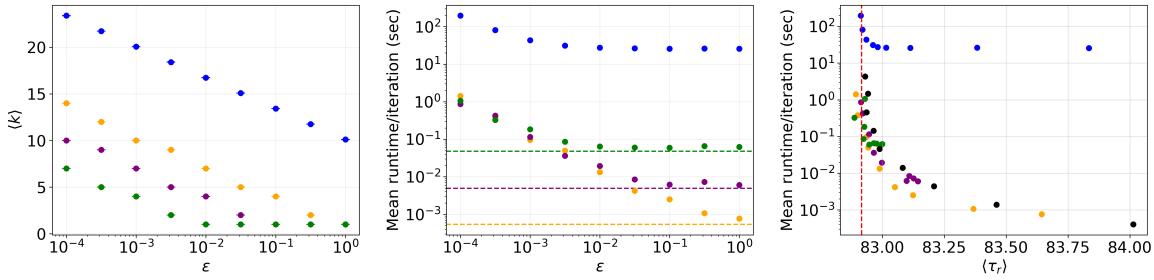

(a) $\langle k \rangle$ (b) Mean runtime per iteration (c) $\langle \tau_r \rangle$ vs. mean runtime

Figure 6: *Speed and accuracy comparisons between the SMRA (•), HMRA with* $\Delta t = 1$ *(•), HMRA with* $\Delta t = 0.1$ *(•), and HMRA with* $\Delta t = 0.01$ *(•). (a) Mean resolution per iteration. (b) Mean runtime per iteration. Dashed lines refer to the mean runtimes of the corresponding first Euler-Maruyama estimates for HMRA. (c) Comparisons between the mean FPT and the mean runtime per iteration of different simulation schemes. SMRA and HMRA simulations taken from Figure 5, Euler-Maruyama (•) plotted simulations with varying* Δt*, vertical red dashed line is the analytical mean FPT.*

Precisely, with the PPF we have proposed an approximation of the Laplace transform by taking the Padé approximation and its partial fraction decomposition [38]. These steps followed by exact inversion yield our PPF approximation. It is accurate and, given that it does not rely on numerical integration, as do most methods, like the Talbot approximation [56, 57], it yields an instantaneous numerical evaluation. The disadvantage of the PPF is that the region of the parametric space where the approximation is limited. But we have identified the region where it is valid.

To overcome this limitation, we have presented the MRA. Given two consecutive points on a trajectory, a property of Wiener processes is that the intermediate of the two points is Gaussian with mean given by the average of the first and last points [58]. The MRA exploits this bridge property by generating intermediate points between intervals of the trajectory. Hence, the MRA can generate finer values up to any threshold of error, compared to other methods for which the level of resolution is fixed in advance [39], making the control of the error difficult.

We have introduced two versions of the MRA, namely the SMRA and HMRA. Either simulation algorithm has shown high accuracy and convergence, this with respect to the exact analytical mean FPT and with respect to the simulation results of the standard Euler-Maruyama algorithm, which is based on a single and very small time increment. It is known that compute the FPT by Euler-Maruyama gives overestimation proportional to the time increment [39]. Thus, both the SMRA and HMRA correct this overestimation through the construction of Brownian bridges. Because the SMRA computes the entire sample path over a large time horizon, (in order to obtain the FPT to an arbitrary accuracy), it requires substantial computational resources. To increase speed and memory efficiency, the HMRA proceeeds as follows: it first approximates the FPT with Euler-Maruyama and then it refines locally the resolution through MRA. This yields a more efficient Monte Carlo technique than either the Euler-Maruyama or the SMRA individually.

Our Monte Carlo methods can readily be used with other Gaussian processes, such as

the Ornstein-Uhlenbeck process (see e.g. p. 229-230 of [59, 60]). Beyond the FPT, our method could be used to estimate the first passage area, namely the area enclosed between the null line and the path of the process up to the FPT, that has recently received substantial attention, cf. e.g. [61]. We envisage that it would be possible to extend our results to non-Gaussian α-stable Lévy processes using generalizations of the Brownian bridge [62, 63, 64]. Lastly, future work could focus on characterizing the optimal parameter choices that balance CPU time consumption and precision, as has been done for jumping processes [65].

7. Code availability statement

The source code (in Python) for the PPF, SMRA and HMRA is available on Github through the following links:

PPF: https://github.com/jarmsmagalang/ppf_approx
SMRA and HMRA: https://github.com/jarmsmagalang/multires

Furthermore, corresponding Python packages can be installed from PyPI at:

PPF: https://pypi.org/project/ppf-approx
SMRA and HMRA: https://pypi.org/project/multires

Acknowledgements

The authors are thankful to David Ginsbourger for his dedicated support and insightful scientific discussions.

This work had been supported by the UniBE ID Grant 2021, the Ruth & Arthur Scherbarth Foundation, the Agencia Estatal de Investigación (AEI, MCI, Spain) MCIN/AEI/10.13039/ 501100011033 and Fondo Europeo de Desarrollo Regional (FEDER, UE) under Project APASOS (PID2021-122256NB-C21/C22) and the María de Maeztu Program for units of Excellence in R&D, grant CEX2021- 001164-M.

References

[1] N. G. van Kampen, Stochastic Processes in Physics and Chemistry, 3rd Edition, North-Holland Personal Library, Elsevier, 2007.

[2] X. Bian, C. Kim, G. E. Karniadakis, 111 years of Brownian motion, Soft Matter 12 (30) (2016) 6331–6346. doi:10.1039/C6SM01153E.
URL https://pubs.rsc.org/en/content/articlelanding/2016/sm/c6sm01153e

[3] A. Libchaber, From Biology to Physics and Back: The Problem of Brownian Movement, Annual Review of Condensed Matter Physics 10 (2019) 275–293. doi:10.1146/annurev-conmatphys-031218-013318.

[4] P. Romanczuk, M. Bär, W. Ebeling, B. Lindner, L. Schimansky-Geier, Active Brownian particles, The European Physical Journal Special Topics 202 (1) (2012) 1–162. doi:10.1140/epjst/e2012-01529-y.
URL https://doi.org/10.1140/epjst/e2012-01529-y

[5] P. Romanczuk, I. D. Couzin, L. Schimansky-Geier, Collective Motion due to Individual Escape and Pursuit Response, Physical Review Letters 102 (1) (2009) 010602. doi:10.1103/PhysRevLett.102.010602.
URL https://link.aps.org/doi/10.1103/PhysRevLett.102.010602

[6] M. L. Woods, C. Carmona-Fontaine, C. P. Barnes, I. D. Couzin, R. Mayor, K. M. Page, Directional Collective Cell Migration Emerges as a Property of Cell Interactions, PLOS ONE 9 (9) (2014) e104969. doi:10.1371/journal.pone.0104969.
URL https://journals.plos.org/plosone/article?id=10.1371/journal.pone.0104969

[7] A. Marcovitz, Y. Levy, Obstacles May Facilitate and Direct DNA Search by Proteins, Biophysical Journal 104 (9) (2013) 2042–2050. doi:10.1016/j.bpj.2013.03.030.
URL https://www.ncbi.nlm.nih.gov/pmc/articles/PMC3647173/

[8] G. Oshanin, O. Vasilyev, P. L. Krapivsky, J. Klafter, Survival of an evasive prey, Proceedings of the National Academy of Sciences 106 (33) (2009) 13696–13701. doi:10.1073/pnas.0904354106.
URL https://www.pnas.org/doi/10.1073/pnas.0904354106

[9] F. Dufresne, H. U. Gerber, Risk theory for the compound poisson process that is perturbed by diffusion, Insurance: Mathematics and Economics 10 (1) (1991) 51–59. doi:10.1016/0167-6687(91)90023-Q.
URL https://doi.org/10.1016/0167-6687(91)90023-Q

[10] R. Gatto, B. Baumgartner, Saddlepoint Approximations to the Probability of Ruin in Finite Time for the Compound Poisson Risk Process Perturbed by Diffusion, Methodology and Computing in Applied Probability 18 (1) (2016) 217–235. doi:10.1007/s11009-014-9412-9.
URL https://doi.org/10.1007/s11009-014-9412-9

[11] R. Gatto, M. Mosimann, Four approaches to compute the probability of ruin in the compound Poisson risk process with diffusion, Mathematical and Computer Modelling 55 (3) (2012) 1169–1185. doi:10.1016/j.mcm.2011.09.041.
URL https://www.sciencedirect.com/science/article/pii/S0895717711005899

[12] S. N. Majumdar, S. Sabhapandit, G. Schehr, Dynamical transition in the temporal relaxation of stochastic processes under resetting, Physical Review E 91 (5) (2015) 052131. doi:10.1103/PhysRevE.91.052131.
URL https://link.aps.org/doi/10.1103/PhysRevE.91.052131

[13] M. R. Evans, S. N. Majumdar, Diffusion with Stochastic Resetting, Physical Review Letters 106 (16) (2011) 160601. doi:10.1103/PhysRevLett.106.160601.
URL https://link.aps.org/doi/10.1103/PhysRevLett.106.160601

[14] A. Chechkin, I. M. Sokolov, Random Search with Resetting: A Unified Renewal Approach, Physical Review Letters 121 (5) (2018) 050601. doi:10.1103/PhysRevLett.121.050601.
URL https://link.aps.org/doi/10.1103/PhysRevLett.121.050601

[15] M. R. Evans, S. N. Majumdar, G. Schehr, Stochastic resetting and applications, Journal of Physics A: Mathematical and Theoretical 53 (19) (2020) 193001. doi:10.1088/1751-8121/ab7cfe.
URL https://dx.doi.org/10.1088/1751-8121/ab7cfe

[16] A. Pal, V. V. Prasad, First Passage under stochastic resetting in an interval, Physical Review E 99 (3) (2019) 032123. doi:10.1103/PhysRevE.99.032123.
URL https://link.aps.org/doi/10.1103/PhysRevE.99.032123

[17] É. Roldán, S. Gupta, Path-integral formalism for stochastic resetting: Exactly solved examples and shortcuts to confinement, Physical Review E 96 (2) (2017) 022130. doi:10.1103/PhysRevE.96.022130.
URL https://link.aps.org/doi/10.1103/PhysRevE.96.022130

[18] A. Nagar, S. Gupta, Diffusion with Stochastic Resetting at Power-Law times, Physical Review E 93 (6) (2016) 060102. doi:10.1103/PhysRevE.93.060102.
URL https://link.aps.org/doi/10.1103/PhysRevE.93.060102

[19] A. Pal, A. Kundu, M. R. Evans, Diffusion under time-dependent resetting, Journal of Physics A: Mathematical and Theoretical 49 (22) (2016) 225001. doi:10.1088/1751-8113/49/22/225001.
URL https://dx.doi.org/10.1088/1751-8113/49/22/225001

[20] L. Kusmierz, S. N. Majumdar, S. Sabhapandit, G. Schehr, First Order Transition for the Optimal Search Time of Lévy Flights with Resetting, Physical Review Letters 113 (22) (2014) 220602. doi:10.1103/PhysRevLett.113.220602.
URL https://link.aps.org/doi/10.1103/PhysRevLett.113.220602

[21] J. M. Meylahn, S. Sabhapandit, H. Touchette, Large deviations for Markov processes with resetting, Physical Review E 92 (6) (2015) 062148. doi:10.1103/PhysRevE.92.062148.
URL https://link.aps.org/doi/10.1103/PhysRevE.92.062148

[22] G. Mercado-Vásquez, D. Boyer, Lotka–Volterra systems with stochastic resetting, Journal of Physics A: Mathematical and Theoretical 51 (40) (2018) 405601. doi:10.1088/1751-8121/aadbc0.
URL https://dx.doi.org/10.1088/1751-8121/aadbc0

[23] P. C. Bressloff, Stochastic resetting and the Mean-Field dynamics of focal adhesions, Physical Review E 102 (2) (2020) 022134. doi:10.1103/PhysRevE.102.022134.
URL https://link.aps.org/doi/10.1103/PhysRevE.102.022134

[24] É. Roldán, A. Lisica, D. Sánchez-Taltavull, S. W. Grill, Stochastic resetting in backtrack recovery by RNA polymerases, Physical Review E 93 (6) (2016) 062411. doi:10.1103/PhysRevE.93.062411.
URL https://link.aps.org/doi/10.1103/PhysRevE.93.062411

[25] A. M. Ramoso, J. A. Magalang, D. Sánchez-Taltavull, J. P. Esguerra, É. Roldán, Stochastic resetting antiviral therapies prevent drug resistance development, Europhysics Letters 132 (5) (2020) 50003. doi:10.1209/0295-5075/132/50003.
URL https://dx.doi.org/10.1209/0295-5075/132/50003

[26] B. Besga, A. Bovon, A. Petrosyan, S. N. Majumdar, S. Ciliberto, Optimal mean First-Passage time for a Brownian searcher subjected to resetting: Experimental and theoretical results, Physical Review Research 2 (3) (2020) 032029. doi:10.1103/PhysRevResearch.2.032029.
URL https://link.aps.org/doi/10.1103/PhysRevResearch.2.032029

[27] O. Tal-Friedman, A. Pal, A. Sekhon, S. Reuveni, Y. Roichman, Experimental Realization of Diffusion with Stochastic Resetting, The Journal of Physical Chemistry Letters

11 (17) (2020) 7350–7355. doi:10.1021/acs.jpclett.0c02122.
URL https://doi.org/10.1021/acs.jpclett.0c02122

[28] G. A. Pavliotis, Stochastic Processes and Applications: Diffusion Processes, the Fokker-Planck and Langevin Equations, 1st Edition, no. 60 in Texts in Applied Mathematics, Springer, New York, 2014.

[29] S. Karlin, H. M. Taylor, A Second Course in Stochastic Processes, Academic Press, an imprint of Elsevier, 1981.

[30] S. Redner, A Guide to First-Passage Processes, Cambridge University Press, Cambridge, 2001. doi:10.1017/CBO9780511606014.
URL https://www.cambridge.org/core/books/guide-to-firstpassage-processes/59066FD9754B42D22B028E33726D1F07

[31] S. Iyer-Biswas, A. Zilman, First-Passage Processes in Cellular Biology, in: Advances in Chemical Physics, Vol. 160, John Wiley & Sons, Ltd, 2016, Ch. 5, pp. 261–306. doi:10.1002/9781119165156.ch5.
URL https://onlinelibrary.wiley.com/doi/abs/10.1002/9781119165156.ch5

[32] J. Aguilar, B. A. García, R. Toral, S. Meloni, J. J. Ramasco, Endemic infectious states below the epidemic threshold and beyond herd immunity, Communications Physics 6 (1) (2023) 187. doi:https://doi.org/10.1038/s42005-023-01302-0.

[33] Y. Zhang, O. K. Dudko, First-Passage Processes in the Genome, Annual Review of Biophysics 45 (1) (2016) 117–134. doi:10.1146/annurev-biophys-062215-010925.
URL https://doi.org/10.1146/annurev-biophys-062215-010925

[34] R. Chicheportiche, J.-P. Bouchaud, Some Applications of First-Passage Ideas to Finance, in: First-Passage Phenomena and Their Applications, World Scientific, 2014, pp. 447–476. doi:10.1142/9789814590297_0018.
URL http://www.worldscientific.com/doi/abs/10.1142/9789814590297_0018

[35] J. Masoliver, J. Perelló, First-Passage and Extremes in Socio-Economic Systems, in: First-Passage Phenomena and Their Applications, World Scientific, 2014, pp. 477–501. doi:10.1142/9789814590297_0019.
URL http://www.worldscientific.com/doi/abs/10.1142/9789814590297_0019

[36] M. Maggiore, A. Riotto, The Excursion Set Theory in Cosmology, in: First-Passage Phenomena and Their Applications, World Scientific, 2014, pp. 532–553. doi:10.1142/9789814590297_0021.
URL http://www.worldscientific.com/doi/abs/10.1142/9789814590297_0021

[37] E. Barkai, D. A. Kessler, Transport and the First Passage Time Problem with Application to Cold Atoms in Optical Traps, in: First-Passage Phenomena and Their Applications, World Scientific, 2014, pp. 502–531. doi:10.1142/9789814590297_0020.
URL http://www.worldscientific.com/doi/abs/10.1142/9789814590297_0020

[38] B. Davies, B. Martin, Numerical inversion of the Laplace transform: A survey and comparison of methods, Journal of Computational Physics 33 (1) (1979) 1–32. doi:10.1016/0021-9991(79)90025-1.
URL https://www.sciencedirect.com/science/article/pii/0021999179900251

[39] S. Asmussen, P. W. Glynn, Stochastic Simulation: Algorithms and Analysis, Vol. 57 of Stochastic Modelling and Applied Probability, Springer, New York, NY, 2007. doi:10.1007/978-0-387-69033-9.
URL http://link.springer.com/10.1007/978-0-387-69033-9

[40] S. B. Yuste, K. Lindenberg, Comment on "Mean first passage time for anomalous diffusion", Physical Review E 69 (3) (2004) 033101. doi:10.1103/PhysRevE.69.033101.
URL https://link.aps.org/doi/10.1103/PhysRevE.69.033101

[41] D. L. Dy, J. P. Esguerra, First-Passage characteristics of biased diffusion in a planar wedge, Physical Review E 88 (1) (2013) 012121. doi:10.1103/PhysRevE.88.012121.
URL https://link.aps.org/doi/10.1103/PhysRevE.88.012121

[42] R. Voituriez, O. Bénichou, First-Passage Statistics for Random Walks in Bounded Domains, in: First-Passage Phenomena and Their Applications, World Scientific, 2014, pp. 145–174. doi:10.1142/9789814590297_0007.
URL http://www.worldscientific.com/doi/abs/10.1142/9789814590297_0007

[43] D. R. Cox, H. D. Miller, The Theory of Stochastic Processes, 1st Edition, Chapman and Hall/CRC, London, 1965.

[44] A. V. Skorokhod, Stochastic Equations for Diffusion Processes in a Bounded Region, Theory of Probability & Its Applications 6 (3) (1961) 264–274. doi:10.1137/1106035.
URL https://epubs.siam.org/doi/10.1137/1106035

[45] A. Pilipenko, An Introduction to Stochastic Differential Equations with Reflection, Vol. 1 of Lectures in Pure and Applied Mathematics, Potsdam University Press, 2014.
URL https://publishup.uni-potsdam.de/opus4-ubp/frontdoor/deliver/index/docId/6949/file/lpam01.pdf

[46] J. M. Harrison, Brownian Motion and Stochastic Flow Systems, John Wiley, New York, 1985.

[47] S. C. Manrubia, E. Lázaro, Viral evolution, Physics of Life Reviews 3 (2) (2006) 65–92. doi:10.1016/j.plrev.2005.11.002.
URL https://www.sciencedirect.com/science/article/pii/S1571064505000436

[48] D. Pillay, M. Zambon, Antiviral drug resistance, BMJ : British Medical Journal 317 (7159) (1998) 660–662. doi:10.1136/bmj.317.7159.660.
URL https://www.ncbi.nlm.nih.gov/pmc/articles/PMC1113839/

[49] D. S. Clutter, M. R. Jordan, S. Bertagnolio, R. W. Shafer, HIV-1 drug resistance and resistance testing, Infection, Genetics and Evolution 46 (2016) 292–307. doi:10.1016/j.meegid.2016.08.031.
URL https://www.sciencedirect.com/science/article/pii/S1567134816303690

[50] Y. L. Luke, On the approximate inversion of some Laplace transforms, Tech. rep., Midwest Research Institute, Aerospace Research Laboratories (1961).
URL https://apps.dtic.mil/sti/citations/AD0259669

[51] I. M. Longman, On the Generation of Rational Function Approximations for Laplace Transform Inversion with an Application to Viscoelasticity, SIAM Journal on Applied Mathematics 24 (4) (1973) 429–440. doi:10.1137/0124045.
URL https://epubs.siam.org/doi/abs/10.1137/0124045

[52] J. E. Akin, J. Counts, The Application of Continued Fractions to Wave Propagation in a Semi-Infinite Elastic Cylindrical Membrane, Journal of Applied Mechanics 36 (3) (1969) 420–424. doi:10.1115/1.3564696.
URL https://doi.org/10.1115/1.3564696

[53] Y. L. Luke, The Special Functions and Their Approximations, Vol. 1 and 2 of Mathematics in Science and Engineering, Academic Press, New York and London, 1969.

[54] G. A. Baker Jr, J. L. Gammel, The Padé approximant, Journal of Mathematical Analysis and Applications 2 (1) (1961) 21–30.

[55] J. H. Mathews, K. D. Fink, Numerical Methods Using MATLAB, 4th Edition, Pearson Prentice Hall, 2004.

[56] A. Talbot, The accurate numerical inversion of Laplace transforms, IMA Journal of Applied Mathematics 23 (1) (1979) 97–120.

[57] J. Abate, W. Whitt, A Unified Framework for Numerically Inverting Laplace Transforms, INFORMS Journal on Computing 18 (4) (2006) 408–421. doi:10.1287/ijoc.1050.0137.
URL https://pubsonline.informs.org/doi/abs/10.1287/ijoc.1050.0137

[58] G. F. Lawler, Introduction to Stochastic Processes, 1st Edition, Chapman and Hall/CRC, New York, 1995.

[59] R. Gatto, Stationary Stochastic Models: An Introduction, 1st Edition, World Scientific Series on Probability Theory and Its Applications: Volume 4, World Scientific Publishing, Singapore, 2022. doi:https://doi.org/10.1142/12710.

[60] A. Dubey, A. Pal, First-passage functionals for Ornstein-Uhlenbeck process with stochastic resetting, Journal of Physics A: Mathematical and Theoretical 56 (2023) 435002. doi:10.1088/1751-8121/acf748.

[61] M. Abundo, The first-passage area of Wiener process with stochastic resetting, Methodology and Computing in Applied Probability (2023) 25:92doi:doi.org/10.1007/s11009-023-10069-4.

[62] S. N. Majumdar, H. Orland, Effective langevin equations for constrained stochastic processes, Journal of Statistical Mechanics: Theory and Experiment 2015 (6) (2015) P06039. doi:10.1088/1742-5468/2015/06/P06039.
URL https://dx.doi.org/10.1088/1742-5468/2015/06/P06039

[63] J. Aguilar, J. W. Baron, T. Galla, R. Toral, Sampling rare trajectories using stochastic bridges, Physical Review E 105 (6) (2022) 064138. doi:10.1103/PhysRevE.105.064138.
URL https://link.aps.org/doi/10.1103/PhysRevE.105.064138

[64] J. Aguilar, R. Gatto, Unified perspective on exponential tilt and bridge algorithms for rare trajectories of discrete markov processes, Phys. Rev. E 109 (2024) 034113. doi:10.1103/PhysRevE.109.034113.
URL https://link.aps.org/doi/10.1103/PhysRevE.109.034113

[65] J. Aguilar, J. J. Ramasco, R. Toral, Biased versus unbiased numerical methods for stochastic simulations, Communications Physics 7 (1) (2024) 155. doi:https://doi.org/10.1038/s42005-024-01648-z.

[66] G. B. Arfken, H. J. Weber, F. E. Harris, Mathematical Methods for Physicists: A Comprehensive Guide, 7th Edition, Academic Press, 2011.

[67] G. A. Whitmore, V. Seshadri, A heuristic derivation of the inverse gaussian distribution, The American Statistician 41 (4) (1987) 280–281. doi:10.1080/00031305.1987.10475503.
URL http://dx.doi.org/10.1080/00031305.1987.10475503

[68] R. S. Chhikara, J. Leroy Folks, The inverse Gaussian distribution, Statistics: A Series of Textbooks and Monographs, CRC Press, Boca Raton, FL, 1988.

[69] A. Godec, R. Metzler, Universal Proximity Effect in Target Search Kinetics in the Few-Encounter Limit, Physical Review X 6 (4) (2016) 041037. doi:10.1103/PhysRevX.6.041037.
URL https://link.aps.org/doi/10.1103/PhysRevX.6.041037

Appendix A Proofs

Proof of Lemma 2.1. We begin by taking the Laplace transform of Eq. (2.2) with respect to t and proceed to solve for the propagator using a procedure similar to the method of undetermined coefficients. Denote by $\mathcal{L}$ the operator of Laplace transform. First, note that swapping integral and derivative operation over different variables yields

$$\mathcal{L}\left(vp'(x,\cdot)\right)(s) = v\tilde{p}'(x,s) \quad \text{and} \quad \mathcal{L}\left(Dp''(x,\cdot)\right)(s) = D\tilde{p}''(x,s)\,.$$

The first term is the only term in the equation that has a derivative dependent on t, which yields

$$\partial_t p(x,t) = s\tilde{p}(x,s) - p(x,0) = s\tilde{p}(x,s) - \delta(x-x_0)$$

where $p(x,0) = \delta(x-x_0)$, taken from the initial condition in Eqs. (2.5). Therefore, the transform of Eq. (2.2) for $\tilde{p}(x,s)$ is given by a nonhomogeneous differential equation

$$s\tilde{p}(x,s) - \delta(x-x_0) + v\tilde{p}'(x,s) - D\tilde{p}''(x,s) = 0\,, \quad s \geq 0\,, \tag{A.1}$$

for $x \in [0,x_0) \cup (x_0,1]$. Rearranging the equation to have the nonhomogeneous term on the right-hand side, we obtain

$$D\tilde{p}''(x) - v\tilde{p}'(x) - s\tilde{p}(x) = -\delta(x-x_0). \tag{A.2}$$

In order to find a solution to Eq. (A.1), let us fix s, denote $\tilde{p}_<(x) = \tilde{p}(x,s)$ for $x \in [0,x_0)$, $\tilde{p}_>(x) = \tilde{p}(x,s)$ for $x \in (x_0,1]$ and search an analytic solution to the associated homogeneous differential equation to Eq. (A.2)

$$D\tilde{p}''(x) - v\tilde{p}'(x) - s\tilde{p}(x) = 0,$$

over these two intervals. The characteristic equation is $D\alpha^2 - v\alpha - s = 0$, with roots, defined in Eq. (2.7),

$$\alpha_\pm = \frac{v \pm \sqrt{v^2+4Ds}}{2D} = \frac{v \pm \omega(s)}{2D} = \rho \pm \theta(s)\,,$$

where the constants are defined by Eq. (2.6). Therefore,

$$\tilde{p}_>(x) = Ae^{\alpha_+ x} + Be^{\alpha_- x} \quad \text{and} \quad \tilde{p}_<(x) = ae^{\alpha_+ x} + be^{\alpha_- x}\,,$$

for some constants a, b, A and B to be determined. From the boundary conditions Eq. (2.4) we obtain

$$\tilde{p}_<(x) = a(e^{\alpha_+ x} - e^{\alpha_- x})$$

and

$$v(Ae^{\alpha_+} + Be^{\alpha_-}) = D(\alpha_+ Ae^{\alpha_+} + \alpha_- Be^{\alpha_-})\,.$$

The latter equation may be rewritten as

$$(D\alpha_+ - v)Ae^{\alpha_+} = (v - D\alpha_-)Be^{\alpha_-} = C(s)\,,$$

implying

$$\tilde{p}_{>}(x) = C\left(\frac{e^{\alpha_+(x-1)}}{D\alpha_+ - v} + \frac{e^{\alpha_-(x-1)}}{v - D\alpha_-}\right).$$

The continuity of $p(\cdot, t)$ (see [29], Chapter 15, Section 5) yields $\tilde{p}_{<}(x_0) = \tilde{p}_{>}(x_0)$, hence one can write

$$C\left(\frac{e^{\alpha_+(x_0-1)}}{D\alpha_+ - v} + \frac{e^{\alpha_-(x_0-1)}}{v - D\alpha_-}\right) = a\left(e^{\alpha_+ x_0} - e^{\alpha_- x_0}\right) = c(s).$$

Consequently, we obtain

$$\tilde{p}_{<}(x) = c(s)\frac{e^{\alpha_+ x} - e^{\alpha_- x}}{e^{\alpha_+ x_0} - e^{\alpha_- x_0}} \quad \text{and} \quad \tilde{p}_{>}(x) = c(s)\frac{\frac{e^{\alpha_+(x-1)}}{D\alpha_+ - v} + \frac{e^{\alpha_-(x-1)}}{v - D\alpha_-}}{\frac{e^{\alpha_+(x_0-1)}}{D\alpha_+ - v} + \frac{e^{\alpha_-(x_0-1)}}{v - D\alpha_-}}.$$

Noticing

$$v - D\alpha_- = D\alpha_+ \quad \text{and} \quad v - D\alpha_+ = D\alpha_-,$$

we have

$$\tilde{p}_{>}(x) = c(s)\frac{\alpha_+ e^{\alpha_+(x-1)} - \alpha_- e^{\alpha_-(x-1)}}{\alpha_+ e^{\alpha_+(x_0-1)} - \alpha_- e^{\alpha_-(x_0-1)}}.$$

Our goal is now to determine the function $c(s) = \tilde{p}(x_0, s)$.

We proceed to examine conditions involving the derivative of p following standard procedures (see e.g. p. 16 of [30] or p. 449 of [66]). We now return to the nonhomogeneous differential equation in Eq. (A.2). Integrating the above equation on a segment around x_0,

$$\int_{x_0-\epsilon}^{x_0+\epsilon} \{D\tilde{p}''(x,s) - v\tilde{p}'(x,s) - s\tilde{p}(x,s)\}\, dx = -\int_{x_0-\epsilon}^{x_0+\epsilon} \delta(x - x_0)\, dx\,, \quad s \geq 0\,, \epsilon > 0$$

then,

$$D\tilde{p}'(x,s)\Big|_{x_0-\epsilon}^{x_0+\epsilon} - v\tilde{p}(x,s)\Big|_{x_0-\epsilon}^{x_0+\epsilon} - \int_{x_0-\epsilon}^{x_0+\epsilon} (s\tilde{p}(x,s))\, dx \;= -1.$$

In the limit $\epsilon \to 0$, the last two terms at the left-hand side tend to zero due to continuity of $\tilde{p}(x,s)$ at $x = x_0$. While the first summand can be rearranged and evaluated in terms of $\tilde{p}'_{<}$ and $\tilde{p}'_{>}$,

$$D\left(\tilde{p}'_{<}(x_0) - \tilde{p}'_{>}(x_0)\right) = 1\,. \tag{A.3}$$

Let us compute the first derivative

$$\tilde{p}'_{<}(x) = c\frac{\alpha_+ e^{\alpha_+ x} - \alpha_- e^{\alpha_- x}}{e^{\alpha_+ x_0} - e^{\alpha_- x_0}},$$

and evaluate it at x_0

$$\begin{aligned}\tilde{p}'_{<}(x_0) &= c\frac{\alpha_+ e^{\alpha_+ x_0} - \alpha_- e^{\alpha_- x_0}}{e^{\alpha_+ x_0} - e^{\alpha_- x_0}} \\ &= c\frac{\alpha_+ e^{\theta x_0} - \alpha_- e^{-\theta x_0}}{e^{\theta x_0} - e^{-\theta x_0}}.\end{aligned}$$

Analogously,

$$\tilde{p}'_{>}(x) = c\frac{\alpha_+^2 e^{\alpha_+(x-1)} - \alpha_-^2 e^{\alpha_-(x-1)}}{\alpha_+ e^{\alpha_+(x_0-1)} - \alpha_- e^{\alpha_-(x_0-1)}}\,,$$

leads to

$$\begin{aligned}\tilde{p}'_{>}(x_0) &= c\frac{\alpha_+^2 e^{\alpha_+(x_0-1)} - \alpha_-^2 e^{\alpha_-(x_0-1)}}{\alpha_+ e^{\alpha_+(x_0-1)} - \alpha_- e^{\alpha_-(x_0-1)}} \\ &= c\frac{\alpha_+^2 e^{\theta(x_0-1)} - \alpha_-^2 e^{-\theta(x_0-1)}}{\alpha_+ e^{\theta(x_0-1)} - \alpha_- e^{-\theta(x_0-1)}}\,.\end{aligned}$$

Therefore, by inserting Eq. (A.3)

$$\begin{aligned}1 &= Dc\left(\frac{\alpha_+ e^{\theta x_0} - \alpha_- e^{-\theta x_0}}{e^{\theta x_0} - e^{-\theta x_0}} - \frac{\alpha_+^2 e^{\theta(x_0-1)} - \alpha_-^2 e^{-\theta(x_0-1)}}{\alpha_+ e^{\theta(x_0-1)} - \alpha_- e^{-\theta(x_0-1)}}\right) \\ &= Dc\,\frac{e^{-\theta}(\alpha_+^2 - \alpha_+\alpha_-) + e^{\theta}(\alpha_-^2 - \alpha_+\alpha_-)}{\alpha_+ e^{\theta(2x_0-1)} + \alpha_- e^{-\theta(2x_0-1)} - \alpha_+ e^{-\theta} - \alpha_- e^{\theta}} \\ &= 2Dc\,\frac{e^{-\theta}\theta(\theta+\rho) + e^{\theta}\theta(\theta-\rho)}{\alpha_+ e^{\theta(2x_0-1)} + \alpha_- e^{-\theta(2x_0-1)} - \alpha_+ e^{-\theta} - \alpha_- e^{\theta}} \\ &= 2Dc\,\frac{\theta(\theta\cosh(\theta) - \rho\sinh(\theta))}{\rho\cosh[\theta(2x_0-1)] + \theta\sinh[\theta(2x_0-1)] - \rho\cosh(\theta) + \theta\sinh(\theta)} \\ &= c\,\frac{\omega(\omega\cosh(\theta) - v\sinh(\theta))}{v\cosh[\theta(2x_0-1)] + \omega\sinh[\theta(2x_0-1)] - v\cosh(\theta) + \omega\sinh(\theta)}\,,\end{aligned}$$

which gives

$$\begin{aligned}c(s) = \tilde{p}(x_0, s) &= \frac{v\cosh[\theta(2x_0-1)] + \omega\sinh[\theta(2x_0-1)] - v\cosh(\theta) + \omega\sinh(\theta)}{\omega^2\cosh(\theta) - v\omega\sinh(\theta)} \\ &= \frac{2\sinh(\theta x_0)\left\{\omega\cosh[\theta(x_0-1)] + v\sinh[\theta(x_0-1)]\right\}}{\omega^2\cosh(\theta) - v\,\omega\sinh(\theta)}\,,\end{aligned}$$

where ω and θ are defined in Eq. (2.6). All in all, we obtain the expression Eqs. (2.8) and (2.9) for the Laplace transform of the propagator. □

Proof of Proposition 3.2. Let us define the distribution function of τ_r by $F_r(t) = \int_0^t f_r(s)ds$ and its *survival function* by $S_r(t) = 1 - F_r(t) = \mathbb{P}(\tau_r > t)$, $t \geq 0$. In view of the known relation

$$f_r(t) = -\partial_t S_r(t)\,, \tag{A.4}$$

we may re-express the expectation of interest in the following way:

$$\mathbb{E}[\tau_r] = \int_0^\infty t f_r(t)\,dt = -\int_0^\infty t\partial_t S_r(t)\,dt = \int_0^\infty S_r(t)\,dt = \tilde{S}_r(0)\,, \tag{A.5}$$

where the tilde always denotes the Laplace transform of a function. In order to find an expression for the latter term, we use a renewal equation that connects the survival function in

the resetting case to the survival function for the evolution without resetting. The following equation is well-known in the literature relative to stochastic resetting and can be found e.g. in [15, 16, 17]

$$S_r(t) = e^{-rt} S_0(t) + r \int_0^t e^{-ru} S_0(u) S_r(t-u)\, du\,.$$

By taking Laplace transform on both sides we obtain

$$\tilde{S}_r(s) = \tilde{S}_0(s+r) + r\tilde{S}_0(s+r)\tilde{S}_r(s)\,,$$

hence, for all s such that $\tilde{S}_0(s+r) \neq r^{-1}$,

$$\tilde{S}_r(s) = \frac{\tilde{S}_0(s+r)}{1 - r\tilde{S}_0(s+r)}\,. \tag{A.6}$$

The link between $\tilde{S}_0(s)$ and $\tilde{f}_0(s)$ is provided by the Laplace transform of Eq. (A.4), which for $r = 0$ yields, for all $s \neq 0$,

$$\tilde{S}_0(s) = \frac{1 - \tilde{f}_0(s)}{s}\,.$$

Plugging the latter into Eq. (A.6) gives for all $s \neq -r$ such that $\tilde{f}_0(s+r) \neq -s/r$,

$$\tilde{S}_r(s) = \frac{1 - \tilde{f}_0(s+r)}{s + r\tilde{f}_0(s+r)}\,, \tag{A.7}$$

and by Eq. (A.5) we finally obtain

$$\mathbb{E}[\tau_r] = \frac{1}{r}\left\{\frac{1}{\tilde{f}_0(r)} - 1\right\}\,. \tag{A.8}$$

All that remains to do is expressing $\tilde{f}$ in terms of what we explicitly know, that is $\tilde{p}$. This is done by evaluating the Laplace transform of the probability current (Eq. (2.3)) at the absorbing boundary $x = 0$

$$\tilde{f}_0(s) = \tilde{J}(0,s) = D\tilde{p}'(0,s) - v\tilde{p}(0,s) = D\tilde{p}'(0,s)\,. \tag{A.9}$$

The probability current $J(x,t)$ is the rate of influx of Brownian particles at the position x, and since $x = 0$ is an absorbing boundary, $J(0,t)$ will give the FPT distribution [30]. This is related to the derivation of the inverse Gaussian distribution using the method of images [67, 68]. Therefore, from Eq. (A.9) we obtain Eq. (3.2) for
$s > -v^2/(4D)$

$$\tilde{f}_0(s) = e^{-\rho x_0}\frac{\omega(s)\cosh\{\theta(s)(x_0-1)\} + v\sinh\{\theta(s)(x_0-1)\}}{\omega(s)\cosh\{\theta(s)\} - v\sinh\{\theta(s)\}}\,, \tag{A.10}$$

as it has been previously shown in [69] and plugging the latter into Eq. (A.8) yields an explicit analytic expression for the mean absorption time

$$\mathbb{E}[\tau_r] = \frac{1}{r}\left\{\frac{e^{\rho x_0}\left(\omega(r)\cosh\{\theta(r)\} - v\sinh\{\theta(r)\}\right)}{\omega(r)\cosh\{\theta(r)(x_0-1)\} + v\sinh\{\theta(r)(x_0-1)\}} - 1\right\}\,,$$

where ρ, ω and θ have been defined in Eq. (2.6). □

Appendix B Implementation of SMRA and HMRA

B.1 MRA

We first consider a simple case of the MRA in the time interval $[0, 1]$. In the algorithm, the discretized Wiener process, $\{W_{k,j}\}$, with k, j nonnegative integers, is obtained through Eqs. (4.2) and (4.3).

Algorithm B.1: Basic MRA

Input: initial position W_0

Output: $\mathbf{W} = \{W_0, \ldots, W_{2^{k-1}}\}, \mathbf{t} = \{0, \ldots, t^\dagger\}$

$k \coloneqq 0$;
$W_1 \coloneqq W \sim \mathcal{N}(0, 1)$;
$\mathbf{W} \coloneqq \{W_0, W_1\}$;
$\mathbf{t} \coloneqq \{0, 1\}$;
while $\mathbf{W}$ *has not reached a stopping condition* **do**
  $k \coloneqq k + 1$;
  $\mathbf{W}^* \coloneqq \emptyset$; $\mathbf{t}^* \coloneqq \emptyset$;
  for $j \in [0, 2^k]$ **do**
    $j' \coloneqq \left\lfloor \frac{j}{2} \right\rfloor$;
    if j *is even* **then**
      $W^*_j \coloneqq W_{j'}$; ▷ note: $W_{j'}$ is j'-th element of $\mathbf{W}$
      $t^*_j \coloneqq t_{j'}$; ▷ note: $t_{j'}$ is j'-th element of $\mathbf{t}$
    else
      $\mu_{int} \coloneqq \frac{W_{j'} + W_{j'+1}}{2}$;
      $\sigma^2_{int} \coloneqq \frac{1}{2^k}$;
      $W^*_j \coloneqq W \sim \mathcal{N}(\mu_{int}, \sigma^2_{int})$;
      $t^*_j \coloneqq \frac{t_{j'} + t_{j'+1}}{2}$;
  $\mathbf{W} \coloneqq \mathbf{W}^*$;
  $\mathbf{t} \coloneqq \mathbf{t}^*$;

This pseudocode will generate the two arrays $\mathbf{W}$ and $\mathbf{t}$, the positions and times respectively of the trajectories. The final resolution level k can be arbitrarily obtained with a given stopping condition.

B.2 Euler-Maruyama trajectory for HMRA

This method is similar to the Euler-Maruyama algorithm described in Algorithm B.3, but modified for use in the hybrid algorithm. This code will output two arrays $\mathbf{X}^E$ and $\mathbf{t}^E$ which are Euler-Maruyama trajectories but below a position threshold $\lambda > 0$. This is because above this certain threshold in the position, an absorption is unlikely to happen. Note that reflection and resetting occur in this algorithm.

Algorithm B.2: `euler`: Generate Euler trajectory below threshold λ

Input: $X_0, t_0, v, D, r, \Delta t, \lambda$
Output: $\mathbf{X}^E, \mathbf{t}^E$

$X \coloneqq X_0$;
$t \coloneqq t_0$;
$\mathbf{X}^E \coloneqq \emptyset$;
$\mathbf{t}^E \coloneqq \emptyset$;
$t^\dagger \coloneqq t_r \sim \mathrm{Exp}(1/r)$;
while $X > 0$ **do**
  if $t \geq t^\dagger$ **then** ▷ `resetting condition`
    $X \coloneqq X_0$;
    $t \coloneqq t^\dagger + t_r, \quad$ where $t_r \sim \mathrm{Exp}(1/r)$;
  else
    $X \coloneqq X + \Delta X, \quad$ where $\Delta X \sim \mathcal{N}(v\,\Delta t, 2D\,\Delta t)$;
    $t \coloneqq \min\{t + \Delta t, t^\dagger\}$;
    if $X \geq 1$ **then** ▷ `reflection condition`
      $X \coloneqq 2 - X$;
  if $X < \lambda$ **then**
    append X to array $\mathbf{X}^E$;
    append t to array $\mathbf{t}^E$;

Algorithm B.3: Euler-Maruyama algorithm for FPT

Input: $X_0, v, D, r, \Delta t$
Output: τ_r

$X \coloneqq X_0$;
$t \coloneqq 0$;
$t^\dagger \coloneqq t_r \sim \mathrm{Exp}(1/r)$;
while $X > 0$ **do**
  if $t \geq t^\dagger$ **then** ▷ `resetting condition`
    $X \coloneqq X_0$;
    $t \coloneqq t^\dagger + t_r, \quad \text{where } t_r \sim \mathrm{Exp}(1/r)$;
  else
    $X \coloneqq X + \Delta X, \quad \text{where } \Delta X \sim \mathcal{N}(v\,\Delta t, 2D\,\Delta t)$;
    $t \coloneqq \min\{t + \Delta t, t^\dagger\}$;
    if $X \geq 1$ **then** ▷ `reflection condition`
      $X \coloneqq 2 - X$;
    else if $X \leq 0$ **then** ▷ `first passage/stopping condition`
      $\tau_r \coloneqq t$;

B.4 SMRA

This code uses the `multires` function found in Appendix B.1. This algorithm generates a Brownian trajectory $\mathbf{X}_k$, $\mathbf{t}_k$ and outputs its corresponding FPT with the absorbing boundary up to an error threshold ϵ.

Recall the simulation parameters $k^\dagger$ discussed in Section 4.2. Parameter $k^\dagger$ is the minimum resolution that the trajectory must have before resetting is allowed, while k^* is the maximum resolution before the FPT is recorded and the algorithm is stopped. Note that $k^* > k^\dagger$.

Algorithm B.4: SMRA

Input: $x_0, v, D, r, \epsilon, k^*$
Output: τ_r

1 $t_0 \coloneqq 0$;
2 $t^\dagger \coloneqq t' \sim \text{Exp}(1/r)$;
3 $k^\dagger \coloneqq -\left\lceil \dfrac{\log(\epsilon)}{\log(2)} \right\rceil$;
4 **while** $\delta_k > \epsilon$ **or** $k < k^*$ **do**
5 $k \coloneqq 0$;
6 $B_f \coloneqq B' \sim \mathcal{N}(x_0 + v(t^\dagger - t_0), 2D(t^\dagger - t_0))$;
7 $\mathbf{B} \coloneqq \{B_0, B_f\}$;
8 $\mathbf{t} \coloneqq \{t_0, t^\dagger\}$;
9 $\mathbf{X} \coloneqq \{x_0\}$;
10 **while** *all* $X \in \mathbf{X} > 0$ **or** $k < k^\dagger$ **do**
11 $k \coloneqq k + 1$;
12 $\delta_k \coloneqq \dfrac{t^\dagger}{2^k}$;
13 $\mathbf{B}, \mathbf{t} \coloneqq \texttt{multires}(\mathbf{B}, \mathbf{t}, D, k, t^\dagger)$;
14 **for** $j = 0$ **to** 2^k **do** ▷ `reflection condition`
15 $\Delta B_j \coloneqq B_{j+1} - B_j$;
16 $X_{j+1} \coloneqq \min\{X_j + \Delta B_j,\ 2 - (X_j + \Delta B_j)\}$;
17 **if** *any* $X \in \mathbf{X} < 0$ **and** $(\delta_k < \epsilon$ **or** $k > k^*)$ **then** ▷ `stopping condition`
18 $\tau_r = \inf\{t \in \mathbf{t} \mid X_t < 0\}$;
19 **break** loops in lines **3** and **9**
20 **else if** $k > k^\dagger$ **then** ▷ `resetting condition`
21 $t_0 \coloneqq t^\dagger$;
22 $t^\dagger \coloneqq t^\dagger + t', t' \sim \text{Exp}(1/r)$;
23 **break** loop in line **9** and **return** to line **3**
24 **else** ▷ `increase resolution`
25 **return** to line **9**

B.5 HMRA

This code uses both the `multires` function from Appendix B.1 and the `euler` function from Appendix B.2. The algorithm begins by generating an Euler-Maruyama trajectory $\mathbf{X}^E$ and $\mathbf{t}^E$ below the position threshold λ. Note that the reflections and resets have occurred in the initial Euler-Maruyama trajectory already.

Algorithm B.5: HMRA

Input: $X_0, v, D, r, \epsilon, \Delta t, k^*, \lambda$
Output: τ_r

1 $t_0 \coloneqq 0$;
2 $k \coloneqq 0$;
3 $\mathbf{X}^E, \mathbf{t}^E \coloneqq \texttt{euler}(X_0, t_0, v, D, r, \Delta t, \lambda)$;
4 $\mathbf{X}^L \coloneqq \emptyset$;
5 $\mathbf{t}^L \coloneqq \emptyset$;
6 **for** $i = 0$ **to** *length of array* $\mathbf{X}^E$ **do**
7 **if** $(t^E_{i+1} - t^E_i) \leq \Delta t$ **then**
8 $X^L_i \coloneqq \{X^E_i, X^E_{i+1}\}$;
9 $t^L_i \coloneqq \{t^E_i, t^E_{i+1}\}$;
10 **while** $\delta_k < \epsilon$ **do**
11 $k \coloneqq k + 1$;
12 $\delta_k \coloneqq \dfrac{t^\dagger}{2^k}$;
13 **for** $\ell = 0$ **to** *length of array* $\mathbf{X}^L$ **do**
14 $X' \coloneqq X^L_\ell$; ▷ `note:` $X^L_\ell = \{X^E_i, \ldots, X^E_{i+1}\}_\ell$
15 $t' \coloneqq t^L_\ell$; ▷ `note:` $t^L_\ell = \{t^E_i, \ldots, t^E_{i+1}\}_\ell$
16 $X^L_\ell, t^L_\ell \coloneqq \texttt{multires}(X', t', D, k, t^\dagger)$;
17 $\mathbf{X}^M \coloneqq$ flattened array of $\mathbf{X}^L$;
18 $\mathbf{t}^M \coloneqq$ flattened array of $\mathbf{t}^L$;
19 **if** *any* $X \in \mathbf{X}^M < 0$ **and** $(\delta_k < \epsilon$ **or** $k > k^*)$ **then** ▷ `stopping condition`
20 $\tau_r = \inf\{t \in \mathbf{t}^M \,|\, X^M_t < 0\}$;
21 **break** loop **10**
22 **else** ▷ `increase resolution`
23 **return** to line **10**

The loop at line 6 splits both $\mathbf{X}^E$ and $\mathbf{t}^E$ into an array of arrays $\mathbf{X}^L$ consisting consecutive elements of the original array, e.g. for $\mathbf{X}^E$: $\mathbf{X}^L = \{\{X^E_0, X^E_1\}, \{X^E_1, X^E_2\}, \ldots\}$. Each array element of both $\mathbf{X}^L$ and $\mathbf{t}^L$ is passed through `multires` and afterwards, the array of arrays is flattened back to a 1D array which is called $\mathbf{X}^M$ and $\mathbf{t}^M$, to check for the first passage and the stopping condition.

Chapter 4

Optimal switching strategies in multi-drug therapies for chronic diseases

Optimal switching strategies in multi-drug therapies for chronic diseases

Juan Magalang,[1,2] Javier Aguilar,[3] Jose Perico Esguerra,[4] Édgar Roldán,[5,*] and Daniel Sanchez-Taltavull[1,†]

[1] *Department of Visceral Surgery and Medicine, Inselspital, Bern University Hospital, University of Bern, Murtenstrasse 35, Bern, 3008, Switzerland*
[2] *Institute of Mathematical Statistics and Actuarial Science, University of Bern, Alpeneggstrasse 22, Bern, 3012, Switzerland*
[3] *Laboratory of Interdisciplinary Physics, Department of Physics and Astronomy "G. Galilei", University of Padova, Padova, Italy*
[4] *Theoretical Physics Group, National Institute of Physics, University of the Philippines Diliman, Quezon City, 1101, Philippines*
[5] *ICTP - The Abdus Salam International Centre for Theoretical Physics, Strada Costiera 11, Trieste, 34151, Italy*

(Dated: September 29, 2024)

Antimicrobial resistance is a threat to public health with millions of deaths linked to drug resistant infections every year. To mitigate resistance, common strategies that are used are combination therapies and therapy switching. However, the stochastic nature of pathogenic mutation makes the optimization of these strategies challenging. Here, we propose a two-scale stochastic model that considers the effective evolution of therapies in a multidimensional efficacy space, where each dimension represents the efficacy of a specific drug in the therapy. The diffusion of therapies within this space is subject to stochastic resets, representing therapy switches. The boundaries of the space, inferred from coarser pathogen-host dynamics, can be either reflecting or absorbing. Reflecting boundaries impede full recovery of the host, while absorbing boundaries represent the development of antimicrobial resistance, leading to therapy failure. We derive analytical expressions for the average absorption times, accounting for both continuous and discrete genomic changes using the frameworks of Langevin and Master equations, respectively. These expressions allow us to evaluate the relevance of times between drug-switches and the number of simultaneous drugs in relation to typical timescales for drug resistance development. We also explore realistic scenarios where therapy constraints are imposed to the number of administered therapies and/or their costs, finding non-trivial optimal drug-switching protocols that maximize the time before antimicrobial resistance develops while reducing therapy costs.

I. INTRODUCTION

Antimicrobial resistance has been recognized as a major threat to public health, with estimates of 4 million deaths associated with resistant bacterial infection in 2019 [1]. This resistance is a consequence of pathogenic evolution, affecting multiple diseases such as tuberculosis [2], HIV/AIDS [3, 4], cancer [5–7], among others. Drug resistant pathogens are more difficult to treat since conventional treatment procedures can no longer be used. This increases the risk of complications due to more aggressive drugs and the economic burden, estimating excess costs of one hundred thousand US dollars per case of multi-drug resistant tuberculosis in 2013 [8]. The extent and severity of drug resistance is expected to increase in the coming years [9, 10], creating the need to determine optimal treatment strategies to minimize the problem.

A common strategy that physicians use to avoid drug resistance is by combining multiple drugs [11, 12]. Combination therapies target multiple biological mechanisms of a pathogen, reducing the likelihood of developing resistances to all drugs combined. When resistances occur, physicians typically replace the therapy [4, 13, 14]. However, stochastic effects can play a role in either the detection of resistance [15, 16], managing adverse effects [17, 18], or the appearance of new drugs in the market [19] which is relevant for chronic illnesses. Therefore, to fully understand the problem we need to simultaneously account for the stochastic effects in therapy switching and the multiple components of combination therapy.

Mathematical models have been used to model drug resistance at different scales, from the biological mechanisms within a pathogen [20, 21], within-host dynamics [22–25], to its epidemiological and economic impact [26–28]. These models have been used to study the effectiveness of public health strategies that mitigate resistance, such as improving hygiene protocols, increasing surveillance, and regulating the use of antimicrobial drugs [26].

Our goal is to develop a mathematical model that can identify optimal strategies of therapy administration and therapy switching rates. In doing so, we present a two-scale mathematical model that describes the efficacy of therapies administered to a host. The first scale accounts for pathogenic evolution which results in changes to the therapy efficacy. This evolution is a direct consequence of pathogenic mutation which is inherently stochastic [29, 30]. The second scale accounts for host-pathogen dynamics of a chronic infection, such as HIV-1 [23, 24] and is linked to the first scale via the infection rate which is determined by the therapy efficacy.

Pathogenic evolution is modeled as a diffusion process

* edgar@ictp.it
† daniel.sanchez@unibe.ch

in multiple dimensions where the position represents the therapy efficacy and therapy changes are modeled using the framework of stochastic resetting [31, 32], which has found applications in biology since very recently [33–36]. While a faithful representation of evolutionary dynamics should bear the discreteness of genomic changes [30], continuous approximations of evolutionary pathways are also used [37] to ease the analysis. The efficacy space also includes a region representing therapy failure. Hence, drug resistance development becomes a first passage time problem [38]. Typically, stochastic resetting problems aim to minimize the first passage time [39–42], but the need to maximize this time emerges naturally in this problem, as it is equivalent to the drug resistance development time [43].

The paper is organized as follows: We first discuss the specifications of the model (Section II). Then we study the dependence of the model on its parameters (Section III) and the effect of imposing restrictions to the amount of administered therapies (Section IV). Finally, we summarize and discuss our results (Section V).

II. MULTI-DRUG STOCHASTIC MODELS

We are interested in modelling a host infected with a pathogen that accounts for the development of drug resistance in two time scales: pathogenic evolution and the host-pathogen dynamics. These two scales are linked by an infection rate, which determines the number of infected cells in the host-pathogen model, and it is reduced with the therapy efficacy, similar to previous models [23–25]. It is known that pathogenic evolution is influenced by more stochastic effects and has slower dynamics than the host-pathogen interactions [29, 30]. Hence, we choose to focus on the scale of evolution and the host-pathogen dynamics are assumed to be at the steady state. By modelling the fluctuation of therapy efficacy due to evolution, we aim to obtain approximations to the time at which drug resistance occurs, which we define as the *resistance development time* (RDT). This quantity is synonymous to the first passage time, defined as the time at which a stochastic process reaches a certain state [38].

Our model considers $N_T \geq 1$ simultaneous and independent therapies, of which the i^{th} therapy efficacy η_i undergoes evolution as a stochastic process. The therapy efficacy scales an infection rate, e.g. $\prod_{i=1}^{N_T}(1-\eta_i)\beta HI$, where β is a constant of infection and at a given time, H is the population of healthy, susceptible cells, and I is the population of actively-infecting cells. The form of the infection rate implies that therapy efficacy is bounded: $\eta_i \in [0,1)\,\forall i$. A therapy efficacy of $\eta_i = 1$ signifies a perfect therapy, as it removes the term for the infection rate. On the other hand, $\eta_i = 0$ refers to an absorbing boundary and signifies a complete failure of the therapy as it maximizes the rate. Figure 1 provides a sketch of the stochastic process being used to model how therapy efficacy changes over time. Further details of the host-pathogen model are given in Appendix A.

Note that it is not necessary for all N_T therapies to reach complete failure for the host to be in a critical state due to an infection of a drug-resistant pathogen. In fig. 1c, we begin to see a decrease in the number of healthy cells even with $\eta_i > 0$. Hence, we consider that the therapy efficacy is below a certain threshold for drug resistance to occur. In this work, we choose $\sqrt{\sum_{i=1}^{N_T}\eta_i^2} \leq \eta_{\min}$ as the condition for drug failure, with $\eta_{\min} = 0.4$.

An essential ingredient of our model is the inclusion of therapy switching at stochastic times. When a therapy is switched out with a different one, the pathogens are exposed to a new stimulus and therefore have to restart the drug resistance development process; we model such switches as a stochastic resetting process [31, 32]. Since we describe the evolution of the multi-therapy efficacy as a stochastic process, we may use the following multivariate stochastic differential equation (SDE)

$$\begin{aligned} \mathrm{d}\boldsymbol{\eta} = &\operatorname{diag}\left(\mathbf{1} - \boldsymbol{\mathcal{I}}_{\boldsymbol{\chi}}(t)\right)\left[\boldsymbol{\mu}(\boldsymbol{\eta},t)\mathrm{d}t + \sqrt{2D}\,\mathrm{d}\boldsymbol{W}(t)\right] \\ &+ \operatorname{diag}\left(\boldsymbol{\mathcal{I}}_{\boldsymbol{\chi}}(t)\right)(\boldsymbol{\eta}_0 - \boldsymbol{\eta}), \end{aligned} \tag{1}$$

where $\boldsymbol{\eta} = \{\eta_1, \eta_2, \ldots, \eta_{N_T}\}$ is a vector containing the N_T therapy efficacies, $\boldsymbol{\mu}(\boldsymbol{\eta}, t)$ is a drift vector affecting each of the therapies, D is the diffusivity (assumed to be isotropic), and $\boldsymbol{W}(t)$ a N_T-dimensional Wiener process. Pathogenic evolution tends towards mutating stronger resistances to improve its survival [29], as such we assume that the drift vector is biased towards therapy failure, $\boldsymbol{\mu}_i < 0$. The operator $\operatorname{diag}(\cdot)$ transforms a vector argument into a square diagonal matrix.

The quantity $\boldsymbol{\mathcal{I}}_{\boldsymbol{\chi}}(t)$ is a vector of indicator functions coupled with $\boldsymbol{\chi}$ that controls the return of the therapy efficacies to its corresponding initial value $\boldsymbol{\eta}_0$. This vector has elements $\mathcal{I}_{\chi_i}(t) = 1$ for $t \in \chi_i$, and $\mathcal{I}_{\chi_i}(t) = 0$ for $t \notin \chi_i$, where $\chi_i = \{0, t^*_{i,1}, t^*_{i,2}, \ldots\}$ for all $1 \leq i \leq N_T$. Here, χ_i is a sequence of partial sums of i.i.d. exponentially-distributed random numbers, i.e. $t^*_{i,j} - t^*_{i,j-1} \sim \mathrm{Exp}(\tau_i)$, with mean $1/\tau_i$, which is the therapy switching rate for the i^{th} therapy.

Solving the RDT statistics associated with the SDE (1) is rather challenging given the geometry of the boundary conditions $\eta_{\min}$ and standard techniques to solve this equation are not known to work [38, 44, 45]. We instead propose two models of an N_T-dimensional fluctuating therapy efficacy with therapy switching that are analogous to eq. (1) that exploits several symmetries and approximations in the space spanned by the therapy efficacy. The first method is a continuous-space model that reduces the dynamics of the multidimensional SDE which allows for the calculation analytical expressions of the mean RDT. The second method is a discrete-space model that explicitly shows the dynamics of the model and produces all the statistical quantities of the RDT.

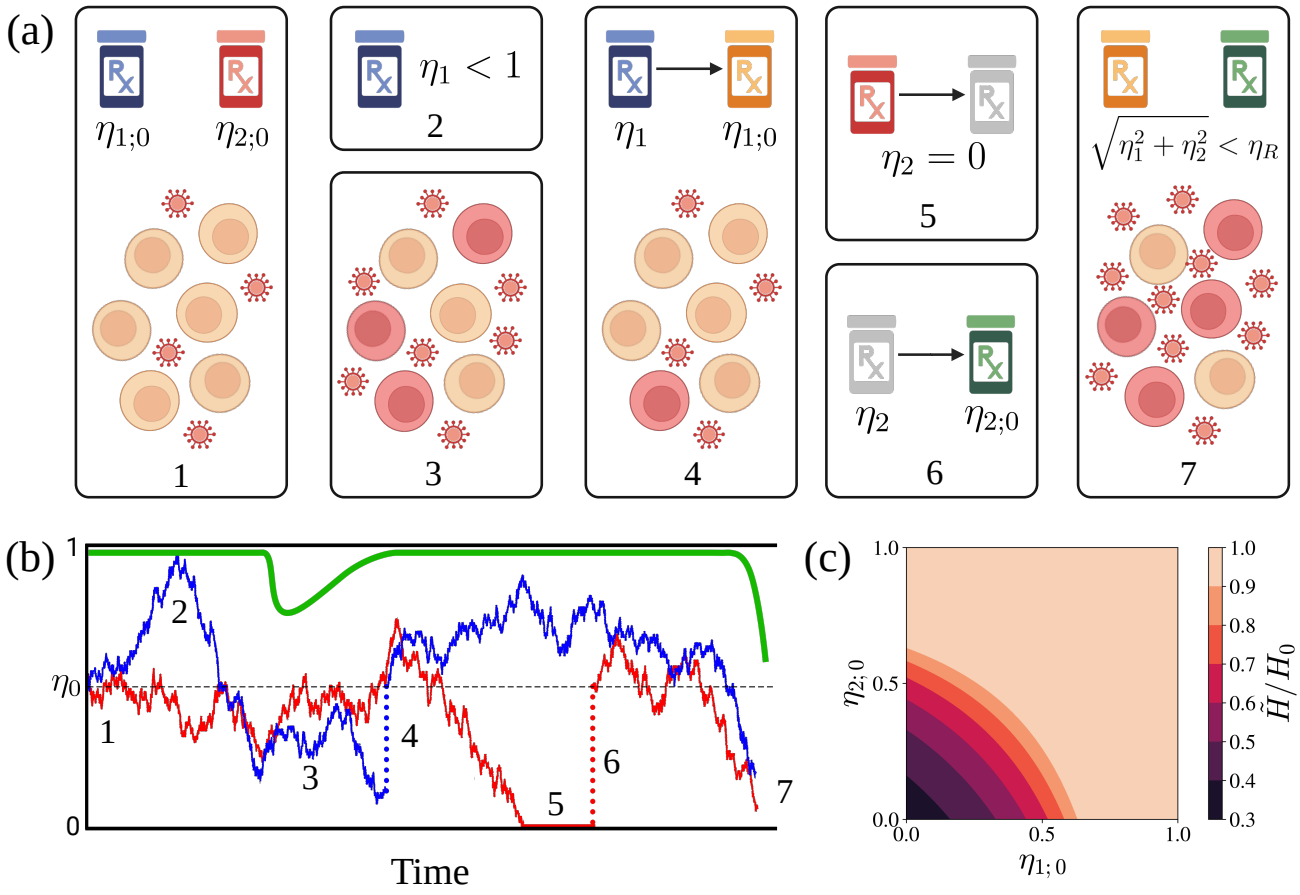

FIG. 1. Schematic representation of the two-scale mathematical model of drug resistance development in terms of the efficacy of an antimicrobial therapy. (a) A diagram showing the host-pathogen scale for two therapies, illustrating how drug resistance emerges and the impact of therapy changes. (b) Illustration of a stochastic trajectory of the efficacies of two therapies (in blue and red) and the normalized number of healthy cells (H/H_0, in green), showing the events described displayed in panel (a): (1) The initial value of therapy efficacy is shown as a black horizontal dashed line. (2) The therapy efficacy is bounded by a reflecting boundary at $\eta = 1$. (3) Healthy cells drop due to a decreases in efficacy of both therapies. (4) Switching one of the therapies. (5) *Partial* absorption due to one of the therapies failing, and does not decrease the healthy population due to the effect of the other therapy. (6) Switching the failed therapy. (7) Failure of both therapies leading to a decrease in the healthy cells down to a critical level. (c) Normalized number of healthy cells at equilibrium as a function of the therapy efficacies, showing the existence of a critical region when both efficacies are low. The analytical expression for the equilibrium of H is computed in Appendix A.

A. Coupled Continuous Model

In our first model of drug resistance development, we assume that the discrete changes in pathogen's genome are small enough to be considered continuous [37]. Furthermore, we consider that the behavior of the multi-drug therapy efficacy is expressed as a single parameter: $\eta = \sqrt{\sum_{i=1}^{N_T} \eta_i^2}$. This choice for the overall therapy efficacy is motivated by the absorbing boundary described in fig. 1c. We find that η evolves following the SDE:

$$\mathrm{d}\eta = (1 - \mathcal{I}_\chi(t)) \left[\frac{\tilde{v}}{\eta} \mathrm{d}t + D \mathrm{d}W(t) \right] + \mathcal{I}_\chi(t)(\eta_0 - \eta), \quad (2)$$

where $\tilde{v} = D[N_T - 1 - (v/D)]$ is an effective drift. Even if the process is one dimensional, the effective drift still depends explicitly on the number of dimensions N_T. Equation (2) also imposes a rotational symmetry in the efficacy space. This symmetry respects the absorbing boundary in fig. 1c, while allowing us to study the efficacy evolution of a therapy with an arbitrary number of drugs. A schematic of this model is found in fig. 2a for $N_T = 2$ and see the detailed derivation of eq. (2) in Appendix B. Using the formalism of the backward Fokker-Planck equation, We derive an analytical expression for the mean RDT conditioned to an initial efficacy η [45, 46],

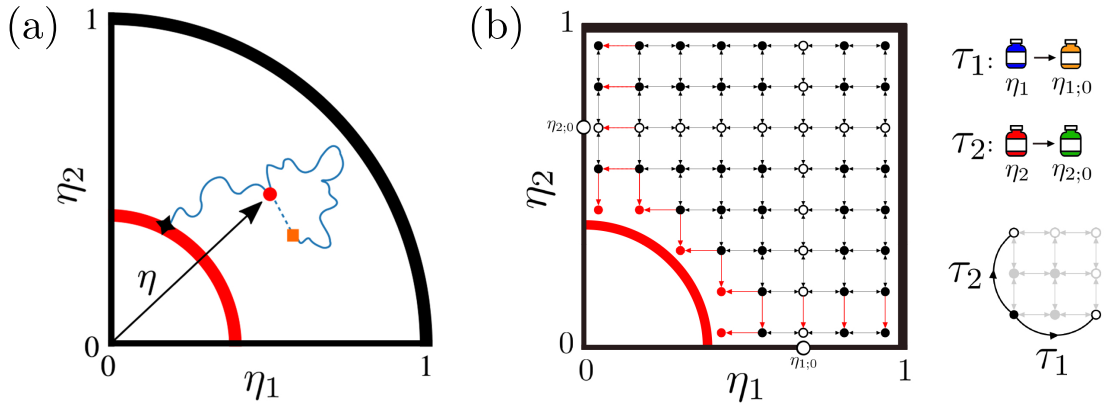

FIG. 2. Sketch of the coupled and uncoupled models for $N_T = 2$ for the efficacy of two drugs. (a) The coupled continuous model, with rotational symmetry and η as the distance from the origin. The trajectories start at the initial efficacy (dot), upon a therapy switch (square) the therapy efficacy goes back to the initial position, and the process stops when it reaches the absorbing region (star). (b) The uncoupled discrete model forms a lattice of $M \times M$ states, with each state corresponding to a value of the efficacy. Changes in therapy efficacy are transitions from one state to an adjacent state. Red states represent the absorbing states of the model. Upon a therapy switch in i^{th} therapy, the system returns to the points labelled in white, $\eta_{i;0}$. Efficacy $\eta_i = 1$ represent reflecting boundaries and $\eta_i = 0$ represents partially absorbing boundaries.

$$\langle T|\eta\rangle = \tau \frac{Y_d(-\mathrm{i}\overline{\eta}_{\max})\left[J_{d-1}\left(-\mathrm{i}\overline{\eta}\right) - \left(\eta/\eta_{\min}\right)^{d-1} J_{d-1}(-\mathrm{i}\overline{\eta}_{\min})\right] + J_d(-\mathrm{i}\overline{\eta}_{\max})\left[Y_{d-1}\left(-\mathrm{i}\overline{\eta}\right) - \left(\eta/\eta_{\min}\right)^{d-1} Y_{d-1}(-\mathrm{i}\overline{\eta}_{\min})\right]}{J_d(-\mathrm{i}\overline{\eta}_{\max})Y_{d-1}(-\mathrm{i}\overline{\eta}) - Y_d(-\mathrm{i}\overline{\eta}_{\max})J_{d-1}(-\mathrm{i}\overline{\eta})}. \tag{3}$$

Here, J_n, Y_n are the Bessel functions of order n of the first and second kind respectively, and $d = 2[(v/D)+N_T]$, where $(v/D) + N_T$ can be interpreted as an effective dimension of the efficacy space. We also introduced rescaled efficacies $\overline{\eta} = \lambda\eta$, $\overline{\eta}_{\min} = \lambda\eta_{\min}$, with $\lambda = (D\tau)^{-1/2}$ and $\overline{\eta}_{\max} = \lambda\eta_{\max}$, with $\eta_{\min}$ and $\eta_{\max}$ as the scaled radial locations of the absorbing and reflecting boundary respectively. The characteristic scale λ is an effective therapy switching rate proportional scaled by genetic diffusion. See Appendix B for the derivation of eq. (3) and further mathematical details.

B. Uncoupled Discrete Model

In the second model of drug resistance, we model the discrete phenotypic changes of a pathogen undergoing mutation [30] as chain of states. We assume that the chain of states is equally-spaced with M states, such that $\eta_i = j/M$, for $j = 0, \ldots, M-1$ and $i = 1, \ldots, N_T$. Transition rates control the evolution of η_i on the chain: rate p_i refers to an increase $\eta_i \to \eta_i + 1/M$, rate q_i refers to a decrease $\eta_i \to \eta_i - 1/M$, and rate $1/\tau_i$ refers to a therapy switch $\eta_i \to \eta_{i;0}$. This model independently evolves and switches the therapy efficacy for all N_T therapies.

For simultaneous therapies, we form a vector of therapy efficacies $\boldsymbol{\eta} = (\eta_1, \ldots, \eta_{N_T})^\top$, which is interpreted as an ordered coordinate, generalizing the chain of M states to an N_T-dimensional lattice of $M^{N_T} \times M^{N_T}$ states. A sketch of how this model is constructed is in fig. 2b for $N_T = 2$. Transitions between states on this lattice can be written as a transition matrix $\mathbf{W}$, and the evolution of the vector $\boldsymbol{\eta}$ is controlled by a master equation

$$\frac{\mathrm{d}p(\boldsymbol{\eta}, t)}{\mathrm{d}t} = \mathbf{W}p(\boldsymbol{\eta}, t), \tag{4}$$

where $p(\boldsymbol{\eta}, t)$ is a column vector of probabilities tracking all N_T therapy efficacies at each time. The details for the construction of the transition matrix $\mathbf{W}$ can be found in Appendix C. This formulation of the model also allows us to utilize simulation methods such as the Gillespie algorithm to generate the trajectories of $\boldsymbol{\eta}$ [47].

To compare the change in state space from continuous to discrete, we obtained an approximate SDE for the uncoupled model, via a Kramers-Moyal expansion [46, 48] that relates the discrete transition rates p_i and q_i to the continuous parameters v_i and D_i. The approximated SDE is a version of the general SDE in eq. (1) but where each N_T therapies evolving independently of one another,

$$\begin{aligned}\mathrm{d}\eta_i = &\left(1 - \mathcal{I}_{\chi_i}(t)\right)\left(-v_i\mathrm{d}t + D_i\mathrm{d}W_i(t)\right) \\ &+ \mathcal{I}_{\chi_i}(t)(\eta_{i;0} - \eta_i),\end{aligned} \tag{5}$$

for $1 \le i \le N_T$. The details of the approximation and how v_i and D_i relates to the discrete transition rates p_i and q_i are found in Appendix C.

We recall that the RDT is computed by taking the time at which the overall therapy efficacy $\sqrt{\sum_{i=1}^{N_T} \eta_i^2}$ reaches

below $\eta_{\min} = 0.4$. For this model, this condition is imposed by removing states and transitions on the lattice that fall below this condition. Consequently, the transition matrix $\mathbf{W}$ is modified as follows:

Let a and b be any two states on the lattice, i.e. $a \equiv (\eta_{1;a}, \dots \eta_{N_T;a})^\top$ and $b \equiv (\eta_{1;b}, \dots \eta_{N_T;b})^\top$. Matrix element W_{ba} will then refer to a transition from state a to state b. The absorbing boundary condition is written for any state on the lattice a and b as $W_{ba} = 0$ and $W_{aa} = 0$, if $\sqrt{\sum_{i=1}^{N_T} \eta_{i;a}^2} \leq \eta_{\min}$.

The full statistics of the RDT for a discrete space of states, e.g. the RDT distribution, mean RDT, and higher moments are known [49]. Let η, η_a, and η_i refer to states on the lattice, η_a is a state along the absorbing boundary, η is the initial state $\eta_0 \equiv (\eta_{1;0}, \dots, \eta_{N_T;0})$, and η_i is any state on the lattice that is neither η nor η_a. The mean time at which the therapy efficacy reaches an absorbing state η_a starting from the initial state η at time t is

$$\langle T|\eta\rangle = \sum_{\forall(\eta_i \to \eta_a)} \left[\mathbf{W}^\top\right]_{\eta_a,\eta_i} \left[(\mathbf{S}^{-1})^2\right]_{\eta_i,\eta}, \qquad (6)$$

where we sum over all single-step transitions that lead to the absorbing boundary $(\eta_i \to \eta_a), \forall \eta_i \neq \eta_a$. The matrix $\mathbf{S}$ is called the *survival* matrix equal to $\mathbf{W}$ with transition elements $(\eta \to \eta_a)$ set to zero, as discussed in [49].

III. RESISTANCE DEVELOPMENT TIME AS A FUNCTION OF THERAPY ADMINISTRATION STRATEGIES

First, we aim to determine the impact of multiple therapies on the overall dynamics, since it is known to induce non-linear effects in the overall efficacy [50]. In this section we investigate parameter regions to see how multiple therapies affect the mean RDT.

A. Switching rates and number of therapies may lead to detrimental effects

In fig. 3, we plot the mean RDT conditioned to the initial therapy efficacy $\langle T|\eta\rangle$ using the coupled model for therapies with and without drug switching. Figures 3a.1 and 3a.2 show that there is an increase in the overall differences between the curves of switching and non-switching as τ decreases. Similarly, figs. 3a.3 and 3a.4 show an increase in the difference between the two curves as N_T increases. This increase is consistent for any τ or N_T, as shown by the analytical results in figs. 3b.1 and 3b.2.

These differences between the curves quantify how much therapy switching may be beneficial or detrimental, as certain initial therapies yield a higher mean RDT for switching and non-switching. This is illustrated in fig. 3c. We also identify the intersection between the two curves η_{th} that marks the transition between the beneficial and detrimental regions. To quantify this difference, the area between the two curves is computed for $\eta_{th} \leq \eta < 1$, which we call S_+, and $0 \leq \eta < \eta_{th}$, S_-. Figures 3d.1 and 3d.2 show that S_+ and S_- decrease with increasing τ, but the opposite happens for increasing N_T, however S_- increases faster with increasing N_T than with τ. This means that if a patient starts N_T therapies with a low initial efficacy, then the detrimental effect is much greater if they choose to switch therapies, in terms of the decrease in the mean RDT.

The remaining parameters of the coupled model, v and D, do not introduce any new phenomenology beyond what is already present in τ and N_T. These parameters are discussed further in Appendix B 2.

B. Determining the probability of detrimental therapy change protocols

Areas where mean RDT is higher for a therapy with or without switching are also observed for the uncoupled model. However, uncoupling means that the therapies evolve independently of one another. The difference of the mean RDT with and without resetting is calculated for all the possible combinations of initial therapy efficacy for $N_T = 2$ in fig. 4. In this figure, the explicit beneficial and detrimental regions is illustrated in 2D space.

Figure 4a is consistent with the results in fig. 3, where the region where therapy switching is greater dominates when it is farther from the absorbing boundary. The same is observed in fig. 4b but for the uncoupled model solved using eq. (6). The uncoupled model allows for switching to be done for only one of the two therapies, as shown in fig. 4c, and the beneficial or detrimental regions now yield a non-trivial gradient. This gradient allows us to obtain insights of where the beneficial and detrimental regions are by using the initial efficacy of the non-switching therapy.

Figure 4d shows that the percentage of space occupied by the beneficial region. This quantity is of interest because it refers to the probability that the therapy design is beneficial for patients if the initial therapy efficacies $\boldsymbol{\eta}$ are uniformly distributed. The beneficial region does not vary much as the switching rate is increased for both the coupled model and for the case of the uncoupled model where both therapies have equal switching rates. This is however not the case for switching only one of the two therapies. The symmetry of the therapy efficacy space is relevant to estimate a priori the probability that a therapy design put patients at risk.

IV. LIMITING THERAPIES REVEALS OPTIMAL STRATEGIES

With the current form of the model, a trivial solution to maximizing the RDT would be an infinite reset rate. However, this infinite switching is not feasible in a re-

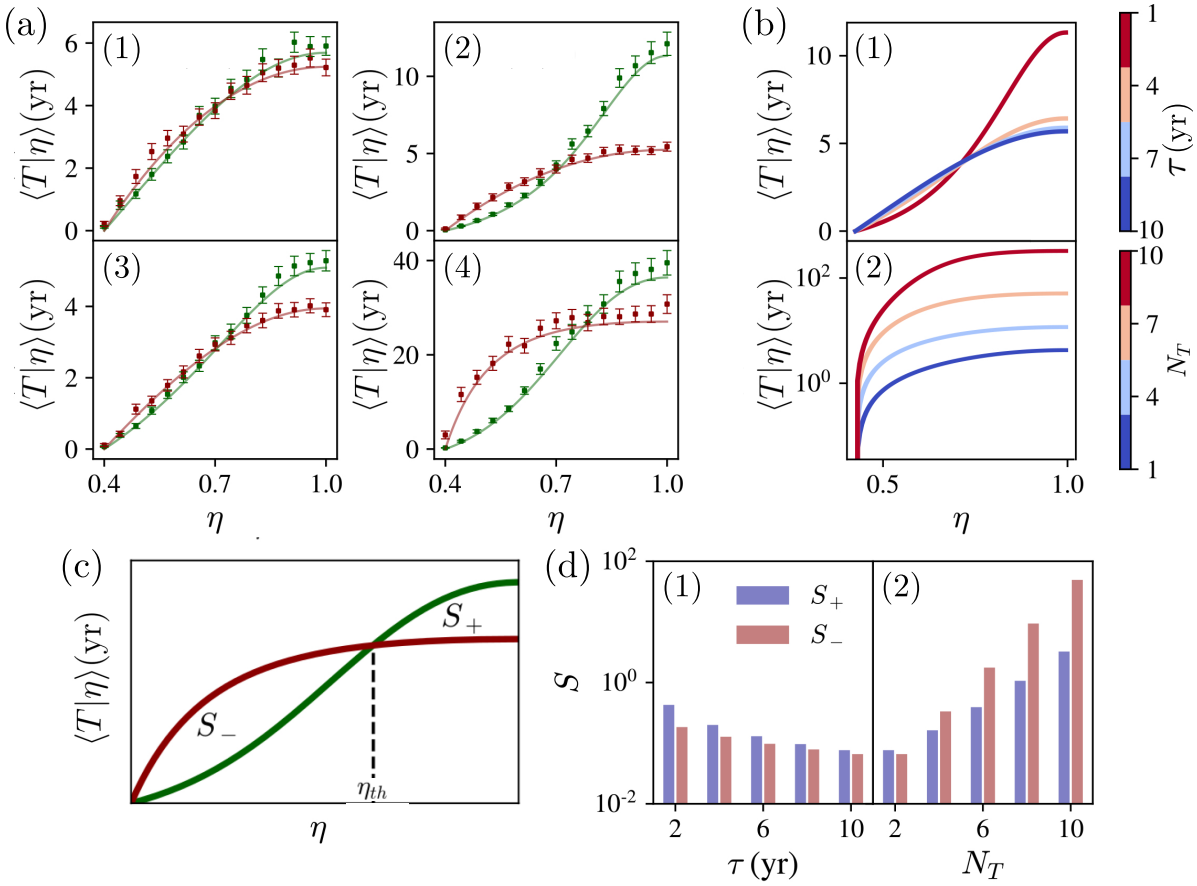

FIG. 3. (a) Mean RDT as a function of initial therapy efficacy for (a.1) $\tau = 10$ yrs and $N_T = 2$, (a.2) $\tau = 1$ yr and $N_T = 2$, (a.3) $N_T = 1$ and $\tau = 3$ yrs, and (a.4) $N_T = 6$ and $\tau = 3$ yrs. (b) Mean RDT as a function of initial therapy efficacy for (b.1) different values of τ and (b.2) different values of N_T. (c) An illustration of the curves for the mean RDT as a function of initial therapy efficacy with and without therapy switching, highlighting the intersection of the curves η_{th}, which define the boundaries of S_+ and S_-. (d) Differences between the areas under the curve before (red) and after (blue) η_{th} (d.1) as a function of τ with $N_T = 2$ and (d.2) as a function of N_T and $\tau = 3$ yrs. Parameters: $v = -8 \cdot 10^{-5}$ days^{-1} and $D = 10^{-4}$ days^{-1}.

alistic clinical scenario because the number of therapies available to a patient is limited. For this reason, in this section we study the effects of imposing limits or costs to a therapy switch. Additionally, we consider differences in the initial therapy efficacy for different therapies.

A. Impact of stochasticity in the initial efficacy

Our first approach to model limited resources in therapies is to include a minimum frequency between therapy switches ($\tau_{\min}$). Also we consider that the efficacy right after therapy switches is a random variable with a complex behavior reflecting the interplay drug-drug and patient-drugs. For simplicity, we assume that the therapy efficacy after switching is sampled from a uniform distribution on the entire therapy efficacy space. Thus we may define an unconditional mean RDT $\langle T\rangle$, which is the conditional mean RDT for the coupled model in eq. (3) integrated over all possible values that the therapy efficacy will take after switching,

$$\langle T\rangle = \frac{1}{\eta_{\max}^{N_T} - \eta_{\min}^{N_T}} \int d\eta\, \eta^{N_T-1}\, \langle T|\eta\rangle. \tag{7}$$

This expression is averaged over the total effective volume of the efficacy space $\eta_{\max}^{N_T} - \eta_{\min}^{N_T}$ for the coupled model, and the η^{N_T-1} term in the integral accounts for the Jacobian of the change form Cartesian to spherical coordinates. See Appendix E for further details.

Within this setting, and for fixed number of simultaneous drugs N_T, there is an optimal value for the average frequency between drug switches τ that maximizes the mean RDT. Furthermore, this optimal value for τ changes abruptly depending on N_T and $\tau_{\min}$. Indeed, we can define a phase S_1 in which the optimal strategy is to apply as many therapy changes as possible since $\tau = \tau_{\min}$. On the contrary, S_2 is another optimal strategy in which no therapy changes are applied, since $\tau \to \infty$.

Figures 5a and 5b show mean RDT curves that correspond to the two phases S_1 and S_2. The curves transi-

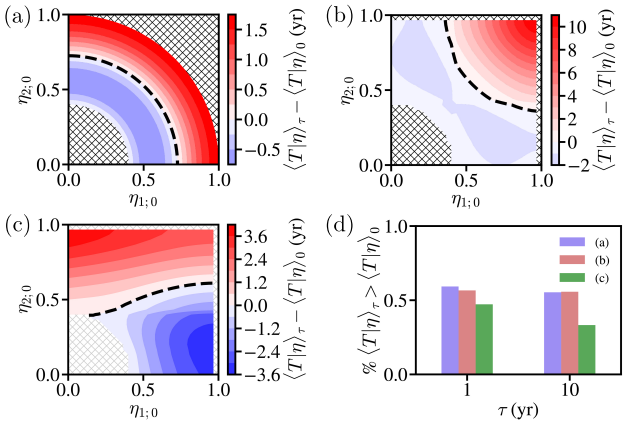

FIG. 4. Difference between the mean RDT with therapy switching and without therapy switching as a function of initial therapy efficacy for (a) the coupled continuous model, (b) uncoupled discrete model with switching allowed for both therapies, and (c) uncoupled discrete model with switching allowed only for 1 therapy η_1. Dashed lines indicate the region where the mean RDTs coincide. (d) The fraction occupied by the initial therapy states that the mean RDT with switching is higher than without switching as a function of τ. Parameters: $\tau = 3$, $N_T = 2$, $v = -8 \cdot 10^{-5}$ days^{-1} and $D = 10^{-4}$ days^{-1}.

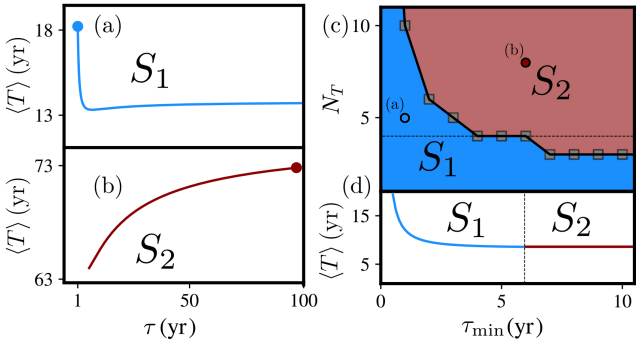

FIG. 5. Unconditional mean RDT as a function of τ for (a) a representative trajectory where the maximum RDT is at τ_{min} (S_1) for $N_T = 5$, $\tau_{min} = 1$ and (b) a representative trajectory where the maximum RDT is not at τ_{min} (S_2) for $N_T = 8$, $\tau_{min} = 6$. Solid dots correspond to the maximum RDT on each curve. (c) Phase diagram separating the regions for cases where the maximum RDT is and is not at τ_{min} as a function of N_T and τ_{min}. Solid dots on the phase diagram correspond to the representative curves in (a) and (b). (d) A transect of the phase diagram for $N_T = 4$, corresponding to the horizontal dotted line in (c).

tion from S_1 in fig. 5a to S_2 in fig. 5b by increasing the allowed minimum average therapy switching frequency from $\tau_{\min} = 1$ and $N_T = 5$ to $\tau_{\min} = 6$ and $N_T = 8$. In fig. 5c we show the boundary separating the phases as a function of N_T and $\tau_{\min}$, with a transect of this phase diagram is shown in fig. 5d. Therapy strategies in the phase S_2 may be more economic than those in S_1, since no drug switches are needed. Hence, for fixed $\tau_{\min}$, increasing the number of simultaneous therapies N_T to enter the phase S_2 could result in a more efficient strategy regarding both the maximization of the mean RDT and the minimization of the therapy costs.

B. Fixing limits and costs to switching therapies

Our next step is to simulate an explicit limit to the amount of therapy switches, let ℓ be the number of allowed switches and switching is no longer allowed after the ℓ^{th} switch. We can identify two methods of optimizing the mean RDT: first by varying the therapy change rate, and second by varying the number of simultaneous therapies.

First, we fix the number of simultaneous therapies to $N_T = 2$. We study the mean RDT as a function of the therapy switching rate for different numbers of allowed switching ℓ. The mean RDT is obtained using simulations of the uncoupled discrete model with the Gillespie algorithm using the transition matrix $\mathbf{W}$ as defined in eq. (4). In fig. 6a, we see a non-monotonic behavior for the mean RDT as the switching rate is varied. This suggests that given a limited number of therapies available, there is an optimal therapy switching rate that will maximize the mean RDT.

Next, we fix the reset rate τ while varying the number of simultaneous therapies N_T. We further constrain this by considering a total number of therapies A_T and that the number of therapies consumed at the ℓ^{th} switch is equal to the number of simultaneous therapies N_T. For example, given $A_T = 12$ total therapies available, for $N_T = 1$ simultaneous therapies then $\ell = 11$ switches are possible, for $N_T = 2$ we have $\ell = 5$, and so on. In general, for any number of N_T and A_T, the number of allowed switches is

$$\ell = \frac{A_T}{N_T} - 1. \tag{8}$$

The mean RDT for this version of limited resetting is computed using simulations of the coupled continuous model using the Euler-Maruyama algorithm of the SDE in eq. (2). Here we see for two orders of magnitude in D, we see a change in the behavior of the mean RDT from an increasing behavior for a larger D and a decreasing behavior for a smaller D. In the model, the diffusion constant D controls how much therapy efficacy fluctuates over time and is proportional to the mutation rate of the infecting pathogen. Figure 6b suggests that pathogens that mutate slower (i.e. smaller D) benefit from fewer simultaneous therapies and more limited resets, while the opposite is true for faster mutating pathogens.

Next, we consider that the therapy switching rate increases with the number of switches, which could reflect a cost [51, 52]. Suppose the number of therapies that have been administered at a certain time is γ, we replace

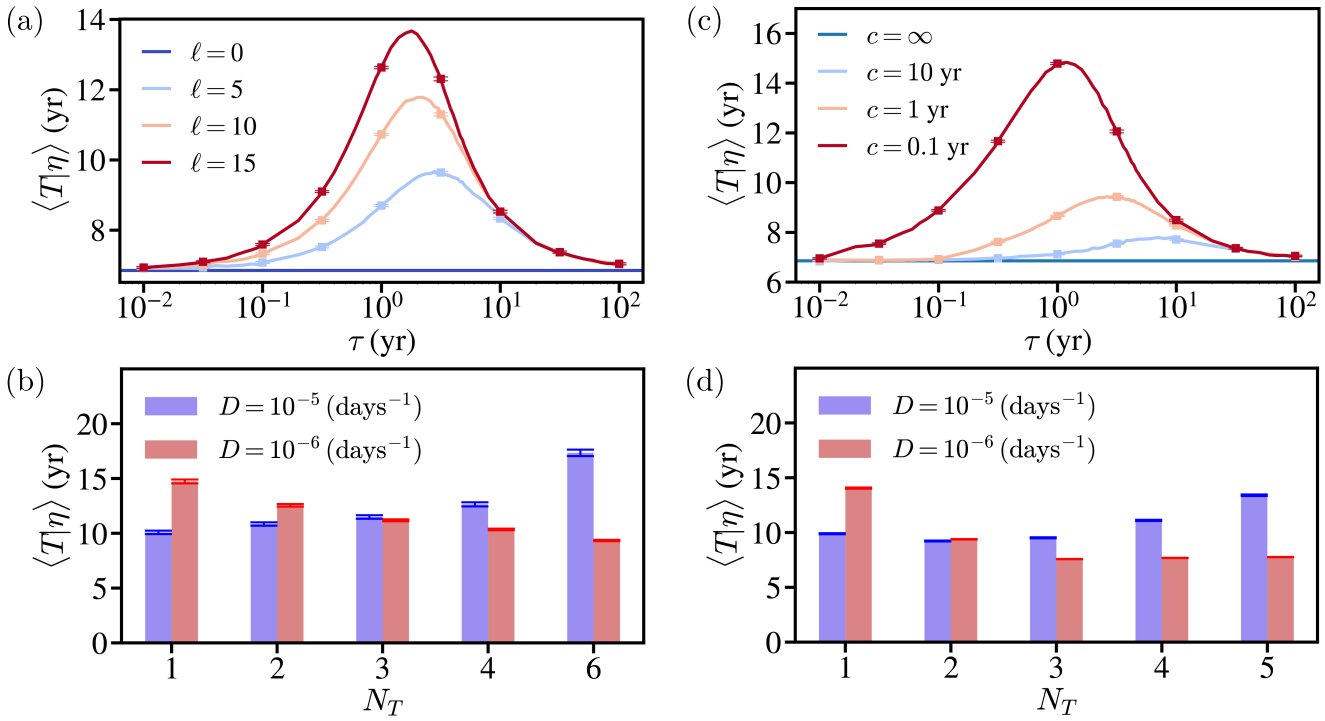

FIG. 6. Mean RDT with limited switching (a) as a function of τ and ℓ using the uncoupled discrete model, and (b) as a function of N_T, two values of D, $A_T = 12$ and ℓ according to eq. (8) using the coupled continuous model. Mean RDT with costed switching (c) as a function of τ and c using the uncoupled discrete model, and (d) as a function of N_T and two values of D using a cost function shown in eq. (10) using the coupled continuous model. Parameters: $v = -8 \cdot 10^{-5}$ days^{-1} and 10^6 simulations.

the therapy switching rate with a function,

$$C(\gamma) = \frac{1}{\tau} \exp\left(-\frac{c}{\tau}\gamma\right), \tag{9}$$

where c is a cost parameter that is proportional to the average time taken for new therapies to be made available to the host and τ is the therapy switching rate without cost. This function ensures that successive switches in the therapy $\gamma \to \infty$ diminishes the therapy switching rate $1/\tau \to 0$.

We see parallels in the simulations of fig. 6a to fig. 6c for the uncoupled discrete model and fig. 6b to fig. 6d for the coupled continuous model. Lower cost parameters c allow for more switching in a shorter amount of time emulating a limit in the therapies. Fixing the number of simultaneous therapies to $N_T = 2$, this results to an existence of an optimal switching rate that maximizes the RDT, as shown in fig. 6c taken from simulations using the Gillespie algorithm.

Furthermore, in fig. 6d, we see the RDT for two values of D for the coupled model. The cost function is altered for the coupled model, since we must consider that each therapy switch changes all N_T therapies at the same time. Lastly, we assume that increasing the number of simultaneous therapies in the coupled model becomes much costlier for each therapy switch, hence we assume that the cost parameter is dependent on N_T, suppose $c = 10^{N_T - 1}$. This yields a modified cost function for the coupled model

$$C(\gamma) = \frac{1}{\tau} \exp\left(-\frac{10^{N_T-1}}{\tau}\gamma\right). \tag{10}$$

Figure 6d suggests that more simultaneous therapies, although costlier, are beneficial for more volatile infections, i.e. higher D, with the opposite being true for lower D. These simulations are performed using the Euler-Maruyama algorithm.

V. DISCUSSION

In this work, we have presented and characterized a stochastic model to study therapy administration strategies that aim to reduce drug resistance development. In particular, we have identified how therapy switches and the combination of therapies impact the resistance development time with and without restrictions on the drug availability.

Our model has extended previous results on stochastic models of therapy administration [43] by accounting for multiple therapies administered to the host, which induce non-linear changes in the overall therapy efficacy [50]. We considered a therapy efficacy that scales the rate

of infection in a host-pathogen model of HIV-1 dynamics allowing us to study chronic diseases [23, 24]. Typically, therapy efficacy is included in the models as a constant rate or functional form for the rate of infection and mutation [20, 23–25, 53]. However, drug resistance can be modelled as a stochastic process [54], allowing our model to account for temporal changes in the therapy efficacy due to the noisy effects of pathogenic evolution.

Our first model is a continuous model that expresses the overall therapy efficacy of combination therapies in a single quantity and therapies are switched simultaneously. The second model, is a discrete model which explicitly accounts for each therapy efficacy independently, allowing for independent therapy switching. Given that therapy switching returns the efficacy to its original value, we were able to use stochastic resetting theory to study the process [32, 39]. The continuous coupled model eases the analytical study, but it has more limitations. On the other hand, the discrete uncoupled model allows for a more realistic study of the process, but it is computationally expensive.

Both models have shown that either increasing the number of simultaneous therapies or the switching rate increases the mean RDT, consistent with the literature on combination and sequential therapies [13, 21, 55–60]. These strategies exploit evolutionary trade-offs that pathogens develop after mutating. The models identified conditions in terms of initial efficacy, for therapy switching to be beneficial or detrimental to patient outcomes. The detrimental effect is observed in case studies where adverse effects have resulted from drug switching [19, 61]. When the switching rates are equal for all therapies, both models show similar results. However, with the discrete model, asymmetries in the switching rates are possible to study and yield qualitative differences in the beneficial and detrimental regions. This shows that using the uncoupled discrete model is necessary when each therapy have different impacts on the patient.

To make the models more realistic, we included restrictions in therapy switching. The different restrictions that we have considered are: a maximum therapy switching rate, limitations in the available therapies, and costs to therapy switching. These restrictions avoid unrealistic strategies such as an infinite therapy switching rate.

Imposing a maximum allowed therapy switching rate allowed us to study the uncertainty in the therapy efficacy after a switch. In this scenario, we identified two strategies: switch therapies as fast as allowed or to not switch at all. A phase diagram for these two strategies in terms of the number of therapies and maximum switching rate have been constructed, suggesting that increasing the number of simultaneous therapies may result to a state where switching therapies is no longer necessary.

Next, we introduced a limitation to the available of therapies by imposing either a finite number or a cost to therapy switching. This allowed us identify optimal values of therapy switching rates. This optimal rate suggests the existence of optimal clinical protocols. In particular, if the stochastic uncontrollable effects lead to the patient to be to the right of the maximum, it is possible to determine the frequency of clinical visits necessary to maximize the mean RDT while minimizing the cost for each visit. Moreover, we characterized the effect of varying the diffusion constant which determines the noise of the process and is correlated to the mutation rate of the infecting pathogen. We have seen that this leads to non-monotonic behavior in the mean RDT as a function of the number of therapies used.

Currently our work only considers a model of drug interaction where drugs are considered to be independent, hence the overall therapy efficacy in the infection rate is expressed as a product $\prod_{i=1}^{N_T}(1-\eta_i)$ [62, 63]. However, different modes of drug interactions may also suppress or amplify the overall therapy efficacy [21], changing the form of this expression. These interactions may also be simultaneous or sequential [50], potentially leading to changes in the optimal reset rates we identified. Furthermore, data obtained from empirical models of drug resistance maybe used to inform the model [64, 65]. While our work aims to study antimicrobial resistance, the model can easily be adapted to study drug resistance and drug switching in chronic or long-term illnesses without a pathogenic vector, such as diabetes [66], COPD [67], and hypertension [68–70].

Taken together, we have provided a mathematical scheme to the study of therapy administration strategies. We have shown and quantified how optimal therapy strategies in terms of therapy switching rates and number of therapies can significantly delay the occurrence of drug resistance within a host.

ACKNOWLEDGMENTS

This work was supported by the Ruth & Arthur Scherbarth Foundation, the UniBE ID Grant 2021, the Agencia Estatal de Investigación (AEI, MCI, Spain) MCIN/AEI/10.13039/501100011033 and Fondo Europeo de Desarrollo Regional (FEDER, UE) under Project APASOS (PID2021- 122256NB-C21/C22) and the María de Maeztu Program for units of Excellence in R&D, grant CEX2021- 001164-M.

[1] C. J. L. Murray and et al., The Lancet **399**, 629 (2022).
[2] D. Liebenberg, B. G. Gordhan, and B. D. Kana, Frontiers in Cellular and Infection Microbiology **12** (2022), 10.3389/fcimb.2022.943545.

[3] A. N. Phillips, J. Stover, V. Cambiano, F. Nakagawa, M. R. Jordan, D. Pillay, M. Doherty, P. Revill, and S. Bertagnolio, The Journal of Infectious Diseases **215**, 1362 (2017).

[4] H. Drechsler and W. G. Powderly, Clinical Infectious Diseases **35**, 1219–1230 (2002).

[5] N. Vasan, J. Baselga, and D. M. Hyman, Nature **575**, 299 (2019).

[6] A. Catalano, D. Iacopetta, J. Ceramella, D. Scumaci, F. Giuzio, C. Saturnino, S. Aquaro, C. Rosano, and M. S. Sinicropi, Molecules **27**, 616 (2022).

[7] J. Maltas, D. S. Tadele, A. Durmaz, C. D. McFarland, M. Hinczewski, and J. G. Scott, PRX Life **2**, 023010 (2024).

[8] N. R. Naylor, R. Atun, N. Zhu, K. Kulasabanathan, S. Silva, A. Chatterjee, G. M. Knight, and J. V. Robotham, Antimicrobial Resistance & Infection Control **7** (2018), 10.1186/s13756-018-0336-y.

[9] J. O'Neill, *Tackling drug-resistant infections globally: final report and recommendations* (Government of the United Kingdom, 2016).

[10] B. J. Langford, M. So, M. Simeonova, V. Leung, J. Lo, T. Kan, S. Raybardhan, M. E. Sapin, K. Mponponsuo, A. Farrell, *et al.*, The Lancet Microbe **4**, e179 (2023).

[11] M. Baym, L. K. Stone, and R. Kishony, Science **351**, aad3292 (2016).

[12] M. Tyers and G. D. Wright, Nature Reviews Microbiology **17**, 141 (2019).

[13] V. I. Band, D. A. Hufnagel, S. Jaggavarapu, E. X. Sherman, J. E. Wozniak, S. W. Satola, M. M. Farley, J. T. Jacob, E. M. Burd, and D. S. Weiss, Nature microbiology **4**, 1627 (2019).

[14] A. D. Haas, O. Keiser, E. Balestre, S. Brown, E. Bissagnene, C. Chimbetete, F. Dabis, M.-A. Davies, C. J. Hoffmann, P. Oyaro, R. Parkes-Ratanshi, S. J. Reynolds, I. Sikazwe, K. Wools-Kaloustian, D. M. Zannou, G. Wandeler, and M. Egger, The Lancet HIV **2**, e271–e278 (2015).

[15] O. Keiser, P. MacPhail, A. Boulle, R. Wood, M. Schechter, F. Dabis, E. Sprinz, and M. Egger, Tropical Medicine & International Health **14**, 1220–1225 (2009).

[16] S. J. Reynolds, G. Nakigozi, K. Newell, A. Ndyanabo, R. Galiwongo, I. Boaz, T. C. Quinn, R. Gray, M. Wawer, and D. Serwadda, AIDS **23**, 697–700 (2009).

[17] K. H. Mayer, H. Drechsler, and W. G. Powderly, Clinical Infectious Diseases **35**, 1219 (2002).

[18] I. Davidson, H. Beardsell, B. Smith, S. Mandalia, M. Bower, B. Gazzard, M. Nelson, and J. Stebbing, Antiviral Research **86**, 227 (2010).

[19] M. G. Kirby, P. Allchorne, T. Appanna, P. Davey, R. Gledhill, J. S. A. Green, D. Greene, and D. J. Rosario, International Journal of Clinical Practice **74** (2019), 10.1111/ijcp.13429.

[20] F. Pinheiro, O. Warsi, D. I. Andersson, and M. Lässig, Nature Ecology & Evolution **5**, 677–687 (2021).

[21] D. I. Andersson, H. Nicoloff, and K. Hjort, Nature Reviews Microbiology **17**, 479–496 (2019).

[22] T. Lee, S. Bonhoeffer, and M. Penny, Results in Physics **34**, 105181 (2022).

[23] L. Rong and A. S. Perelson, PLoS Computational Biology **5**, e1000533 (2009).

[24] A. P. Duncan Callaway, Bulletin of Mathematical Biology **64**, 29 (2002).

[25] O. Sharomi and A. Gumel, Journal of Biological Dynamics **2**, 323–345 (2008).

[26] A. M. Niewiadomska, B. Jayabalasingham, J. C. Seidman, L. Willem, B. Grenfell, D. Spiro, and C. Viboud, BMC Medicine **17** (2019), 10.1186/s12916-019-1314-9.

[27] H. Heesterbeek, R. M. Anderson, V. Andreasen, S. Bansal, D. De Angelis, C. Dye, K. T. D. Eames, W. J. Edmunds, S. D. W. Frost, S. Funk, T. D. Hollingsworth, T. House, V. Isham, P. Klepac, J. Lessler, J. O. Lloyd-Smith, C. J. E. Metcalf, D. Mollison, L. Pellis, J. R. C. Pulliam, M. G. Roberts, and C. Viboud, Science **347** (2015), 10.1126/science.aaa4339.

[28] N. T. Hillock, T. L. Merlin, J. Turnidge, and J. Karnon, Applied Health Economics and Health Policy **20**, 479–486 (2022).

[29] S. C. Manrubia, Current Opinion in Virology **2**, 531–537 (2012).

[30] A. Papkou, L. Garcia-Pastor, J. A. Escudero, and A. Wagner, Science **382**, eadh3860 (2023).

[31] M. R. Evans and S. N. Majumdar, Physical Review Letters **106**, 160601 (2011).

[32] M. R. Evans, S. N. Majumdar, and G. Schehr, Journal of Physics A: Mathematical and Theoretical **53**, 193001 (2020).

[33] T. Rotbart, S. Reuveni, and M. Urbakh, Physical Review E **92**, 060101 (2015).

[34] É. Roldán, A. Lisica, D. Sánchez-Taltavull, and S. W. Grill, Physical Review E **93**, 062411 (2016).

[35] A. Lisica, C. Engel, M. Jahnel, É. Roldán, E. A. Galburt, P. Cramer, and S. W. Grill, Proceedings of the National Academy of Sciences **113**, 2946 (2016).

[36] P. C. Bressloff, Journal of Physics A: Mathematical and Theoretical **53**, 355001 (2020).

[37] J. Wang, K. Zhang, L. Xu, and E. Wang, Proceedings of the National Academy of Sciences **108**, 8257 (2011).

[38] S. Redner, *A guide to first-passage processes* (Cambridge University Press, 2001).

[39] M. R. Evans and S. N. Majumdar, Journal of Physics A: Mathematical and Theoretical **44**, 435001 (2011).

[40] A. Pal and V. V. Prasad, Physical Review E **99** (2019), 10.1103/physreve.99.032123.

[41] L. Kuśmierz and E. Gudowska-Nowak, Physical Review E **92** (2015), 10.1103/physreve.92.052127.

[42] A. Pal and S. Reuveni, Physical Review Letters **118** (2017), 10.1103/physrevlett.118.030603.

[43] A. Ramoso, J. Magalang, D. Sánchez-Taltavull, J. Esguerra, and E. Roldán, EPL (Europhysics Letters) **132**, 50003 (2020).

[44] D. L. Dy and J. P. Esguerra, Phys. Rev. E **88**, 012121 (2013).

[45] C. Gardiner, in *Stochastic Methods*, Springer series in synergetics (Springer Berlin Heidelberg, Berlin, Heidelberg, 2008) pp. 1–22.

[46] N. G. V. Kampen, *Stochastic Processes in Physics and Chemistry* (Elsevier, 2007).

[47] D. T. Gillespie, The Journal of Physical Chemistry **81**, 2340–2361 (1977).

[48] D. T. Gillespie, The Journal of Chemical Physics **72**, 5363 (1980).

[49] P. E. Harunari, A. Dutta, M. Polettini, and E. Roldán, Physical Review X **12** (2022), 10.1103/physrevx.12.041026.

[50] R. Roemhild, T. Bollenbach, and D. I. Andersson, Nature Reviews Microbiology **20**, 478–490 (2022).

[51] J. C. Sunil, R. A. Blythe, M. R. Evans, and S. N. Majumdar, Journal of Physics A: Mathematical and Theoretical **56**, 395001 (2023).
[52] B. De Bruyne and F. Mori, Phys. Rev. Res. **5**, 013122 (2023).
[53] S. Baral, R. Raja, P. Sen, and N. M. Dixit, WIREs Systems Biology and Medicine **11** (2019), 10.1002/wsbm.1446.
[54] M. C. F. Prosperi, R. D'Autilia, F. Incardona, A. De Luca, M. Zazzi, and G. Ulivi, Bioinformatics **25**, 1040 (2008), https://academic.oup.com/bioinformatics/article-pdf/25/8/1040/50287497/bioinformatics_25_8_1040.pdf.
[55] H. Nicoloff, K. Hjort, B. R. Levin, and D. I. Andersson, Nature Microbiology **4**, 504–514 (2019).
[56] R. Roemhild and H. Schulenburg, Evolution, Medicine, and Public Health **2019**, 37–45 (2019).
[57] C. E. H. Rosenkilde, C. Munck, A. Porse, M. Linkevicius, D. I. Andersson, and M. O. A. Sommer, Nature Communications **10** (2019), 10.1038/s41467-019-08529-y.
[58] L. Imamovic and M. O. A. Sommer, Science Translational Medicine **5** (2013), 10.1126/scitranslmed.3006609.
[59] A. Batra, R. Roemhild, E. Rousseau, S. Franzenburg, S. Niemann, and H. Schulenburg, eLife **10** (2021), 10.7554/elife.68876.
[60] M. Oette, E. Schülter, M. Rosen-Zvi, Y. Peres, M. Zazzi, A. Sönnerborg, D. Struck, A. Altmann, R. Kaiser, and the EuResist Network Study Group, Intervirology **55**, 160 (2012), https://karger.com/int/article-pdf/55/2/160/2942682/000332018.pdf.
[61] J. Sochman and M. Podzimkova, International Journal of Cardiology **99**, 145–146 (2005).
[62] W. R. Greco, G. Bravo, and J. C. Parsons, Pharmacol. Rev. **47**, 331 (1995).
[63] C. I. BLISS, Annals of Applied Biology **26**, 585–615 (1939).
[64] D. Chen, G. Liu, H. Du, J. Wee, R. Wang, J. Chen, J. Shen, and G.-W. Wei, ArXiv (2024).
[65] P. Lamirande, E. A. Gaffney, M. Gertz, P. K. Maini, J. R. Crawshaw, and A. Caruso, arXiv preprint arXiv:2404.04086 (2024).
[66] H. E. Lebovitz and M. A. Banerji, European Journal of Pharmacology **490**, 135–146 (2004).
[67] F. Braido, F. Lavorini, F. Blasi, I. Baiardini, and G. W. Canonica, International Journal of Chronic Obstructive Pulmonary Disease , 2601 (2015).
[68] M. C. S. Wong, W. W. S. Tam, C. S. K. Cheung, E. L. H. Tong, A. C. H. Sek, G. John, N. T. Cheung, B. P. Y. Yan, C. M. Yu, S. Leeder, and S. Griffiths, PLoS ONE **8**, e53625 (2013).
[69] J. Václavík, P. Vysočanová, J. Seidlerová, P. Zajíček, O. Petrák, J. Dlask, and J. Krýza, Medicine **93**, e168 (2014).
[70] V. G. Athyros, K. Tziomalos, A. Karagiannis, and D. P. Mikhailidis, Expert Opinion on Pharmacotherapy **11**, 2943–2946 (2010).

Appendix A: Steady states of the host-pathogen model

The host-pathogen considered in this paper is a model of chronic infection, specifically HIV-1 [23, 24]. This model is modified to consider N_T simultaneous and independent therapies, each with an efficacy η_i. Each therapy efficacy is multiplied to one another, following the framework for independently-acting therapies [50, 62, 63]. This model tracks three cell populations: healthy cells H, latently-infecting cells L, and actively-infecting cells I:

$$\begin{aligned}\dot{H} &= \alpha - \lambda_H H - \beta H I \prod_{i=1}^{N_T}(1-\eta_i),\\ \dot{L} &= \epsilon\beta H I \prod_{i=1}^{N_T}(1-\eta_i) + pL - \frac{pL^2}{K} - a_L L - \lambda_L L,\\ \dot{I} &= (1-\epsilon)\beta H I \prod_{i=1}^{N_T}(1-\eta_i) + a_L L - \lambda_I I.\end{aligned} \tag{A1}$$

The rates and parameters of the model are described as follows: Healthy cells are generated with a constant rate of α and die at a rate of $\lambda_H H$, where λ_H is a death constant for healthy cells. Furthermore, these healthy cells are converted into either latently-infecting or actively infecting cells with a rate $\beta H I \prod_{i=1}^{N_T}(1-\eta_i)$, with β as a constant of infection and η as the therapy efficacy. Constant ϵ beside the infection rate in $\dot{L}$ is the probability that infection will yield a latently-infected cell. Conversely, $1-\epsilon$ beside the infection rate in $\dot{I}$ is the probability that the infection will yield and actively-infecting cell.

Latently-infecting cells proliferate with a rate pL, with p as a constant of proliferation, limited by a carrying capacity K with a rate $(pL^2)/K$, and die off with a rate $\lambda_L L$. Finally, latently-infecting cells can transform to actively-infecting cells with a rate aL, with a as a constant of activation, and actively-infecting cells die off with a rate of $\lambda_I I$.

We assume that the host-pathogen model is at equilibrium, hence we solve for the fixed points of the model by setting each equation in (A1) equal to zero and solving for H,L, and I, which we now denote as $\widetilde{H}$, $\widetilde{L}$, and $\widetilde{I}$. We first obtain a trivial fixed point at $\widetilde{H} = \alpha/\lambda_H, \widetilde{L} = 0, \widetilde{I} = 0$ and a non-trivial fixed point given by the following:

$$\begin{aligned}\widetilde{H} &= \frac{\alpha}{\lambda_H + b\widetilde{I}},\\ \widetilde{L} &= \frac{[\lambda_I b\widetilde{I} + (\lambda_I\lambda_H - (1-\epsilon)b\alpha)]\widetilde{I}}{a_L(b\widetilde{I} + \lambda_H)},\\ \widetilde{I} &= S + T - \frac{x_2}{3x_1}.\end{aligned} \tag{A2}$$

Where,

$$\begin{aligned}S &= \sqrt[3]{R + \sqrt{Q^3 + R^2}},\\ T &= \sqrt[3]{R - \sqrt{Q^3 + R^2}},\\ Q &= \frac{3x_1x_3 - x_2^2}{ax_1^2},\\ R &= \frac{9x_1x_2x_3 - 27x_1^2x_4 - 2x_2^2}{54x_1^3},\\ x_1 &= -p\lambda_I^2 b^2,\\ x_2 &= -(2p\lambda_I bc - dKa_L\lambda_I b^2),\\ x_3 &= \epsilon b^2\alpha K a_L^2 - pc^2 + dKa_L\lambda_H - \lambda_I b,\\ x_4 &= \epsilon b\alpha K a_L^2\lambda_H + dKa_L\lambda_H c,\\ b &= \prod_{i=1}^{N_T}(1-\eta_i)\beta,\\ c &= \lambda_I\lambda_H - (1-\epsilon)b\alpha,\\ d &= p - a_L - \lambda_L.\end{aligned} \tag{A3}$$

The fixed point $\widetilde{H}$ is used to compute the diagram in fig. 1c, where $\widetilde{H}$ is computed for $N_T = 2$ and varying η_1 and η_2. This maps the amount of healthy cells at equilibrium to the space of therapy efficacy.

The parameter values used to generate the diagram in fig. 1c are as follows:

Parameter	Description	Value	Unit
H_0	Initial H population	599326	cells/mL
L_0	Initial L population	45	cells/mL
I_0	Initial I population	11	cells/mL
α	Rate of H recruitment	6000	cells/(mL day)
λ_H	H death rate constant	0.01	1/day
η_i	Efficacy of the i^{th} therapy	varies	
N_T	Number of therapies	varies	
β	Infection rate constant	$5 \cdot 10^{-6}$	mL/day
ϵ	Fraction of infections yielding $H \to L$	0.01	
$1-\epsilon$	Fraction of infections yielding $H \to I$	0.99	
p	L proliferation rate constant	0.2	1/day
K	Carrying capacity of L cells	100	cells/mL
a_L	Activation rate constant of L cells	0.1	1/day
λ_L	L death rate constant	0.01	1/day
λ_I	I death rate constant	1	1/day

The values for H_0, L_0, and I_0 on the table have been calculated using eq. (A2) with $N_T = 2$ and $\eta_1 = \eta_2 = 0.8$.

Appendix B: Coupled model

1. Model derivation

In this section we derive eq. (2) from the main text. We will elaborate without including the possibility of executing stochastic resets, since the SDE with resets is readily obtained from the equation without resets adding the indicator functions with the process χ, as explained in the main text. Consider a general time-homogeneous multidimensional SDE in the Îto sense,

$$\mathrm{d}\boldsymbol{\eta} = \boldsymbol{\mu}(\boldsymbol{\eta})\mathrm{d}t + \boldsymbol{\sigma}(\boldsymbol{\eta})\mathrm{d}\boldsymbol{W}(t). \tag{B1}$$

The Fokker-Planck representation of such process reads

$$\partial_t \rho_t(\boldsymbol{\eta}) = -\nabla\cdot\left[\rho_t(\boldsymbol{\eta})\boldsymbol{\mu}(\boldsymbol{\eta})\right] + \nabla^2\left[\boldsymbol{\sigma}(\boldsymbol{\eta})\boldsymbol{\sigma}^{\intercal}(\boldsymbol{\eta})\rho_t\right]. \tag{B2}$$

The above equation is invariant under orthogonal transformations of the diffusion matrix. Indeed, let $\boldsymbol{S}$ be an orthogonal matrix such that $\boldsymbol{S}\boldsymbol{S}^{\intercal} = \boldsymbol{I}$, then the process

$$\mathrm{d}\boldsymbol{\eta} = \boldsymbol{\mu}(\boldsymbol{\eta})\mathrm{d}t + \boldsymbol{S}\boldsymbol{\sigma}(\boldsymbol{\eta})\mathrm{d}\boldsymbol{W}(t), \tag{B3}$$

is statistically indistinguishable from the process in eq. (B1) as both of them have the same associated Fokker-Planck equation.

Let us reduce the generality of the equations presented so far to adapt to the kind of models studied in the main text. In particular, we study isotropic and constant diffusion matrices,

$$\boldsymbol{\sigma} = \sqrt{2D}\boldsymbol{I}. \tag{B4}$$

Also, for the case of the coupled model we consider that therapies interact in such a way that the drift in the efficacy space is rotationally invariant,

$$\boldsymbol{\mu}(\boldsymbol{\eta}) = \boldsymbol{\eta} f(\eta), \tag{B5}$$

with $\eta = \sqrt{\boldsymbol{\eta}\cdot\boldsymbol{\eta}}$. Thus, the resulting rotationally invariant SDE reads

$$\mathrm{d}\boldsymbol{\eta} = \boldsymbol{\eta}\, f(\eta) + \sqrt{2D}\,\mathrm{d}\boldsymbol{W}(t). \tag{B6}$$

The idea now is to do a change of variables to spherical coordinates with one radius η and $N_T - 1$ angles $\phi_1, \ldots, \phi_{N_T-1}$ using Îto's rule [45, 46]. By doing so, we find that the radial drift only depends on η,

$$\sum_{i=1}^{N_T} \partial_{\eta_i}\eta\,\mathrm{d}\eta_i + D\partial^2_{\eta_i}\eta\,\mathrm{d}t = \left(\eta f(\eta) + D\frac{N_T-1}{\eta}\right)\mathrm{d}t. \tag{B7}$$

The radial diffusion will, in principle, depend both on the radial and angular variables. However, it can be shown that there is always an orthogonal transformation $\boldsymbol{S}$ making the evolution for the radial component independent of the angular variables,

$$\mathrm{d}\eta = \left(\eta f(\eta) + D\frac{N_T-1}{\eta}\right)\mathrm{d}t + \sqrt{2D}\,\mathrm{d}W(t). \tag{B8}$$

So far we did not make an explicit choice for the rotational invariant drift function f. Evolution will tend to make nocive agents more resistent to the therapy and with a velocity increasing as the therapy is less effective. A minimal choice of f reproducing such mechanisms reads

$$f(\eta) = -\frac{v}{\eta^2}. \tag{B9}$$

Introducing this choice for f in eq. (B8) together with the possibility of experience stochastic resets we obtain eq. (2) of the main text.

2. Effect of parameters

In the main text we analyzed in detail the effect of the number of simultaneous drugs in the therapy (N_T) and the average frequency between therapy switching, τ, in the average RDT (see Fig. 3 in the main text). Nevertheless, the coupled model depends on two more parameters: the diffusion constant D and the constant v tuning the radial drift. On the one hand, v only appears in our coupled model as a subtraction to the the number of simultaneous drugs. Therefore, we can analyze changes in the drift as effective changes in the number of therapies N_T, which was properly analyzed. Indeed, our model with parameter choice $v = v_0 + \Delta v$, $N_T = n_0$ produces the same results that realizations with $v = v_0$ and $N_T = n_0 - \Delta v/D$. Thus, no new phenomenology is expected when varying v. On the other hand the last free parameter D is also not relevant as it can be absorbed through a change of variables of the time. Thus choices on D can be seen as choices of time units.

3. Mean first passage times

The equation for conditioned mean RDT, $\langle T|\eta\rangle$, can be obtained using the backward Fokker-Planck equation formalism (see e.g. [45, 46]). In particular, from the adjoin Fokker-Planck operator associated to the coupled model [eq. (2)] follows the equation

$$\begin{aligned} D\frac{d-1}{\eta}\frac{\mathrm{d}}{\mathrm{d}\eta}\langle T|\eta\rangle + D\frac{\mathrm{d}^2}{\mathrm{d}\eta^2}\langle T|\eta\rangle \\ +\frac{1}{\tau}\left(\langle T|\eta_r\rangle - \langle T|\eta\rangle\right) = -1. \end{aligned} \tag{B10}$$

Where $d = v/D + N_T$, η is the initial efficacy of the therapy and η_r is the efficacy right after therapy switch. See further details on the derivation of eq.(B10) in [31, 39].

Using the change of variables $G(\eta) = -\langle T|\eta_r\rangle + \langle T|\eta\rangle$, eq. (B10) becomes

$$\frac{\mathrm{d}^2}{\mathrm{d}\eta^2}G(\eta) + \frac{d-1}{\eta}\frac{\mathrm{d}}{\mathrm{d}\eta}G(\eta) + \frac{1}{\lambda^2}G(\eta) = -\frac{1}{D}, \tag{B11}$$

with $\lambda = \sqrt{\tau D}$. Eq. (B11) has $G_p(\eta) = \tau$ as particular solution. The changes of variable $\eta = i\lambda\, x$, and $G(x) = g(x)\, x^{-\frac{d}{2}}$ transform the homogeneous part of the equation for G in a Bessel equation,

$$x^2 \frac{\mathrm{d}^2}{\mathrm{d}x^2} g(x) + x \frac{\mathrm{d}}{\mathrm{d}x} g(x) + (x - \beta^2) g(x) = 0, \tag{B12}$$

with $\beta = \frac{d}{2} - 1$. Therefore, the general solution for eq. (B10) reads

$$\langle T|\eta\rangle = \eta^{\beta} \left[c_1 J_{\beta}(-i\bar{\eta}) + c_2 Y_{\beta}(-i\bar{\eta})\right] + \tau + c_3. \tag{B13}$$

With $\bar{\eta} = \eta/\lambda$. Two of the three unknown constants of eq. (B13) are determined through the boundary conditions,

$$\langle T|\eta\rangle(\eta_{\min}) = 0, \tag{B14}$$

$$\frac{\mathrm{d}}{\mathrm{d}\eta} \langle T|\eta\rangle|_{\eta=\eta_{\max}} = 0, \tag{B15}$$

where $\eta_{\min}$ and $\eta_{\max}$ are the radial locations of the absorbing and reflecting boundary respectively. The third equation is provided by the self-consistent relation

$$\langle T|\eta_r\rangle = c_3. \tag{B16}$$

The resulting equation for the average absorption time with initial condition η and resetting state η_r reads

$$\begin{aligned} \frac{\langle T|\eta\rangle}{\tau} = & \frac{J_{\beta+1}(-i\bar{\eta}_{\max})}{Z(\eta_r)} \left(\left(\frac{\eta_r}{\eta_{\min}}\right)^{\beta} Y_{\beta}(-i\bar{\eta}_{\min}) \right. \\ & \left. + \left(\frac{\eta_r}{\eta}\right)^{\beta} Y_{\beta}(-i\bar{\eta}) \right) \\ & - \frac{Y_{\beta+1}(-i\bar{\eta}_{\max})}{Z(\eta_r)} \left(\left(\frac{\eta_r}{\eta_{\min}}\right)^{\beta} J_{\beta}(-i\bar{\eta}_{\min}) \right. \\ & \left. + \left(\frac{\eta_r}{\eta}\right)^{\beta} J_{\beta}(-i\bar{\eta}) \right), \end{aligned} \tag{B17}$$

with

$$\begin{aligned} Z(\eta) = & J_{\beta+1}(-i\bar{\eta}_{\max}) Y_{\beta}(-i\frac{\eta}{\lambda}) \\ & - Y_{\beta+1}(-i\bar{\eta}_{\max}) J_{\beta}(-i\frac{\eta}{\lambda}), \end{aligned} \tag{B18}$$

and $\bar{\eta} = \eta/\lambda$, $\bar{\eta}_{\max} = \eta_{\max}/\lambda$, and $\bar{\eta}_{\min} = \eta_{\min}/\lambda$. Eq. (3) is obtained from eq.(B17) fixing the resetting state to be equal to the initial condition of the process, $\eta_r = \eta$.

Appendix C: Derivation of uncoupled model

1. Markov chain transition rates

The transitions outlined in Section II B can be written as a Master equation:

$$\begin{aligned} \frac{\mathrm{d}p(\boldsymbol{\eta}, t)}{\mathrm{d}t} = & \sum_{i=1}^{N_T} \frac{1}{\tau_i} \delta(\eta_i - \eta_{i;0}) \\ & + p_i p\left(\eta_i - \frac{1}{M}, t\right) \\ & + q_i p\left(\eta_i + \frac{1}{M}, t\right) \\ & - \left(p_i + q_i + \frac{1}{\tau_i}\right) p(\eta_i, t)\,, \end{aligned} \tag{C1}$$

where $\eta_{i;0}$ is the initial therapy efficacy of the i^{th} therapy and $\delta(\eta_i - \eta_{i;0})$ is a Dirac delta function centered at the displacement of the current efficacy from the initial efficacy $\eta_i - \eta_{i;0}$. We note that this master equation is similar in form to the master equation presented in [31], but is generalized by considering a Markov process on a lattice.

Terms p_i and q_i are the Markov jump rates to adjacent states that respectively increase or decrease the therapy efficacy. Taking a Kramers-Moyal expansion to the above allows us to obtain a Fokker-Planck equation [46, 48]. This is done by performing a second-order Taylor expansion on the terms in the master equation that are shifted by $1/M$. This expansion is performed such that the $1/M$ terms will be factored outside of the propagators, i.e. Expanding $p(\eta_i + (1/M), \ldots, \eta_{N_T}, t)$ centered at $\eta_i + (1/M) = \eta_i$, $p(\eta_i - (1/M), \ldots, \eta_{N_T}, t)$ at $\eta_i - (1/M) = \eta_i$, and so on. Performing these expansions and simplifying,

$$\begin{aligned} \frac{\mathrm{d}p(\boldsymbol{\eta}, t)}{\mathrm{d}t} = & \sum_{i=1}^{N_T} \frac{1}{\tau_i} \delta(\eta_i - \eta_{1;0}) - \frac{1}{\tau_i} p(\eta_i, t) \\ & - \frac{p_i - q_i}{N} \frac{\partial p(\eta_i, t)}{\partial \eta_i} \\ & + \frac{p_i + q_i}{2M^2} \frac{\partial^2 p(\eta_i, t)}{\partial \eta_1^2} \end{aligned} \tag{C2}$$

with the following effective drift and diffusion parameters:

$$v_i = \frac{p_i - q_i}{M}, \quad D_i = \frac{p_i + q_i}{2M^2}. \tag{C3}$$

Inverting these parameters,

$$\begin{aligned} p_i &= \frac{1}{2}\left(2D_i M_i^2 + v_1 M_i\right) \\ q_i &= \frac{1}{2}\left(2D_i M_i^2 - v_i M_i\right). \end{aligned} \tag{C4}$$

We obtain the jump rates in the discrete space in terms of parameters used by the continuous space. As such, we

are able to use the master equation formulation by constructing a transition matrix as discussed in the following section.

2. Generating the transition matrix

Sums of transition rates p_i and q_i, and therapy switching rate $1/\tau_i$ occupy the elements of the transition matrix $\mathbf{W}$ in eq. (4). For any two states on the lattice a and b, $\mathbf{W}$ has positive elements W_{ab} referring to the transition rates from state b to a, and negative diagonal elements $W_{aa} = -\sum_{b\neq a} W_{ab}$ referring to the escape rates from state a.

In practice, to make the transition matrix $\mathbf{W}$, it is simpler to start with the transition matrix from a complete $M^{N_T} \times M^{N_T}$ lattice graph, and add and remove nodes and edges as needed until we end up with the desired graph. Adding and removing edges and nodes from the complete lattice is written as a sum of matrices, $\mathbf{W} = \mathbf{M} + \mathbf{R} - \mathbf{C} - \mathbf{P}$, where $\mathbf{M}$ is the transition matrix of the complete lattice, $\mathbf{R}$ refers to the transition matrix of transitions towards the set of reset states, $\mathbf{C}$ refers to transitions that lead towards the completely absorbing states, and $\mathbf{P}$ refers to transitions that lead towards the partially absorbing states. With this transition matrix, we may use expressions that are available to Markov chains [49] in computing for the RDT statistics, as discussed further in Section II B.

Appendix D: Behavior of η_{th}

Within the coupled model, η_{th} is defined as the threshold for the initial therapy efficacy separating detrimental therapies ($\eta < \eta_{\mathrm{th}}$) from beneficial therapies ($\eta > \eta_{\mathrm{th}}$). We can use our analytical expression in eq. (3) to compute η_{th} solving the equation

$$\langle T|\eta\rangle - \langle T|\eta\rangle_\infty = 0, \tag{D1}$$

where $\langle T|\eta\rangle_\infty$ is the average absorption time with no therapy switches,

$$\langle T|\eta\rangle_\infty = \lim_{\tau\to\infty} \langle T|\eta\rangle. \tag{D2}$$

In fig. 7a we show that η_{th} is not very sensible to changes in the typical time between resets (τ). Contrary, variations in the number of simultaneous drugs (N_T) will in general affect η_{th} (see fig. 7b).

If we assume that η is a random variable with uniform distribution, then the probability that $\eta > \eta_{\mathrm{th}}$ and the therapy design results beneficial for the patient reads

$$p = \frac{\eta_{\max}^{N_T} - \eta_{\mathrm{th}}^{N_T}}{\eta_{\max}^{N_T} - \eta_{\min}^{N_T}}. \tag{D3}$$

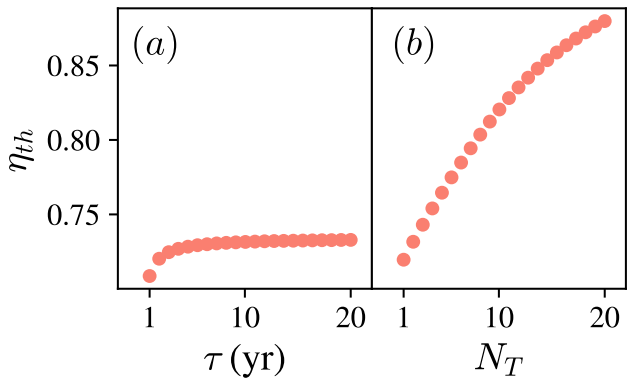

FIG. 7. Intersection of the mean RDT curves with and without resetting η_{th} (a) as a function of τ with $N_T = 2$, and (b) as a function of N_T with $\tau = 3$ (yr). Intersection η_{th} computed from the numerical solution of eq. (D2).

Appendix E: Unconditioned mean resistance development time

The unconditioned mean RDT is obtained from its conditioned version through marginalization,

$$\langle T\rangle = \int d\boldsymbol{\eta}\, \rho\,(\boldsymbol{\eta})\ \langle T|\boldsymbol{\eta}\rangle, \tag{E1}$$

where $\rho\,(\boldsymbol{\eta})$ is the distribution of therapy efficacy right after drug switch. When the distribution $\rho\,(\boldsymbol{\eta})$ is uniform, eq.(E1) becomes the integral of $\langle T|\boldsymbol{\eta}\rangle$ over all possible values of the therapy efficacy after therapy switch weighted by the volume of the efficacy space, which we call Ω,

$$\langle T\rangle = \frac{1}{\Omega}\int_\Omega d\boldsymbol{\eta}\,\langle T|\boldsymbol{\eta}\rangle, \tag{E2}$$

In the context of the coupled model, the conditioned expectation of T only depends on the radial distance $\eta = \sqrt{\boldsymbol{\eta}\cdot\boldsymbol{\eta}}$, and the volume of the efficacy space reads

$$\Omega = V(N_T)\left(\eta_{\max}^{N_T} - \eta_{\min}^{N_T}\right), \tag{E3}$$

where $V(N_T)$ is the volume of the hipersphere of N_T dimensions and unit radius. Integrating over angular variables and bearing in mind the Jacobian of the change of coordinates from Cartesian to spherical coordinates, the integral over the efficacy space for the coupled model can be rewritten as

$$\int_\Omega d\boldsymbol{\eta}\,\langle T|\boldsymbol{\eta}\rangle = V(N_T)\int_{\eta_{\min}}^{\eta_{\max}} d\eta\,\eta^{N_T-1}\langle T|\eta\rangle. \tag{E4}$$

Eq. (7) in the main text is obtained inserting eqs. (E3) and (E4) in eq. (E2).

Chapter 5

Discussion and Outlook

This thesis has introduced a model of drug resistance development within a host undergoing a chronic infection using an infection rate that evolves as a bounded Brownian motion with stochastic resetting in multiple dimensions. One of the boundaries is an absorbing state indicating the emergence of drug resistance as the infection rate is at its maximum. The time at which the process reaches this boundary is an important quantity to characterize as it is equivalent to the time at which a therapy has failed, which recasts the problem into a first passage time problem [51].

A thorough study of the probability distribution of the first passage time or resistance development time has been provided in this work, where novel analytical and simulation methods have been introduced to obtain this probability distribution. Methods to approximate the inversion of the Laplace transform of first passage time have been proposed to study rare events and long-term drug resistance times. On the other hand, for early events and short term resistance times, an error-variable simulation algorithm for Brownian motion has also been developed. Furthermore, the computation of the first passage time moments of a multidimensional Brownian motion in both continuous and discrete state spaces have also been derived in detail, with either choice in the state space specialized for clinical interventions that a physician may use to mitigate resistances. These are therapy switching and combination therapy, represented in the stochastic process by stochastic resetting and multidimensionality, respectively. Either strategy targets evolutionary trade-offs that a pathogen develops after mutation [26].

Administering a single therapy is a straightforward intervention to suppress an infection. This also allows for the focused study of the effects of therapy switching, which has been shown to increase therapy efficacy [16, 25]. The SDE in eq. (2.7) that was considered for single therapy scenarios is an arithmetic Brownian motion, which imposes a constant drift and diffusion coefficients. To extend the applicability of the model, other processes may be considered such as the Ornstein-Uhlenbeck process [53] with the SDE:

$$\mathrm{d}X_t = -vX_t\,\mathrm{d}t + \sqrt{2D}\,\mathrm{d}W_t. \tag{5.1}$$

Stochastic resetting in Ornstein-Uhlenbeck processes have also been studied, where a Laplace transform for the propagator of this process is known [113]. Ornstein-Uhlenbeck

processes are characterized by a position-dependent drift. In terms of the model, the drift parameter dictates how potent each mutation is in developing resistances and bringing the therapy efficacy to a minimum. The inclusion of a position-dependent drift will represent an effect in which mutations will tend to develop resistances faster since the therapy is creating a stronger selective pressure towards mutations with higher levels of resistance [1, 43].

Furthermore, closed-form approximations to the inversion of the Laplace transform of the FPT distribution have been derived in Chapter 3 called the PPF method, however it has a limited region of validity in the space of parameters due to strict conditions in the method that have been imposed. However, these conditions may be relaxed to consider a larger space of parameters. Recall that the first step of the PPF is to approximate a function $g_{m,n}(u)$ using the Padé approximation yielding a numerator $p_m(u) = \sum_{j=0}^{m} = a_j s^j$ and denominator $q_n(u) = \sum_{j=0}^{n} = b_j s^j$. This is followed by partial fraction decomposition (PFD) where the set of roots of $q_n(u)$ along with PFD coefficients are obtained. These are used in the last step which is the inversion. These last two steps may be generalized to include cases where the roots obtained from the denominator of the PFD are complex.

Proposition 5.0.1 (Laplace inversion with complex roots and coefficients obtained from PFD)**.** *The inversion with complex partial fraction decomposition roots and coefficients is given by*

$$f_{m,n}(t) = \sum_{j=1}^{n_1} \sum_{i=1}^{l_j} \frac{\gamma_{j,i}}{(i-1)!} t^{i-1} \exp(\alpha_j t) + \sum_{j=1}^{n_2} \sum_{i=1}^{l_j^\dagger} \frac{2R_{j,i}}{(i-1)!} t^{i-1} \exp(\phi_{j,i}\, \sigma_j t) \cos(\omega_j t + \phi_{j,i}), \tag{5.2}$$

for $t > 0$. The first sum of the expression corresponds to the n_1 real roots of the denominator, with roots α_j, multiplicities l_j, and coefficients $\gamma_{j,i}$. The second sum corresponds to the complex roots of the denominator, of which will always come in n_2 conjugate pairs $\alpha_j^\dagger, \overline{\alpha}_j^\dagger$ with coefficients $\gamma_{j,i}^\dagger, \overline{\gamma}_{j,i}^\dagger$. The coefficients of the complex sum are as follows:

$$\sigma_j = \mathrm{Re}(\alpha_j^\dagger), \quad \omega_j = \mathrm{Im}(\alpha_j^\dagger), \quad R_{j,i} = |\gamma_{j,i}^\dagger|, \quad \phi_{j,i} = \tan^{-1}\left(\frac{\mathrm{Im}(\gamma_{j,i}^\dagger)}{\mathrm{Re}(\gamma_{j,i}^\dagger)}\right) \tag{5.3}$$

The proof is outlined in Appendix A.5.

On the other hand, the usage of multiple therapies or combination therapies are also used to improve the efficacy of a therapy and have shown to have a nonlinear effect in the therapy efficacy as it changes over time [22, 23]. For example, highly active antiretroviral therapies for HIV-1 are a combination of two or more drugs that target different replication mechanisms of the virus [34]. Optimal choices between the number of therapies involved in combination therapy and therapy switching rates were discussed extensively in Chapter 4. However, it has been assumed that the therapies act independently of one another, this is called a null model of drug interaction and hence the efficacies for all therapies are multiplicative [27, 28]. To model synergistic

or antagonistic drug interactions, the fluctuation of each therapy must influence one another. In terms of the model, the multidimensional Brownian SDE is isotropic which means that the diffusion parameter D is constant. Anisotropic diffusion assumes the use of a diffusion matrix $\boldsymbol{\sigma}(\boldsymbol{X}_t, t)$ with nonzero diagonals that account for the interaction of each component of the Wiener process with one another.

Limited and costed resetting were also introduced in this chapter as a constraint to therapy switching. The inclusion of this constraint revealed optimal therapy switching rates that maximize the mean time to develop resistances. This optimal rate suggests the optimal time for a patient to receive a regular check-up by their physician as well, which can be modeled with deterministic resetting. Deterministic resetting is a predetermined and periodic reset of the stochastic process back to its initial position. The inclusion of deterministic resetting in the constrained stochastic resetting problem is hypothesized to show nontrivial optimal behavior among therapy administration strategies in terms of stochastic and deterministic therapy switching rates.

The distribution of times at which a therapy may fail within a host may be used in larger scales of infection as well. Agent-based models of an infectious disease that is prone to develop resistances may be used to model how fast drug resistant pathogens spread among populations of hosts. The agents, representing hosts, may sample from the resistance development time distribution to represent the time at which their within-host infection rate is at a maximum, increasing their individual pathogenic load, which also increases the probability to infect another host. With this model, the effectiveness of pharmaceutical interventions may be quantified such as the therapy administration strategies at epidemiological scales, as demonstrated similarly in [11, 13].

To conclude, this work has provided an extensive framework of a mathematical model of drug resistance in terms of the inherently noisy fluctuations caused by pathogenic mutation and therapy administration strategies that mitigate the development of resistance. Several mathematical techniques that compute for the probability distribution of the time at which drug resistance has emerged have been derived that highlight different scenarios and therapy administration strategies. These techniques have been used to demonstrate how optimal therapy administration strategies mitigate the development of drug resistance.

Bibliography

[1]S. Manrubia and E. Lazero, "Viral evolution", Physics of Life Reviews **3**, 65–92 (2006).

[2]D. Pillay and M. Zambon, "Antiviral drug resistance", BMJ : British Medical Journal **317**, 660–662 (1998).

[3]A. Papkou, L. Garcia-Pastor, J. A. Escudero, and A. Wagner, "A rugged yet easily navigable fitness landscape", Science **382** (2023).

[4]J. W. Drake, B. Charlesworth, D. Charlesworth, and J. F. Crow, "Rates of spontaneous mutation", Genetics **148**, 1667–1686 (1998).

[5]M. Kimura and T. Ohta, "Stepwise mutation model and distribution of allelic frequencies in a finite population.", Proceedings of the National Academy of Sciences **75**, 2868–2872 (1978).

[6]C. J. L. Murray, K. S. Ikuta, F. Sharara, L. Swetschinski, G. Robles Aguilar, A. Gray, C. Han, C. Bisignano, P. Rao, E. Wool, S. C. Johnson, A. J. Browne, M. G. Chipeta, F. Fell, S. Hackett, G. Haines-Woodhouse, B. H. Kashef Hamadani, E. A. P. Kumaran, B. McManigal, S. Achalapong, R. Agarwal, S. Akech, S. Albertson, J. Amuasi, J. Andrews, A. Aravkin, E. Ashley, F.-X. Babin, F. Bailey, S. Baker, B. Basnyat, A. Bekker, R. Bender, J. A. Berkley, A. Bethou, J. Bielicki, S. Boonkasidecha, J. Bukosia, C. Carvalheiro, C. Castañeda-Orjuela, V. Chansamouth, S. Chaurasia, S. Chiurchiù, F. Chowdhury, R. Clotaire Donatien, A. J. Cook, B. Cooper, T. R. Cressey, E. Criollo-Mora, M. Cunningham, S. Darboe, N. P. J. Day, M. De Luca, K. Dokova, A. Dramowski, S. J. Dunachie, T. Duong Bich, T. Eckmanns, D. Eibach, A. Emami, N. Feasey, N. Fisher-Pearson, K. Forrest, C. Garcia, D. Garrett, P. Gastmeier, A. Z. Giref, R. C. Greer, V. Gupta, S. Haller, A. Haselbeck, S. I. Hay, M. Holm, S. Hopkins, Y. Hsia, K. C. Iregbu, J. Jacobs, D. Jarovsky, F. Javanmardi, A. W. J. Jenney, M. Khorana, S. Khusuwan, N. Kissoon, E. Kobeissi, T. Kostyanev, F. Krapp, R. Krumkamp, A. Kumar, H. H. Kyu, C. Lim, K. Lim, D. Limmathurotsakul, M. J. Loftus, M. Lunn, J. Ma, A. Manoharan, F. Marks, J. May, M. Mayxay, N. Mturi, T. Munera-Huertas, P. Musicha, L. A. Musila, M. M. Mussi-Pinhata, R. N. Naidu, T. Nakamura, R. Nanavati, S. Nangia, P. Newton, C. Ngoun, A. Novotney, D. Nwakanma, C. W. Obiero, T. J. Ochoa, A. Olivas-Martinez, P. Olliaro, E. Ooko, E. Ortiz-Brizuela, P. Ounchanum, G. D. Pak, J. L. Paredes, A. Y. Peleg, C. Perrone, T. Phe, K. Phommasone, N. Plakkal, A. Ponce-de-Leon, M. Raad, T. Ramdin, S. Rattanavong, A. Riddell, T. Roberts, J. V. Robotham, A. Roca, V. D. Rosenthal, K. E.

Rudd, N. Russell, H. S. Sader, W. Saengchan, J. Schnall, J. A. G. Scott, S. Seekaew, M. Sharland, M. Shivamallappa, J. Sifuentes-Osornio, A. J. Simpson, N. Steenkeste, A. J. Stewardson, T. Stoeva, N. Tasak, A. Thaiprakong, G. Thwaites, C. Tigoi, C. Turner, P. Turner, H. R. van Doorn, S. Velaphi, A. Vongpradith, M. Vongsouvath, H. Vu, T. Walsh, J. L. Walson, S. Waner, T. Wangrangsimakul, P. Wannapinij, T. Wozniak, T. E. M. W. Young Sharma, K. C. Yu, P. Zheng, B. Sartorius, A. D. Lopez, A. Stergachis, C. Moore, C. Dolecek, and M. Naghavi, "Global burden of bacterial antimicrobial resistance in 2019: a systematic analysis", The Lancet **399**, 629–655 (2022).

[7]M. Naghavi, S. E. Vollset, K. S. Ikuta, L. R. Swetschinski, A. P. Gray, E. E. Wool, G. Robles Aguilar, T. Mestrovic, G. Smith, C. Han, R. L. Hsu, J. Chalek, D. T. Araki, E. Chung, C. Raggi, A. Gershberg Hayoon, N. Davis Weaver, P. A. Lindstedt, A. E. Smith, U. Altay, N. V. Bhattacharjee, K. Giannakis, F. Fell, B. McManigal, N. Ekapirat, J. A. Mendes, T. Runghien, O. Srimokla, A. Abdelkader, S. Abd-Elsalam, R. G. Aboagye, H. Abolhassani, H. Abualruz, U. Abubakar, H. J. Abukhadijah, S. Aburuz, A. Abu-Zaid, S. Achalapong, I. Y. Addo, V. Adekanmbi, T. E. Adeyeoluwa, Q. E. S. Adnani, L. A. Adzigbli, M. S. Afzal, S. Afzal, A. Agodi, A. J. Ahlstrom, A. Ahmad, S. Ahmad, T. Ahmad, A. Ahmadi, A. Ahmed, H. Ahmed, I. Ahmed, M. Ahmed, S. Ahmed, S. A. Ahmed, M. A. Akkaif, S. Al Awaidy, Y. Al Thaher, S. O. Alalalmeh, M. T. AlBataineh, W. A. Aldhaleei, A. A. S. Al-Gheethi, N. B. Alhaji, A. Ali, L. Ali, S. S. Ali, W. Ali, K. Allel, S. Al-Marwani, A. Alrawashdeh, A. Altaf, A. B. Al-Tammemi, J. A. Al-Tawfiq, K. H. Alzoubi, W. A. Al-Zyoud, B. Amos, J. H. Amuasi, R. Ancuceanu, J. R. Andrews, A. Anil, I. A. Anuoluwa, S. Anvari, A. E. Anyasodor, G. L. C. Apostol, J. Arabloo, M. Arafat, A. Y. Aravkin, D. Areda, A. Aremu, A. A. Artamonov, E. A. Ashley, M. O. Asika, S. S. Athari, M. M. W. Atout, T. Awoke, S. Azadnajafabad, J. M. Azam, S. Aziz, A. Y. Azzam, M. Babaei, F.-X. Babin, M. Badar, A. A. Baig, M. Bajcetic, S. Baker, M. Bardhan, H. J. Barqawi, Z. Basharat, A. Basiru, M. Bastard, S. Basu, N. S. Bayleyegn, M. A. Belete, O. O. Bello, A. Beloukas, J. A. Berkley, A. S. Bhagavathula, S. Bhaskar, S. S. Bhuyan, J. A. Bielicki, N. I. Briko, C. S. Brown, A. J. Browne, D. Buonsenso, Y. Bustanji, C. G. Carvalheiro, C. A. Castañeda-Orjuela, M. Cenderadewi, J. Chadwick, S. Chakraborty, R. M. Chandika, S. Chandy, V. Chansamouth, V. K. Chattu, A. A. Chaudhary, P. R. Ching, H. Chopra, F. R. Chowdhury, D.-T. Chu, M. Chutiyami, N. Cruz-Martins, A. G. da Silva, O. Dadras, X. Dai, S. D. Darcho, S. Das, F. P. De la Hoz, D. M. Dekker, K. Dhama, D. Diaz, B. F. R. Dickson, S. G. Djorie, M. Dodangeh, S. Dohare, K. G. Dokova, O. P. Doshi, R. K. Dowou, H. L. Dsouza, S. J. Dunachie, A. M. Dziedzic, T. Eckmanns, A. Ed-Dra, A. Eftekharimehrabad, T. C. Ekundayo, I. El Sayed, M. Elhadi, W. El-Huneidi, C. Elias, S. J. Ellis, R. Elsheikh, I. Elsohaby, C. Eltaha, B. Eshrati, M. Eslami, D. W. Eyre, A. O. Fadaka, A. F. Fagbamigbe, A. Fahim, A. Fakhri-Demeshghieh, F. O. Fasina, M. M. Fasina, A. Fatehizadeh, N. A. Feasey, A. Feizkhah, G. Fekadu, F. Fischer, I. Fitriana, K. M. Forrest, C. Fortuna Rodrigues, J. E. Fuller, M. A. Gadanya, M. Gajdács, A. P. Gandhi, E. E. Garcia-Gallo, D. O. Garrett, R. K. Gautam, M. W. Gebregergis, M. Gebrehiwot, T. G. Gebremeskel, C.

Geffers, L. Georgalis, R. M. Ghazy, M. Golechha, D. Golinelli, M. Gordon, S. Gulati, R. D. Gupta, S. Gupta, V. K. Gupta, A. D. Habteyohannes, S. Haller, H. Harapan, M. L. Harrison, A. I. Hasaballah, I. Hasan, R. S. Hasan, H. Hasani, A. H. Haselbeck, M. S. Hasnain, I. I. Hassan, S. Hassan, M. S. Hassan Zadeh Tabatabaei, K. Hayat, J. He, O. E. Hegazi, M. Heidari, K. Hezam, R. Holla, M. Holm, H. Hopkins, M. M. Hossain, M. Hosseinzadeh, S. Hostiuc, N. R. Hussein, L. D. Huy, E. D. Ibáñez-Prada, A. Ikiroma, I. M. Ilic, S. M. S. Islam, F. Ismail, N. E. Ismail, C. D. Iwu, C. J. Iwu-Jaja, A. Jafarzadeh, F. Jaiteh, R. Jalilzadeh Yengejeh, R. D. G. Jamora, J. Javidnia, T. Jawaid, A. W. J. Jenney, H. J. Jeon, M. Jokar, N. Jomehzadeh, T. Joo, N. Joseph, Z. Kamal, K. K. Kanmodi, R. S. Kantar, J. A. Kapisi, I. M. Karaye, Y. S. Khader, H. Khajuria, N. Khalid, F. Khamesipour, A. Khan, M. J. Khan, M. T. Khan, V. Khanal, F. F. Khidri, J. Khubchandani, S. Khusuwan, M. S. Kim, A. Kisa, V. A. Korshunov, F. Krapp, R. Krumkamp, M. Kuddus, M. Kulimbet, D. Kumar, E. A. P. Kumaran, A. Kuttikkattu, H. H. Kyu, I. Landires, B. K. Lawal, T. T. T. Le, I. M. Lederer, M. Lee, S. W. Lee, A. Lepape, T. L. Lerango, V. S. Ligade, C. Lim, S. S. Lim, L. W. Limenh, C. Liu, X. Liu, X. Liu, M. J. Loftus, H. I. M Amin, K. L. Maass, S. B. Maharaj, M. A. Mahmoud, P. Maikanti-Charalampous, O. M. Makram, K. Malhotra, A. A. Malik, G. D. Mandilara, F. Marks, B. A. Martinez-Guerra, M. Martorell, H. Masoumi-Asl, A. G. Mathioudakis, J. May, T. A. McHugh, J. Meiring, H. N. Meles, A. Melese, E. B. Melese, G. Minervini, N. S. Mohamed, S. Mohammed, S. Mohan, A. H. Mokdad, L. Monasta, A. Moodi Ghalibaf, C. E. Moore, Y. Moradi, E. Mossialos, V. Mougin, G. D. Mukoro, F. Mulita, B. Muller-Pebody, E. Murillo-Zamora, S. Musa, P. Musicha, L. A. Musila, S. Muthupandian, A. J. Nagarajan, P. Naghavi, F. Nainu, T. S. Nair, H. H. R. Najmuldeen, Z. S. Natto, J. Nauman, B. P. Nayak, G. T. Nchanji, P. Ndishimye, I. Negoi, R. I. Negoi, S. A. Nejadghaderi, Q. P. Nguyen, E. A. Noman, D. C. Nwakanma, S. O'Brien, T. J. Ochoa, I. A. Odetokun, O. A. Ogundijo, T. R. Ojo-Akosile, S. R. Okeke, O. C. Okonji, A. T. Olagunju, A. Olivas-Martinez, A. A. Olorukooba, P. Olwoch, K. I. Onyedibe, E. Ortiz-Brizuela, O. Osuolale, P. Ounchanum, O. T. Oyeyemi, M. P. P A, J. L. Paredes, R. R. Parikh, J. Patel, S. Patil, S. Pawar, A. Y. Peleg, P. Peprah, J. Perdigão, C. Perrone, I.-R. Petcu, K. Phommasone, Z. Z. Piracha, D. Poddighe, A. J. Pollard, R. Poluru, A. Ponce-De-Leon, J. Puvvula, F. N. Qamar, N. H. Qasim, C. D. Rafai, P. Raghav, L. Rahbarnia, F. Rahim, V. Rahimi-Movaghar, M. Rahman, M. A. Rahman, H. Ramadan, S. K. Ramasamy, P. S. Ramesh, P. W. Ramteke, R. K. Rana, U. Rani, M.-M. Rashidi, D. Rathish, S. Rattanavong, S. Rawaf, E. M. M. Redwan, L. F. Reyes, T. Roberts, J. V. Robotham, V. D. Rosenthal, A. G. Ross, N. Roy, K. E. Rudd, C. J. Sabet, B. A. Saddik, M. R. Saeb, U. Saeed, S. Saeedi Moghaddam, W. Saengchan, M. Safaei, A. Saghazadeh, N. Saheb Sharif-Askari, A. Sahebkar, S. S. Sahoo, M. Sahu, M. Saki, N. Salam, Z. Saleem, M. A. Saleh, Y. L. Samodra, A. M. Samy, A. Saravanan, M. Satpathy, A. E. Schumacher, M. Sedighi, S. Seekaew, M. Shafie, P. A. Shah, S. Shahid, M. J. Shahwan, S. Shakoor, N. Shalev, M. A. Shamim, M. A. Shamshirgaran, A. Shamsi, A. Sharifan, R. P. Shastry, M. Shetty, A. Shittu, S. Shrestha, E. E. Siddig, T. Sideroglou, J. Sifuentes-Osornio, L. M. L. R. Silva, E. A. F. Simões, A. J. H.

Simpson, A. Singh, S. Singh, R. Sinto, S. S. M. Soliman, S. Soraneh, N. Stoesser, T. Z. Stoeva, C. K. Swain, L. Szarpak, S. S. T Y, S. Tabatabai, C. Tabche, Z. M.-A. Taha, K.-K. Tan, N. Tasak, N. Y. Tat, A. Thaiprakong, P. Thangaraju, C. C. Tigoi, K. Tiwari, M. R. Tovani-Palone, T. H. Tran, M. Tumurkhuu, P. Turner, A. J. Udoakang, A. Udoh, N. Ullah, S. Ullah, A. G. Vaithinathan, M. Valenti, T. Vos, H. T. L. Vu, Y. Waheed, A. S. Walker, J. L. Walson, T. Wangrangsimakul, K. G. Weerakoon, H. F. L. Wertheim, P. C. M. Williams, A. A. Wolde, T. M. Wozniak, F. Wu, Z. Wu, M. K. K. Yadav, S. Yaghoubi, Z. S. Yahaya, A. Yarahmadi, S. Yezli, Y. E. Yismaw, D. K. Yon, C.-W. Yuan, H. Yusuf, F. Zakham, G. Zamagni, H. Zhang, Z.-J. Zhang, M. Zielińska, A. Zumla, S. H. H. Zyoud, S. H. Zyoud, S. I. Hay, A. Stergachis, B. Sartorius, B. S. Cooper, C. Dolecek, and C. J. L. Murray, "Global burden of bacterial antimicrobial resistance 1990–2021: a systematic analysis with forecasts to 2050", The Lancet **404**, 1199–1226 (2024).

[8]J. O'Neill, *Tackling drug-resistant infections globally: final report and recommendations* (Government of the United Kingdom, 2016).

[9]World Health Organization, *Antimicrobial resistance. global report on surveillance* (World Health Organization, Genève, Switzerland, Apr. 2014).

[10]R. Laxminarayan, A. Duse, C. Wattal, A. K. M. Zaidi, H. F. L. Wertheim, N. Sumpradit, E. Vlieghe, G. L. Hara, I. M. Gould, H. Goossens, C. Greko, A. D. So, M. Bigdeli, G. Tomson, W. Woodhouse, E. Ombaka, A. Q. Peralta, F. N. Qamar, F. Mir, S. Kariuki, Z. A. Bhutta, A. Coates, R. Bergstrom, G. D. Wright, E. D. Brown, and O. Cars, "Antibiotic resistance-the need for global solutions", en, Lancet Infect. Dis. **13**, 1057–1098 (2013).

[11]A. M. Niewiadomska, B. Jayabalasingham, J. C. Seidman, L. Willem, B. Grenfell, D. Spiro, and C. Viboud, "Population-level mathematical modeling of antimicrobial resistance: a systematic review", BMC Medicine **17**, 10.1186/s12916-019-1314-9 (2019).

[12]B. J. Langford, M. So, M. Simeonova, V. Leung, J. Lo, T. Kan, S. Raybardhan, M. E. Sapin, K. Mponponsuo, A. Farrell, E. Leung, J.-P. R. Soucy, A. Cassini, D. MacFadden, N. Daneman, and S. Bertagnolio, "Antimicrobial resistance in patients with covid-19: a systematic review and meta-analysis", The Lancet Microbe **4**, e179–e191 (2023).

[13]H. Heesterbeek, R. M. Anderson, V. Andreasen, S. Bansal, D. De Angelis, C. Dye, K. T. D. Eames, W. J. Edmunds, S. D. W. Frost, S. Funk, T. D. Hollingsworth, T. House, V. Isham, P. Klepac, J. Lessler, J. O. Lloyd-Smith, C. J. E. Metcalf, D. Mollison, L. Pellis, J. R. C. Pulliam, M. G. Roberts, and C. Viboud, "Modeling infectious disease dynamics in the complex landscape of global health", Science **347**, 10.1126/science.aaa4339 (2015).

[14]F. Schaumburg, F. C. Onwugamba, R. Akulenko, G. Peters, A. Mellmann, R. Köck, and K. Becker, "A geospatial analysis of flies and the spread of antimicrobial resistant bacteria", International Journal of Medical Microbiology **306**, 566–571 (2016).

[15]F. C. Onwugamba, J. R. Fitzgerald, K. Rochon, L. Guardabassi, A. Alabi, S. Kühne, M. P. Grobusch, and F. Schaumburg, "The role of 'filth flies' in the spread of antimicrobial resistance", Travel Medicine and Infectious Disease **22**, 8–17 (2018).

[16]R. Roemhild and H. Schulenburg, "Evolutionary ecology meets the antibiotic crisis", Evolution, Medicine, and Public Health **2019**, 37–45 (2019).

[17]L. Imamovic and M. O. A. Sommer, "Use of collateral sensitivity networks to design drug cycling protocols that avoid resistance development", Science Translational Medicine **5**, 10.1126/scitranslmed.3006609 (2013).

[18]C. E. H. Rosenkilde, C. Munck, A. Porse, M. Linkevicius, D. I. Andersson, and M. O. A. Sommer, "Collateral sensitivity constrains resistance evolution of the ctx-m-15 β-lactamase", Nature Communications **10**, 10.1038/s41467-019-08529-y (2019).

[19]F. Pinheiro, O. Warsi, D. I. Andersson, and M. Lässig, "Metabolic fitness landscapes predict the evolution of antibiotic resistance", Nature Ecology & Evolution **5**, 677–687 (2021).

[20]L. Rong, M. A. Gilchrist, Z. Feng, and A. S. Perelson, "Modeling within-host hiv-1 dynamics and the evolution of drug resistance: trade-offs between viral enzyme function and drug susceptibility", Journal of Theoretical Biology **247**, 804–818 (2007).

[21]S. Hernando-Amado, P. Laborda, and J. L. Martínez, "Tackling antibiotic resistance by inducing transient and robust collateral sensitivity", Nature Communications **14**, 10.1038/s41467-023-37357-4 (2023).

[22]V. I. Band, D. A. Hufnagel, S. Jaggavarapu, E. X. Sherman, J. E. Wozniak, S. W. Satola, M. M. Farley, J. T. Jacob, E. M. Burd, and D. S. Weiss, "Antibiotic combinations that exploit heteroresistance to multiple drugs effectively control infection", Nature microbiology **4**, 1627–1635 (2019).

[23]D. I. Andersson, H. Nicoloff, and K. Hjort, "Mechanisms and clinical relevance of bacterial heteroresistance", Nature Reviews Microbiology **17**, 479–496 (2019).

[24]H. Nicoloff, K. Hjort, B. R. Levin, and D. I. Andersson, "The high prevalence of antibiotic heteroresistance in pathogenic bacteria is mainly caused by gene amplification", Nature Microbiology **4**, 504–514 (2019).

[25]A. Batra, R. Roemhild, E. Rousseau, S. Franzenburg, S. Niemann, and H. Schulenburg, "High potency of sequential therapy with only β-lactam antibiotics", eLife **10**, 10.7554/elife.68876 (2021).

[26]R. Roemhild, T. Bollenbach, and D. I. Andersson, "The physiology and genetics of bacterial responses to antibiotic combinations", Nature Reviews Microbiology **20**, 478–490 (2022).

[27]C. I. BLISS, "The toxicity of poisons applied jointly", Annals of Applied Biology **26**, 585–615 (1939).

[28]W. R. Greco, G. Bravo, and J. C. Parsons, "The search for synergy: a critical review from a response surface perspective", en, Pharmacol. Rev. **47**, 331–385 (1995).

[29]M. G. Kirby, P. Allchorne, T. Appanna, P. Davey, R. Gledhill, J. S. A. Green, D. Greene, and D. J. Rosario, "Prescription switching: rationales and risks", International Journal of Clinical Practice **74**, 10.1111/ijcp.13429 (2019).

[30]V. G. Athyros, K. Tziomalos, A. Karagiannis, and D. P. Mikhailidis, "To switch (statins) or not to switch? that is the question", Expert Opinion on Pharmacotherapy **11**, 2943–2946 (2010).

[31]M. Y. Wei, M. K. Ito, J. D. Cohen, E. A. Brinton, and T. A. Jacobson, "Predictors of statin adherence, switching, and discontinuation in the usage survey: understanding the use of statins in america and gaps in patient education", Journal of Clinical Lipidology **7**, 472–483 (2013).

[32]J. Sochman and M. Podzimkova, "Not all statins are alike: induced rhabdomyolysis on changing from one statin to another one", International Journal of Cardiology **99**, 145–146 (2005).

[33]F. Clavel and A. J. Hance, "Hiv drug resistance", New England Journal of Medicine **350**, 1023–1035 (2004).

[34]R. W. Shafer and J. M. Schapiro, "HIV-1 drug resistance mutations: an updated framework for the second decade of HAART", en, AIDS Rev. **10**, 67–84 (2008).

[35]D. S. Clutter, M. R. Jordan, S. Bertagnolio, and R. W. Shafer, "HIV-1 drug resistance and resistance testing", Infection, Genetics and Evolution **46**, 292–307 (2016).

[36]L. Rong and A. S. Perelson, "Modeling latently infected cell activation: viral and latent reservoir persistence, and viral blips in HIV-infected patients on potent therapy", PLoS Computational Biology **5**, edited by R. Antia, e1000533 (2009).

[37]A. P. Duncan Callaway, "HIV-1 infection and low steady state viral loads", Bulletin of Mathematical Biology **64**, 29–64 (2002).

[38]M. C. F. Prosperi, R. D'Autilia, F. Incardona, A. De Luca, M. Zazzi, and G. Ulivi, "Stochastic modelling of genotypic drug-resistance for human immunodeficiency virus towards long-term combination therapy optimization", Bioinformatics **25**, 1040–1047 (2008).

[39]D. Liebenberg, B. G. Gordhan, and B. D. Kana, "Drug resistant tuberculosis: implications for transmission, diagnosis, and disease management", Frontiers in Cellular and Infection Microbiology **12**, 10.3389/fcimb.2022.943545 (2022).

[40]E. Temkin, N. Fallach, J. Almagor, B. P. Gladstone, E. Tacconelli, and Y. Carmeli, "Estimating the number of infections caused by antibiotic-resistant escherichia coli and klebsiella pneumoniae in 2014: a modelling study", The Lancet Global Health **6**, e969–e979 (2018).

[41]N. J. White, "Antimalarial drug resistance", Journal of Clinical Investigation **113**, 1084–1092 (2004).

[42]A. M. Ramoso, J. A. Magalang, D. Sánchez-Taltavull, J. P. Esguerra, and É. Roldán, "Stochastic resetting antiviral therapies prevent drug resistance development", Europhysics Letters **132**, 50003 (2020).

[43]T. Lee, S. Bonhoeffer, and M. Penny, "The competition dynamics of resistant and sensitive infections", Results in Physics **34**, 105181 (2022).

[44]O. Sharomi and A. Gumel, "Dynamical analysis of a multi-strain model of hiv in the presence of anti-retroviral drugs", Journal of Biological Dynamics **2**, 323–345 (2008).

[45]N. T. Hillock, T. L. Merlin, J. Turnidge, and J. Karnon, "Modelling the future clinical and economic burden of antimicrobial resistance: the feasibility and value of models to inform policy", Applied Health Economics and Health Policy **20**, 479–486 (2022).

[46]Y. L. Luke, *On the approximate inversion of some Laplace transforms*, tech. rep. (Midwest Research Institute, Aerospace Research Laboratories, 1961) Chap. Technical Reports.

[47]I. M. Longman, "On the Generation of Rational Function Approximations for Laplace Transform Inversion with an Application to Viscoelasticity", SIAM Journal on Applied Mathematics **24**, 429–440 (1973).

[48]J. H. Mathews and K. D. Fink, *Numerical Methods Using MATLAB*, 4th ed. (Pearson Prentice Hall, 2004).

[49]G. F. Lawler, *Introduction to Stochastic Processes*, 1st (Chapman and Hall/CRC, New York, July 1995).

[50]S. Asmussen and P. W. Glynn, *Stochastic Simulation: Algorithms and Analysis*, Vol. 57, Stochastic Modelling and Applied Probability (Springer, New York, NY, 2007).

[51]S. Redner, *A Guide to First-Passage Processes* (Cambridge University Press, Cambridge, 2001).

[52]D. L. Dy and J. P. Esguerra, "First-Passage characteristics of biased diffusion in a planar wedge", Physical Review E **88**, 012121 (2013).

[53]C. Gardiner, "A historical introduction", in *Stochastic methods*, Springer series in synergetics (Springer Berlin Heidelberg, Berlin, Heidelberg, 2008), pp. 1–22.

[54]J. Wang, K. Zhang, L. Xu, and E. Wang, "Quantifying the waddington landscape and biological paths for development and differentiation", Proceedings of the National Academy of Sciences **108**, 8257–8262 (2011).

[55]P. E. Harunari, A. Dutta, M. Polettini, and É. Roldán, "What to learn from a few visible transitions' statistics?", Physical Review X **12**, 10.1103/physrevx.12.041026 (2022).

[56]S. Karlin and H. M. Taylor, *A Second Course in Stochastic Processes* (Academic Press, an imprint of Elsevier, 1981).

[57]R. Gatto, *Stationary stochastic models: an introduction*, 1st, World Scientific Series on Probability Theory and Its Applications: Volume 4 (World Scientific Publishing, Singapore, July 2022).

[58]N. Zlatanov and L. Kocarev, "Random walks on networks: cumulative distribution of cover time", Physical Review E **80**, 10.1103/physreve.80.041102 (2009).

[59]A. P. Riascos, D. Boyer, P. Herringer, and J. L. Mateos, "Random walks on networks with stochastic resetting", Physical Review E **101**, 10.1103/physreve.101.062147 (2020).

[60]D. T. Gillespie, "Approximating the master equation by fokker–planck-type equations for single-variable chemical systems", The Journal of Chemical Physics **72**, 5363–5370 (1980).

[61]N. G. van Kampen, *Stochastic Processes in Physics and Chemistry*, 3rd ed., North-Holland Personal Library (Elsevier, 2007).

[62]D. R. Cox and H. D. Miller, *The Theory of Stochastic Processes*, 1st (Chapman and Hall/CRC, London, 1965).

[63]A. V. Skorokhod, "Stochastic Equations for Diffusion Processes in a Bounded Region", Theory of Probability & Its Applications **6**, 264–274 (1961).

[64]X. Bian, C. Kim, and G. E. Karniadakis, "111 years of Brownian motion", Soft Matter **12**, 6331–6346 (2016).

[65]M. R. Evans and S. N. Majumdar, "Diffusion with Stochastic Resetting", Physical Review Letters **106**, 160601 (2011).

[66]M. R. Evans, S. N. Majumdar, and G. Schehr, "Stochastic resetting and applications", Journal of Physics A: Mathematical and Theoretical **53**, 193001 (2020).

[67]S. N. Majumdar, S. Sabhapandit, and G. Schehr, "Dynamical transition in the temporal relaxation of stochastic processes under resetting", Physical Review E **91**, 052131 (2015).

[68]A. Chechkin and I. M. Sokolov, "Random Search with Resetting: A Unified Renewal Approach", Physical Review Letters **121**, 050601 (2018).

[69]S. Karlin and H. Taylor, *A first course in stochastic processes*, First course in stochastic processes / Samuel Karlin; Howard M. Taylor Bd. 1 (Elsevier Science, 1975).

[70]R. Voituriez and O. Bénichou, "First-Passage Statistics for Random Walks in Bounded Domains", in *First-Passage Phenomena and Their Applications* (World Scientific, May 2014), pp. 145–174.

[71]V. Giorno, A. G. Nobile, L. M. Ricciardi, and L. Sacerdote, "Some remarks on the rayleigh process", Journal of Applied Probability **23**, 398–408 (1986).

[72]R. Gutiérrez, R. Gutiérrez-Sánchez, and A. Nafidi, "The stochastic rayleigh diffusion model: statistical inference and computational aspects. applications to modelling of real cases", Applied Mathematics and Computation **175**, 628–644 (2006).

[73]G. A. Pavliotis, *Stochastic Processes and Applications: Diffusion Processes, the Fokker-Planck and Langevin Equations*, 1st, Texts in Applied Mathematics 60 (Springer, New York, 2014).

[74]G. A. Whitmore and V. Seshadri, "A heuristic derivation of the inverse gaussian distribution", The American Statistician **41**, 280–281 (1987).

[75]R. S. Chhikara and J. Leroy Folks, *The inverse gaussian distribution*, Statistics: A Series of Textbooks and Monographs (CRC Press, Boca Raton, FL, Sept. 1988).

[76]J. Abate and W. Whitt, "A Unified Framework for Numerically Inverting Laplace Transforms", INFORMS Journal on Computing **18**, 408–421 (2006).

[77]A. M. Cohen, *Numerical Methods for Laplace Transform Inversion*, Vol. 5 (Springer Science & Business Media, 2007).

[78]D. P. Gaver, "Observing stochastic processes, and approximate transform inversion", Operations Research **14**, 444–459 (1966).

[79]H. Stehfest, "Algorithm 368: numerical inversion of laplace transforms [d5]", Communications of the ACM **13**, 47–49 (1970).

[80]A. Talbot, "The accurate numerical inversion of Laplace transforms", IMA Journal of Applied Mathematics **23**, 97–120 (1979).

[81]I. S. Gradshteyn and I. M. Ryzhik, *Table of integrals, series, and products*, Seventh, Translated from the Russian, Translation edited and with a preface by Alan Jeffrey and Daniel Zwillinger, With one CD-ROM (Windows, Macintosh and UNIX) (Elsevier/Academic Press, Amsterdam, 2007), pp. xlviii+1171.

[82]D. E. Knuth, "An algorithm for brownian zeroes", Computing **33**, 89–94 (1984).

[83]D. T. Gillespie, "Exact stochastic simulation of coupled chemical reactions", The Journal of Physical Chemistry **81**, 2340–2361 (1977).

[84]O. Bénichou, M. Coppey, M. Moreau, P.-H. Suet, and R. Voituriez, "Optimal search strategies for hidden targets", Physical Review Letters **94**, 10.1103/physrevlett.94.198101 (2005).

[85]A. Arenas, A. Díaz-Guilera, J. Kurths, Y. Moreno, and C. Zhou, "Synchronization in complex networks", Physics Reports **469**, 93–153 (2008).

[86]P. Romanczuk, I. D. Couzin, and L. Schimansky-Geier, "Collective Motion due to Individual Escape and Pursuit Response", Physical Review Letters **102**, 010602 (2009).

[87]R. Pastor-Satorras and A. Vespignani, "Epidemic spreading in scale-free networks", Physical Review Letters **86**, 3200–3203 (2001).

[88]J. Aguilar, B. A. García, R. Toral, S. Meloni, and J. J. Ramasco, "Endemic infectious states below the epidemic threshold and beyond herd immunity", Communications Physics **6**, 1–11 (2023).

[89]E. Barkai and D. A. Kessler, "Transport and the First Passage Time Problem with Application to Cold Atoms in Optical Traps", in *First-Passage Phenomena and Their Applications* (World Scientific, May 2014), pp. 502–531.

[90]M. Maggiore and A. Riotto, "The Excursion Set Theory in Cosmology", in *First-Passage Phenomena and Their Applications* (World Scientific, May 2014), pp. 532–553.

[91]J. Masoliver and J. Perelló, "First-Passage and Extremes in Socio-Economic Systems", in *First-Passage Phenomena and Their Applications* (World Scientific, May 2014), pp. 477–501.

[92]R. Chicheportiche and J.-P. Bouchaud, "Some Applications of First-Passage Ideas to Finance", in *First-Passage Phenomena and Their Applications* (World Scientific, May 2014), pp. 447–476.

[93]R. Gatto and M. Mosimann, "Four approaches to compute the probability of ruin in the compound Poisson risk process with diffusion", Mathematical and Computer Modelling **55**, 1169–1185 (2012).

[94]R. Gatto and B. Baumgartner, "Saddlepoint Approximations to the Probability of Ruin in Finite Time for the Compound Poisson Risk Process Perturbed by Diffusion", Methodology and Computing in Applied Probability **18**, 217–235 (2016).

[95]Y. Zhang and O. K. Dudko, "First-Passage Processes in the Genome", Annual Review of Biophysics **45**, 117–134 (2016).

[96]M. L. Woods, C. Carmona-Fontaine, C. P. Barnes, I. D. Couzin, R. Mayor, and K. M. Page, "Directional Collective Cell Migration Emerges as a Property of Cell Interactions", PLOS ONE **9**, e104969 (2014).

[97]S. Iyer-Biswas and A. Zilman, "First-Passage Processes in Cellular Biology", in *Advances in Chemical Physics*, Vol. 160 (John Wiley & Sons, Ltd, 2016) Chap. 5, pp. 261–306.

[98]G. Mercado-Vásquez and D. Boyer, "Lotka–Volterra systems with stochastic resetting", Journal of Physics A: Mathematical and Theoretical **51**, 405601 (2018).

[99]P. C. Bressloff, "Stochastic resetting and the Mean-Field dynamics of focal adhesions", Physical Review E **102**, 022134 (2020).

[100]É. Roldán, A. Lisica, D. Sánchez-Taltavull, and S. W. Grill, "Stochastic resetting in backtrack recovery by RNA polymerases", Physical Review E **93**, 062411 (2016).

[101]B. Besga, A. Bovon, A. Petrosyan, S. N. Majumdar, and S. Ciliberto, "Optimal mean First-Passage time for a Brownian searcher subjected to resetting: Experimental and theoretical results", Physical Review Research **2**, 032029 (2020).

[102]O. Tal-Friedman, A. Pal, A. Sekhon, S. Reuveni, and Y. Roichman, "Experimental Realization of Diffusion with Stochastic Resetting", The Journal of Physical Chemistry Letters **11**, 7350–7355 (2020).

[103]A. Pal and V. V. Prasad, "First Passage under stochastic resetting in an interval", Physical Review E **99**, 032123 (2019).

[104]É. Roldán and S. Gupta, "Path-integral formalism for stochastic resetting: Exactly solved examples and shortcuts to confinement", Physical Review E **96**, 022130 (2017).

[105]S. B. Yuste and K. Lindenberg, "Comment on "Mean first passage time for anomalous diffusion"", Physical Review E **69**, 033101 (2004).

[106]N. Masuda, M. A. Porter, and R. Lambiotte, "Random walks and diffusion on networks", Physics Reports **716–717**, 1–58 (2017).

[107]J. D. Noh and H. Rieger, "Random walks on complex networks", Physical Review Letters **92**, 10.1103/physrevlett.92.118701 (2004).

[108]A. Nagar and S. Gupta, "Diffusion with Stochastic Resetting at Power-Law times", Physical Review E **93**, 060102 (2016).

[109]A. Pal, A. Kundu, and M. R. Evans, "Diffusion under time-dependent resetting", Journal of Physics A: Mathematical and Theoretical **49**, 225001 (2016).

[110]B. De Bruyne and F. Mori, "Resetting in stochastic optimal control", Physical Review Research **5**, 10.1103/physrevresearch.5.013122 (2023).

[111]J. C. Sunil, R. A. Blythe, M. R. Evans, and S. N. Majumdar, "The cost of stochastic resetting", Journal of Physics A: Mathematical and Theoretical **56**, 395001 (2023).

[112]L. Kusmierz, S. N. Majumdar, S. Sabhapandit, and G. Schehr, "First Order Transition for the Optimal Search Time of Lévy Flights with Resetting", Physical Review Letters **113**, 220602 (2014).

[113]J. M. Meylahn, S. Sabhapandit, and H. Touchette, "Large deviations for Markov processes with resetting", Physical Review E **92**, 062148 (2015).

[114]A. M. Wensing, V. Calvez, F. Ceccherini-Silberstein, C. Charpentier, H. F. Günthard, R. Paredes, R. W. Shafer, and D. D. Richman, "2019 Update of the Drug Resistance Mutations in HIV-1", Topics in Antiviral Medicine **27**, 111–121 (2019).

[115]R. Gatto, *Stochastische modelle der aktuariellen risikotheorie – eine mathematische einführung, 2nd edition* (Springer, 2020).

Appendix A

Proofs

A.1 Proof of Proposition 2.1.1

Proof. Let X_t be the current state of a random walk at time t on a chain of states spaced apart by $1/M$. Let the following probabilities define how the the random walk evolves in an infinitesimal amount of time Δt,

$$\begin{aligned} X_{t+\Delta t} &= X_t - \frac{1}{M}, && \text{with probability } p\Delta t \\ X_{t+\Delta t} &= X_t + \frac{1}{M}, && \text{with probability } q\Delta t \end{aligned}$$

The probability distribution that at the next infinitesimal amount of time Δt that a random walk would be at state $X_{t+\Delta t} = x$ coming from an initial state x_0 is given by

$$\begin{aligned} P(x, t+\Delta t|x_0) =& p\Delta t\, P\left(x - \frac{1}{M}, t\middle|x_0\right) + q\Delta t\, P\left(x + \frac{1}{M}, t\middle|x_0\right) \\ & - (p+q)\Delta t\, P(x,t|x_0) + P(x,t|x_0) \\ \frac{P(x,t+\Delta t|x_0) - P(x,t|x_0)}{\Delta t} =& p\, P\left(x - \frac{1}{M}, t\middle|x_0\right) + q\, P\left(x + \frac{1}{M}, t\middle|x_0\right) \\ & - (p+q)\, P(x_i,t|x_0) \end{aligned}$$

Letting $\Delta \to 0$ turns the fraction in the left hand side into

$$\frac{P(x,t+\Delta t|x_0) - P(x,t|x_0)}{\Delta t} \approx \frac{\mathrm{d}}{\mathrm{d}t} P(x,t|x_0).$$

From this, the master equation eq. (2.3) is derived,

$$\frac{\mathrm{d}}{\mathrm{d}t} P(x,t|x_0) = p\, P\left(x - \frac{1}{M}, t\middle|x_0\right) + q\, P\left(x + \frac{1}{M}, t\middle|x_0\right) - (p+q)\, P(x,t|x_0).$$

□

A.2 Proof of Proposition 2.1.2

Proof. On the probability terms with states displaced by $1/M$ on the master equation (2.3), a second-order Taylor expansion is performed centered on x. For the first term of the master equation,

$$\begin{aligned} p\,P\left(x-\frac{1}{M},t\middle|x_0\right) \approx & \, p\,P\left(x,t|x_0\right)+p\left(x-\frac{1}{M}-x\right)\frac{\partial}{\partial x}P\left(x,t|x_0\right) \\ & +p\left(x-\frac{1}{M}-x\right)^2\frac{\partial^2}{\partial x^2}P\left(x,t|x_0\right) \\ = & \, p\,P\left(x,t|x_0\right)-\frac{p}{M}\frac{\partial}{\partial x}P\left(x,t|x_0\right)+\frac{p^2}{M^2}\frac{\partial^2}{\partial x^2}P\left(x,t|x_0\right). \end{aligned}$$

Similarly, for the second term,

$$q\,P\left(x+\frac{1}{M},t\middle|x_0\right) \approx q\,P\left(x,t|x_0\right)+\frac{q}{M}\frac{\partial}{\partial x}P\left(x,t|x_0\right)+\frac{q^2}{M^2}\frac{\partial^2}{\partial x^2}P\left(x,t|x_0\right)$$

The total derivative on the left-hand side of the master equation is now re-written as a partial derivative with respect to time for consistency. Combining together and collecting propagator terms by increasing orders of the partial derivative, the master equation is now written as

$$\frac{\partial}{\partial t}P(x,t|x_0)=-\left(\frac{p-q}{M}\right)\frac{\partial}{\partial x}P(x,t|x_0)+\left(\frac{p+q}{2M^2}\right)\frac{\partial^2}{\partial x^2}P(x,t|x_0).$$

Letting $v=(p-q)/M$ and $D=(p+q)/(2M^2)$, the Fokker-Planck equation (2.5) is derived. □

A.3 Derivation of the Fokker-Planck equation from the SDE

The following products of infinitesimals $\mathrm{d}t$ and $\mathrm{d}W_t$ are important identities in Itô calculus [53]:

$$\mathrm{d}t^2=0, \qquad \mathrm{d}W_t\,\mathrm{d}t=0, \qquad \mathrm{d}W_t^2=\mathrm{d}t \tag{A.1}$$

The first two identities is from the fact that $\mathrm{d}t$ and $\mathrm{d}W$ are infinitely small, hence $\mathrm{d}t^2$ and $\mathrm{d}W\,\mathrm{d}t$ will be negligible. The third identity is from the quadratic variation of the Wiener process W_t, since the increments of the Wiener process are defined to have a variance that is linearly proportional to the time increment. Substituting the $\mathrm{d}x$ terms into Itô's formula (2.10) with $\mathrm{d}X_t$ in the SDE (2.7) with the identities (A.1),

$$
\begin{aligned}
\mathrm{d}g(x,t) &= \frac{\partial}{\partial t}g(x,t)\,\mathrm{d}t + \frac{\partial}{\partial x}g(x,t)\left(-v\,\mathrm{d}t + \sqrt{2D}\,\mathrm{d}W_t\right) \\
&\quad + \frac{1}{2}\frac{\partial^2}{\partial x^2}g(x,t)\left(-v\,\mathrm{d}t + \sqrt{2D}\,\mathrm{d}W_t\right)^2 \\
\mathrm{d}g(x,t) &= \frac{\partial}{\partial t}g(x,t)\,\mathrm{d}t + \frac{\partial}{\partial x}g(x,t)\left(-v\,\mathrm{d}t + \sqrt{2D}\,\mathrm{d}W_t\right) \\
&\quad + \frac{1}{2}\frac{\partial^2}{\partial x^2}g(x,t)\left(-v^2\,\mathrm{d}t^2 - 2v\sqrt{2D}\,\mathrm{d}t\,\mathrm{d}W_t + 2D\,\mathrm{d}W_t^2\right)
\end{aligned}
$$

Using the identities in eq. (A.1),

$$
\mathrm{d}g(x,t) = \frac{\partial}{\partial t}g(x,t)\,\mathrm{d}t + \frac{\partial}{\partial x}g(x,t)\left(-v\,\mathrm{d}t + \sqrt{2D}\,\mathrm{d}W_t\right) + D\frac{\partial^2}{\partial x^2}g(x,t)\,\mathrm{d}t
$$

Collecting terms with $\mathrm{d}t$,

$$
\mathrm{d}g(x,t) = \left(\frac{\partial}{\partial t}g(x,t)\,\mathrm{d}t - v\frac{\partial}{\partial x}g(x,t)\,\mathrm{d}t + D\frac{\partial^2}{\partial x^2}g(x,t)\,\mathrm{d}t\right) + \sqrt{2D}\frac{\partial}{\partial x}g(x,t)\,\mathrm{d}W_t
$$

Taking the expectation of both sides of the equation with respect to x,

$$
\mathbb{E}\left[g(x,t)\right] = \int_{-\infty}^{\infty} g(x,t)P(x,t)\,\mathrm{d}x,
$$

and further noting that by the definition of the Wiener process, the expectation of the Wiener increment $\mathrm{d}W_t$ is zero,

$$
\begin{aligned}
\mathrm{d}\mathbb{E}[g(x,t)] &= \mathbb{E}\left[\frac{\partial}{\partial t}g(x,t) - v\frac{\partial}{\partial x}g(x,t) + D\frac{\partial^2}{\partial x^2}g(x,t)\right]\mathrm{d}t \\
\frac{\mathrm{d}}{\mathrm{d}t}\int_{-\infty}^{\infty} g(x,t)P(x,t)\,\mathrm{d}x &= \int_{-\infty}^{\infty}\left[\frac{\partial}{\partial t}g(x,t) - v\frac{\partial}{\partial x}g(x,t) + D\frac{\partial^2}{\partial x^2}g(x,t)\right]P(x,t)\,\mathrm{d}x \\
\frac{\mathrm{d}}{\mathrm{d}t}\int_{-\infty}^{\infty} g(x,t)P(x,t)\,\mathrm{d}x &= \int_{-\infty}^{\infty} P(x,t)\frac{\partial}{\partial t}g(x,t)\,\mathrm{d}x \\
&\quad + \int_{-\infty}^{\infty}\left[-v\frac{\partial}{\partial x}g(x,t) + D\frac{\partial^2}{\partial x^2}g(x,t)\right]P(x,t)\,\mathrm{d}x.
\end{aligned}
$$

By the product rule of derivatives, the lefthand side of the equation must be

$$
\frac{\mathrm{d}}{\mathrm{d}t}\int_{-\infty}^{\infty} g(x,t)P(x,t)\,\mathrm{d}x = \int_{-\infty}^{\infty} P(x,t)\frac{\partial}{\partial t}g(x,t)\,\mathrm{d}x + \int_{-\infty}^{\infty} g(x,t)\frac{\partial}{\partial t}P(x,t)\,\mathrm{d}x.
$$

Note that the first term of the sum above is equal to the first term of the righthand side of the preceding equation, hence it can be simplified further to

$$
\int_{-\infty}^{\infty} g(x,t)\frac{\partial}{\partial t}P(x,t)\,\mathrm{d}x = \int_{-\infty}^{\infty}\left[-v\frac{\partial}{\partial x}g(x,t) + D\frac{\partial^2}{\partial x^2}g(x,t)\right]P(x,t)\,\mathrm{d}x.
$$

Since $g(x,t)$ is an arbitrarily smooth test function, we may write

$$\frac{\partial}{\partial t}P(x,t) = -v\frac{\partial}{\partial x}P(x,t) + D\frac{\partial^2}{\partial x^2}P(x,t),$$

which is the Fokker-Planck equation in eq. (2.5). □

A.4 Proof of Proposition 2.2.3

Given a twice-differentiable function $g(\boldsymbol{x},t)$, take the multivariate second-order Taylor expansion of its differential $\mathrm{d}g$ is

$$\mathrm{d}g(\boldsymbol{x},t) = \frac{\partial}{\partial t}g(\boldsymbol{x},t)\mathrm{d}t + \frac{1}{2}\frac{\partial^2}{\partial t^2}g(\boldsymbol{x},t)\mathrm{d}t^2 + \sum_{i=1}^{N}\frac{\partial}{\partial x_i}g(\boldsymbol{x},t)\mathrm{d}\boldsymbol{x} + \frac{1}{2}\mathrm{d}\boldsymbol{x}H_{\boldsymbol{x}}g(\boldsymbol{x},t)\mathrm{d}\boldsymbol{x}^\top,$$

where $H_{\boldsymbol{x}}$ is the Hessian matrix with respect to $\boldsymbol{x}$ with elements $\partial^2/(\partial x_i \partial x_j), \forall i,j$. Since $\mathrm{d}t^2 = 0$ and $\mathrm{d}\boldsymbol{x}$ is given by eq. (2.16),

$$\begin{aligned}
\mathrm{d}g(\boldsymbol{x},t) =& \frac{\partial}{\partial t}g(\boldsymbol{x},t)\mathrm{d}t + \sum_{i=1}^{N}\frac{\partial}{\partial x_i}g(\boldsymbol{x},t)\left[\boldsymbol{\mu}\left(\boldsymbol{x},t\right)\,\mathrm{d}t + \boldsymbol{\sigma}\left(\boldsymbol{x},t\right)\,\mathrm{d}\boldsymbol{W}_t\right] \\
&+ \frac{1}{2}\sum_{i=1}^{N}\sum_{j=1}^{N}\left[\boldsymbol{\mu}\left(\boldsymbol{x},t\right)\,\mathrm{d}t + \boldsymbol{\sigma}\left(\boldsymbol{x},t\right)\,\mathrm{d}\boldsymbol{W}_t\right]\left[\boldsymbol{\mu}\left(\boldsymbol{x},t\right)\,\mathrm{d}t + \boldsymbol{\sigma}\left(\boldsymbol{x},t\right)\,\mathrm{d}\boldsymbol{W}_t\right]^\top \frac{\partial}{\partial x_i}\frac{\partial}{\partial x_j}g(\boldsymbol{x},t) \\
=& \frac{\partial}{\partial t}g(\boldsymbol{x},t)\mathrm{d}t + \sum_{i=1}^{N}\frac{\partial}{\partial x_i}g(\boldsymbol{x},t)\left[\boldsymbol{\mu}\left(\boldsymbol{x},t\right)\,\mathrm{d}t + \boldsymbol{\sigma}\left(\boldsymbol{x},t\right)\,\mathrm{d}\boldsymbol{W}_t\right] \\
&+ \frac{1}{2}\sum_{i=1}^{N}\sum_{j=1}^{N}\Big[\boldsymbol{\mu}\left(\boldsymbol{x},t\right)\boldsymbol{\mu}\left(\boldsymbol{x},t\right)^\top\,\mathrm{d}t^2 + \boldsymbol{\mu}\left(\boldsymbol{x},t\right)\sigma(\boldsymbol{x},t)^\top\mathrm{d}t\mathrm{d}\boldsymbol{W}_t \\
&+ \boldsymbol{\sigma}\left(\boldsymbol{x},t\right)^\top\,\mathrm{d}t\,\mathrm{d}\boldsymbol{W}_t^\top\mu(\boldsymbol{x},t) + \boldsymbol{\sigma}\left(\boldsymbol{x},t\right)\boldsymbol{\sigma}\left(\boldsymbol{x},t\right)^\top\,\mathrm{d}\boldsymbol{W}_t^2\Big]\frac{\partial}{\partial x_i}\frac{\partial}{\partial x_j}g(\boldsymbol{x},t).
\end{aligned}$$

Since $\mathrm{d}\boldsymbol{W}_t\,\mathrm{d}t = 0$ and $\mathrm{d}\boldsymbol{W}_t^2 = \mathrm{d}t$,

$$\begin{aligned}
\mathrm{d}g(\boldsymbol{x},t) =& \frac{\partial}{\partial t}g(\boldsymbol{x},t)\mathrm{d}t + \sum_{i=1}^{N}\boldsymbol{\mu}\left(\boldsymbol{x},t\right)\frac{\partial}{\partial x_i}g(\boldsymbol{x},t)\mathrm{d}t + \sum_{i=1}^{N}\boldsymbol{\sigma}\left(\boldsymbol{x},t\right)\,\frac{\partial}{\partial x_i}g(\boldsymbol{x},t)\mathrm{d}\boldsymbol{W}_t \\
&+ \frac{1}{2}\sum_{i=1}^{N}\sum_{j=1}^{N}\boldsymbol{\sigma}\left(\boldsymbol{x},t\right)\boldsymbol{\sigma}\left(\boldsymbol{x},t\right)^\top\,\mathrm{d}t\frac{\partial}{\partial x_i}\frac{\partial}{\partial x_j}g(\boldsymbol{x},t) \\
=& \left[\frac{\partial}{\partial t}g(\boldsymbol{x},t) + \sum_{i=1}^{N}\boldsymbol{\mu}\left(\boldsymbol{x},t\right)\frac{\partial}{\partial x_i}g(\boldsymbol{x},t)\right. \\
&\left. + \frac{1}{2}\sum_{i=1}^{N}\sum_{j=1}^{N}\boldsymbol{\sigma}\left(\boldsymbol{x},t\right)\boldsymbol{\sigma}\left(\boldsymbol{x},t\right)^\top\frac{\partial}{\partial x_i}\frac{\partial}{\partial x_j}g(\boldsymbol{x},t)\right]\mathrm{d}t + \sum_{i=1}^{N}\boldsymbol{\sigma}\left(\boldsymbol{x},t\right)\,\frac{\partial}{\partial x_i}g(\boldsymbol{x},t)\mathrm{d}\boldsymbol{W}_t
\end{aligned}$$

Writing down $\boldsymbol{\sigma}$ in terms of matrix elements $\sigma_{i,j}, \forall i, j$ and defining the product $\boldsymbol{\sigma}\boldsymbol{\sigma}^\top$ to be the diffusion tensor, defined in eq. (2.18), we obtain Itô's formula solved for the multivariate SDE in eq. (2.16). □

A.5 Proof of Proposition 5.0.1

Let $g_{m,n}(u) = p_m(u)/q_n(u)$ be a function approximated using the Padé approximation with a rational function of polynomials, with numerator $p_m(u) = \sum_{j=0}^{m} = a_j s^j$ and denominator $q_n(u) = \sum_{j=0}^{n} = b_j s^j$. Given the form of the Laplace transform of the propagator, the coefficients a_j and b_j must always be real.

To obtain the partial fraction decomposition, the roots of $q_n(u)$ must first be computed. By the fundamental theorem of algebra, $q_n(u)$ may be written as

$$q_n(u) = (u-\alpha_1)^{l_1} \dots (u-\alpha_{n_1})^{l_{n_1}} (u^2 - c_1 u + d_1)^{l_1^\dagger} \dots (u^2 - c_{n_2} u + d_{n_2})^{l_{n_2}^\dagger} \tag{A.2}$$

The trinomial terms in the product may be factored further to yield roots that are complex conjugate pairs

$$q_n(u) = (u-\alpha_1)^{l_1} \dots (u-\alpha_{n_1})^{l_{n_1}} (u-\alpha_1^\dagger)^{l_1^\dagger} (u-\overline{\alpha}_1^\dagger)^{l_1^\dagger} \dots (u-\alpha_{n_2}^\dagger)^{l_{n_2}^\dagger} (u-\overline{\alpha}_{n_2}^\dagger)^{l_{n_2}^\dagger}. \tag{A.3}$$

Thus, the roots of $q_n(u)$ are separated into the real roots α_j for $j = 1, \dots, n_1$ and the complex conjugate roots $\alpha_j^\dagger, \overline{\alpha}_j^\dagger$ for $j = 1, \dots, n_2$, and $n_1 + 2n_2 = n$ retrieves the degree of $q_n(u)$. The partial fraction decomposition of $g_{m,n}(u)$ is

$$g_{m,n}(u) = \sum_{j=1}^{n_1} \sum_{i=1}^{l_j} \frac{\gamma_{j,i}}{(u-\alpha_j)^i} + \sum_{j=1}^{n_2} \sum_{i=1}^{l_j^\dagger} \left[\frac{\gamma_{j,i}^\dagger}{(u-\alpha_j^\dagger)^i} + \frac{\overline{\gamma}_{j,i}^\dagger}{(u-\overline{\alpha}_j^\dagger)^i} \right], \tag{A.4}$$

where $\gamma_{j,i}$, $\gamma_{j,i}^\dagger$, and $\overline{\gamma}_{j,i}^\dagger$ are coefficients that may be obtained using the residue method or by cf. e.g. [115] p. 233-234.

Note that regardless of whether the root or coefficient is real or complex-valued, the partial fractions can still be used to obtain a Laplace inversion, e.g.

$$\mathcal{L}^{-1}\left(\frac{\gamma}{(u-\alpha)^i} \right) = \frac{\gamma}{(i-1)!} t^{i-1} \exp(\alpha t), \tag{A.5}$$

for an arbitrary γ and α. Suppose that the complex roots will have the form $\alpha^\dagger = \sigma + \mathrm{i}\omega$ and complex conjugate $\overline{\alpha}_j = \sigma - \mathrm{i}\omega$. These roots will have coefficients γ and $\overline{\gamma}$ that may be expressed into polar coordinates with radius $R = |\gamma^\dagger|$ and angle $\phi = \tan^{-1}(\mathrm{Im}(\gamma^\dagger)/\mathrm{Re}(\gamma^\dagger))$. The inversion of the sum of the partial fractions for these complex

roots would be

$$\begin{aligned}
\mathcal{L}^{-1}\left(\frac{\gamma^{\dagger}}{[u-(\sigma+\omega\mathrm{i})]^{i}}+\frac{\overline{\gamma}^{\dagger}}{[u-(\sigma-\omega\mathrm{i})]^{i}}\right) =& \frac{R\exp(\mathrm{i}\phi)}{(i-1)!}t^{i-1}\exp[(\sigma+\mathrm{i}\omega)t] \\
&+\frac{R\exp(-\mathrm{i}\phi)}{(i-1)!}t^{i-1}\exp[(\sigma-\mathrm{i}\omega)t] \\
=& \frac{Rt^{i-1}\exp(\sigma t)}{(i-1)!}\big[\exp(\mathrm{i}\phi)\exp(\mathrm{i}\omega t) \\
&+\exp(-\mathrm{i}\phi)\exp(-\mathrm{i}\omega t)\big] \\
=& \frac{2Rt^{i-1}\exp(\sigma t)}{(i-1)!}\frac{\exp[\mathrm{i}(\omega t+\phi)]+\exp[-\mathrm{i}(\omega t+\phi)]}{2} \\
=& \frac{2R\exp(\sigma t)}{(i-1)!}t^{i-1}\cos(\omega t+\phi)
\end{aligned}$$

Therefore, taking the sums of the two Laplace transform inversions, we obtain the inversion of the full function $g_{m,n}(u)$ even with complex roots in the denominator from the partial fraction decomposition step. □

Declaration of consent

on the basis of Article 18 of the PromR Phil.-nat. 19

Name/First Name: Juan Antonio Magalang

Registration Number: 21-128-665

Study program: PhD Statistics

Bachelor ☐ Master ☐ Dissertation ☑

Title of the thesis: Stochastic models of drug resistance development

Supervisor: Prof. Dr. Riccardo Gatto
PD Dr. Daniel Sanchez-Taltavull

I declare herewith that this thesis is my own work and that I have not used any sources other than those stated. I have indicated the adoption of quotations as well as thoughts taken from other authors as such in the thesis. I am aware that the Senate pursuant to Article 36 paragraph 1 litera r of the University Act of September 5th, 1996 and Article 69 of the University Statute of June 7th, 2011 is authorized to revoke the doctoral degree awarded on the basis of this thesis.
For the purposes of evaluation and verification of compliance with the declaration of originality and the regulations governing plagiarism, I hereby grant the University of Bern the right to process my personal data and to perform the acts of use this requires, in particular, to reproduce the written thesis and to store it permanently in a database, and to use said database, or to make said database available, to enable comparison with theses submitted by others.

Bern, 26.11.2024

Place/Date

Signature